METROLOGICAL TECHNIQUES TO STUDY PRIMARY AND SECONDARY HEMOSTASIS

By

Sandra Michelle Baker

A DISSERTATION

Presented to the Department of Biomedical Engineering
of the Oregon Health & Science University
School of Medicine
in partial fulfillment of
the requirements for the degree of

Doctor of Philosophy
in Biomedical Engineering

October 2015

Department of Biomedical Engineering
School of Medicine
Oregon Health & Science University

CERTIFICATE OF APPROVAL

This is to certify that the Ph.D. dissertation of
Sandra Michelle Baker
has been approved

Owen J. T. McCarty, Ph.D.
Associate Professor, Dissertation Advisor

Monica T. Hinds, Ph.D.
Associate Professor

Michael Recht, M.D., Ph.D.
Adjunct Associate Professor

Xiaolin Nan, Ph.D.
Assistant Professor

Jason Taylor, M.D., Ph.D.
Associate Professor

To my parents and husband,

for their never-ending patience, support, and love.

TABLE OF CONTENTS

List of Figures

Chapter 1: Introduction

Chapter 2: Common Materials and Methods

Chapter 3: Development of Label-free Imaging Techniques for the Quantification of Volume, Mass, and Density of Thrombus Formation

Chapter 4: Development of a Method to Quantify Platelet Adhesion and Aggregation under Static Conditions

Chapter 5: Assessment of Neonatal Platelet Adhesion, Activation, and Aggregation

Chapter 6: Role of Coagulation in the Recruitment of Colon Adenocarcinoma Cells to Thrombus under Shear

Chapter 7: Conclusions and Future Directions

List of Tables and Equations

Tables

Equations

List of Abbreviations

ACT	activated clotting time
ADP	adenosine diphosphate
APC	activated protein C
aPTT	activated partial thromboplastin time
AT	antithrombin
ATP	adenosine triphosphate
BSA	bovine serum albumin
CAM	chorioallantoic membrane
CLEC-2	C-type lectin receptor-2
CMAC	7-amino-4-chloromethylcoumarin
CMTMR	5-(and-6)-(((4-chloromethyl)benzoyl)amino)tetramethylrhodamine
CRP	collagen-related peptide
CTI	corn trypsin inhibitor
DAPI	4',6-diamidino-2-phenylindole
DIC	differential interference contrast
DMEM	Dulbecco's Modified Eagle Medium
DMSO	dimethyl sulfoxide
DNA	deoxyribonucleic acid
EC	endothelial cell
ECM	extracellular matrix
ELISA	enzyme-linked immunosorbent assay
EPCR	endothelial protein C receptor

FACS	fluorescence-activated cell sorting
FBS	fetal bovine serum
FcRγ	Fc receptor γ
FG	fibrinogen
FITC	fluorescein isothiocyanate
FII	coagulation factor II, prothrombin
FIIa	activated coagulation factor II, thrombin
FIX(a)	(activated) coagulation factor IX
FV(a)	(activated) coagulation factor V
FVII(a)	(activated) coagulation factor VII
FVIII(a)	(activated) coagulation factor VIII
FX(a)	(activated) coagulation factor X
FXI(a)	(activated) coagulation factor XI
FXII(a)	(activated) coagulation factor XII
FXIII(a)	(activated) coagulation factor XIII
Gla	glutamic acid
GP	glycoprotein
GPCR	G protein-coupled receptor
GPIb	glycoprotein Ib or CD42b
GPIIb/IIIa	glycoprotein IIb/IIIa or integrin $\alpha_{IIb}\beta_3$
HTDIC	Hilbert transform differential interference contrast
IPA	impedance platelet aggregometry
IR	infrared

ITAM	immunoreceptor tyrosine-based activation motif
LTA	light transmission aggregometry
NA	numerical aperture
NaCit	sodium citrate
NIQPM	non-interferometric quantitative phase microscopy
OCT	optimal cutting temperature
PAR	protease-activated receptor
PBS	phosphate buffered saline
PDMS	polydimethylsiloxane
PE	phycoerythrin
PECAM-1	platelet endothelial cell adhesion molecule 1 or CD31
PFA	paraformaldehyde
PFA-100	platelet function analyzer-100
PLA	polylactic acid
PLC	phospholipase C
PMMA	polymethylmethacrylate
PMN	polymorphonuclear leukocyte
PMT	photomultiplier tube
PPACK	D-phenylalanyl-L-prolyl-L-arginine chloromethyl ketone
PR	photoresist
PS	phosphatidylserine
PT	prothrombin time
RBC	red blood cell

ROI	region of interest
SEM	standard error of the mean
SM	scanning mirrors
TEG	thromboelastography
TF	tissue factor
TFPI	tissue factor pathway inhibitor
TRAP-6	thrombin receptor activator 6
TT	thrombin time
TxA_2	thromboxane A_2
VE	vascular endothelial
VWF	von Willebrand factor
v/v	volume/volume
WBC	white blood cell
w/v	weight/volume
α_{IIb}	CD41 or glycoprotein IIb
β_3	CD61

Acknowledgements

First, I would like to express my sincere gratitude to my dissertation advisor, Dr. Owen McCarty. His immense knowledge, patience, motivation, and guidance has helped me throughout my graduate education and to grow as a scientist and engineer. I could not have imagined having a better advisor and mentor for my Ph.D. study. It has been an exciting and rewarding four years working in his laboratory, and I look forward to seeing its future growth and successes.

In addition to my advisor, I would like to thank my dissertation committee members, Dr. Monica Hinds, Dr. Michael Recht, Dr. Xiaolin Nan, and Dr. Jason Taylor, for their insightful comments, support, and careful assessment of my work. Dr. Monica Hinds' invaluable insight and encouragement have been a great help to my research, and I am very grateful at her willingness to serve as chair of my dissertation defense committee. The translational research project with Dr. Michael Recht has taught me about successful collaborations and has had a significant impact on my future career path. I am exceedingly thankful for Dr. Michael Recht and Dr. Jason Taylor's important and instrumental clinical perspective for my dissertation. I want to thank Dr. Xiaolin Nan for his perceptive questions and comments, and I am immensely thankful for his participation in my dissertation defense committee.

I am grateful to Dr. Xavier Trepat for welcoming me into his laboratory at the Institute for Bioengineering of Catalonia. I enjoyed working closely with Dr. Dobryna Zalvidea, and I want to thank her for teaching me about photonics and microscopy and letting me

work with her expensive lasers. I was fortunate to have worked with Arlyng González and Natalia Castro, who helped with not only my research, but my Spanish as well.

I had the privilege of working with a phenomenal group of scientists in the McCarty laboratory. I am immensely grateful to Kevin Phillips, Joseph Aslan, Kristina Haley, Cristina Puy Garcia, Jiaqing Pang, Garth Tormoen, Flor Cianchetti, Asako Itakura, Jevgenia Zilberman-Rudenko, Rachel Rigg, Laura Healy, Kate Garland, and Annachiara Mitrugno for their insightful advice and encouragement in research, writing, and graduate school and for being an incredible group of co-workers and friends. I want to thank the ever hardworking interns, Chantal Wiesenekker, Kathleen Rees, Zoë Wong, Juliana Porter, Branden Kusanto, Cassandra Loren, and Ishan Patel, who have been wonderful additions to our lab. Additionally, I want to thank everyone on the 13th floor for their technical assistance and blood donations.

I could not have done this without the continuous support, love, and encouragement from my family and friends. I am especially grateful to my parents, Dan and Julie, for always being there for me and for motivating me throughout my graduate education. And lastly, I would like to extend my deepest thanks to my husband and best friend, Thiago, whose faithful patience and support is ever appreciated.

Abstract

Metrological techniques to study primary and secondary hemostasis

Sandra M. Baker

Department of Biomedical Engineering
School of Medicine
Oregon Health & Science University

October 2015
Dissertation Advisor: Owen J. T. McCarty, Ph.D.

Hemostasis is the physiological process of cessation of bleeding at sites of vascular injury. Primary hemostasis consists of the recruitment of blood platelets and the formation of platelet aggregates at the site of vessel damage. Secondary hemostasis occurs with activation of blood plasma coagulation proteins to generate insoluble fibrin around platelet aggregates to form a thrombus. Similar mechanisms of action can lead to the activation of platelets and the coagulation cascade in diseased blood vessels, resulting in pathological thrombus formation, while the failure to fully activate these pathways can lead to bleeding complications. Thus, there is a need for accurate, reproducible measurement systems for monitoring platelet function and coagulation, detecting disease states, and evaluating efficacy of novel antithrombotic therapeutics. This dissertation centers on the development of metrological techniques to study the mechanisms of thrombosis and hemostasis.

Common microscopy techniques are useful for mechanistic studies but are limited when quantitatively evaluating physical features of biological specimens. Here we present the

development and utilization of label-free imaging techniques to investigate the physical parameters (e.g., volume and mass) of platelet aggregates and thrombi formed in response to exposure to combinations of procoagulant agonists under shear flow conditions. These techniques revealed that coagulation restricts platelet aggregate growth at high physiologic shear rates and the formation of fibrin significantly increases clot density while thrombus volume remains constant.

Accurate assessment of platelet function is critical for identifying platelet function disorders and measuring the effect of antiplatelet therapies. This dissertation presents the development of an assay that utilizes the biophysical property of platelet concentration, in conjunction with label-free, quantitative imaging techniques to assess platelet function under static conditions. The utility of this technique to evaluate antiplatelet therapies was demonstrated by the inhibition of glycoprotein (GP) IIb/IIIa abrogating platelet aggregation and significantly reducing sample volume and mass at high platelet concentrations on collagen-coated surfaces.

The developing hemostatic system in neonates is functionally distinct from adults. However, blood volume limitations have hindered the evaluation of platelet function in neonates. Here we describe the development of four small volume, whole blood, platelet function assays for assessing neonatal platelet adhesion, activation, and aggregation under static and fluid shear conditions. With these assays, we show that neonatal platelets activate to a lesser degree relative to adult platelets, GPIIb/IIIa mediates neonatal platelet

adhesion and aggregation on collagen surfaces under fluid shear, and neonatal platelets adhere to collagen in a von Willebrand factor-dependent manner.

Thrombotic events are highly associated with cancer and metastasis; however, the role of coagulation in facilitating metastasis is ill-defined. This dissertation presents the development of a technique that evaluates cancer cell interactions with platelet aggregates and thrombi under fluid shear conditions. Utilization of this technique revealed that coagulation and fibrin formation promotes metastatic colon adenocarcinoma cell adhesion and arrest to thrombi, and demonstrated that the presence of polymorphonuclear leukocytes enhanced cancer cell-thrombi interactions.

Collectively, this dissertation presents the development of novel measurement systems to study the pathways that contribute to thrombosis and hemostasis.

Chapter 1: Introduction

1.1 Overview of Hemostasis and Relation to Disease

Maintenance of the highly regulated human hemostatic system is dependent on the delicate balance of the pro- and anticoagulant systems of primary and secondary hemostasis and fibrinolysis. Upon vessel wall damage, the process of primary hemostasis is immediately activated to recruit platelets and form platelet aggregates. Secondary hemostasis is initiated with the activation of the coagulation cascade to generate fibrin around the platelet aggregates, forming a thrombus, or hemostatic plug. Simultaneously, the process of fibrinolysis is activated to restrict clot size and prevent the formation of pathologic thrombi. Effective hemostasis requires a sufficient amount of functional platelets, coagulation factors, and fibrinolytic proteins and adequately responsive blood vasculature.

Hemostatic and thrombotic complications are associated with various pathological states, including cardiovascular disease, which is the leading cause of death in the United States (Mozaffarian *et al.* 2015). In the year 2011 alone, cardiovascular disease, which includes heart failure, coronary heart disease, and stroke, was responsible for 787,000 deaths in the United States, with prevention and treatment of this disease costing more than $320.1 billion (Mozaffarian *et al.* 2015). These staggering statistics indicate that there is a clear need for a deeper understanding of pathways that underlie thrombosis and hemostasis. The development of new techniques to assess the activation of platelets and the coagulation cascade in normal and pathological states may aid in revealing mechanisms associated with cardiovascular disease and the development of novel therapeutics. This

chapter will discuss the process of primary and secondary hemostasis, the role of platelets and coagulation pathways in disease, and currently available measurement systems for studying hemostasis.

1.2 Blood and Vascular Cell Physiology

Blood is primarily composed of blood cells suspended in an aqueous solution of plasma, which contains water, plasma proteins, dissolved nutrients, and waste products. Blood cells, consisting of red blood cells (RBCs), white blood cells (WBCs), and platelets, and the vascular endothelial cells (ECs) lining the blood vessel wall intricately work together in the dynamic shear environment of blood circulation to maintain hemostasis.

1.2.1 Red blood cells

As the most abundant cell type in the blood, RBCs comprise approximately 99% of all blood cells at a concentration of 4.7 – 6.1 million cells/μL in humans (Dzierzak and Philipsen 2013). RBCs play a critical role transporting oxygen from the lungs to other tissues in the body via the circulatory system. Human RBCs are anucleated cells that possess a biconcave disk shape with a diameter of 5.5 – 8.8 μm and a thickness of 2 μm at the periphery and 1 μm at the narrowest point (center) (Aarts *et al.* 1983). Some of the most important physical features of RBCs are their high elasticity and deformability, which allows them to circulate through the reticuloendothelial system and capillaries as small as 3 μm in diameter. During transit through blood vessels, RBCs contribute to hemostasis by concentrating in the center of vessels, forcing the smaller platelets to the vessel walls for continually assessing vascular integrity (Woldhuis *et al.* 1992).

1.2.2 White blood cells

WBCs, or leukocytes, make up about 1% of total blood cells and play an important role in the human immune system. The main types of WBCs are granulocytes, monocytes, and lymphocytes. Granulocytes contain δ-granules in their cytoplasm and are classified into three types: neutrophils, eosinophils, and basophils, which circulate the blood at 5×10^9, 4×10^7, and 4×10^7 cells/L, respectively (Fulkerson and Rothenberg 2013; Mócsai 2013). Human neutrophils are the most common type of granulocytes and play a key role in host innate immunity against bacterial infection. WBCs can express molecules, such as tissue factor (TF), which can influence hemostasis (Ahn *et al.* 2005).

1.2.3 Platelets

Platelets are discoid, anucleate blood cells critical to the process of primary hemostasis. Platelets are the smallest cells in the blood, with a diameter of 2 to 4 μm, a thickness of 70 – 90 Å, and a density of 1.04 – 1.08 g/mL (Polanowska-Grabowska, Raha and Gear 1992). Platelets are formed via fragmentation of magakaryocyte cytoplasm in the bone marrow and circulate the vasculature at a concentration of 150 – 350 billion cells/L for about 5 – 9 days in humans (Daly 2011). Platelets are anuclear but possess other common cellular structures, such as mitochondria, Golgi, lysosomes, α- and δ-granules, and microtubules. Platelets contain an open canalicular system, which is a dense tubular system that plays an important role in rapidly transporting platelet releasate, including agonists, into and out of the cell. During normal physiological blood flow, platelets typically remain in a quiescent, inactive state and only activate in response to blood vessel damage.

1.2.4 Endothelial cells

The luminal surface of blood vessels is lined with a confluent monolayer of ECs. ECs incorporate biochemical and physical signals to control leukocyte adhesion and platelet adhesion and activation (Granger *et al.* 2010). ECs locally mediate these processes through membrane-bound factors, such as TF, thrombomodulin, and E-selectin, as well as secreted factors, such as nitric oxide and prostacyclin (Cines *et al.* 1998). During normal, laminar blood flow, ECs produce factors that maintain quiescence of platelets and inhibit leukocyte adhesion. However, vessel wall damage results in ECs expressing and secreting molecules, such as TF and von Willebrand factor (VWF), that promote primary and secondary hemostasis (Camerer, Kolstø and Prydz 1996).

1.2.5 Hemorheology

The dynamic process of blood circulation is governed by the rheological properties of blood cells, plasma, and the vasculature. Hemorheology, which is the science of flow and deformation of blood through vessels, is dependent on blood viscosity, hematocrit, protein concentration, RBC deformability, wall shear stress, shear rate, and the geometry of blood vessels (Marossy *et al.* 2009). Wall shear stress is the frictional shear force exerted on vessel walls by flowing blood. Under normal physiological conditions, wall shear stresses of flowing blood ranges from 15 to 70 dynes/cm^2 in large straight arteries and from 1 to 6 dynes/cm^2 in veins (Kroll *et al.* 1996). Shear rate, which is the ratio of blood velocity to vessel diameter, ranges from 100 – 2,000 s^{-1} in large arteries, from 30 – 160 s^{-1} in veins, and from 400 – 1,600 s^{-1} in arterioles and capillaries, respectively (Yang 1989; Lipowsky 2005; Papaioannou and Stefanadis 2005). However, disease states can

alter the shear stresses in vessels, resulting in changes of EC morphology, induction of an inflammatory response, and increased expression of cell adhesion molecules (Li, Haga and Chien 2005; White and Frangos 2007). Quantitative understanding of blood flow dynamics and hemorheology will aid in improving designs of implants (e.g., heart valves, artificial hearts) and flow devices (e.g., dialysis machines, blood oxygenators), developing drugs and drug delivery vehicles, and elucidating the complex interplay between fluid flow characteristics and cardiovascular diseases (Popel and Johnson 2005; Cho and Cho 2011).

1.3 Primary Hemostasis

1.3.1 Mechanism of platelet adhesion

At sites of vascular injury, primary hemostasis is initiated when platelets adhere to the site via interactions with VWF and extracellular matrix (ECM) proteins. VWF is a large, multimeric blood glycoprotein produced by ECs. When vessels are damaged, ECM collagens are exposed to the blood, resulting in plasma VWF recruitment to the site. In the flowing blood vessel, platelets transiently interact with and tether to the bound VWF via the platelet glycoprotein (GP) Ibα (CD42b) (Figure 1.1). GPIbα is present on the platelet surface in complex with the transmembrane polypeptides GPIbβ, GPIX, and GPV to form the GPIb/IX/V complex (Sakariassen *et al.* 1986). Platelet tethering to VWF slows down flowing platelets enough to allow for stable adhesion interactions with the ECM primarily through integrin interactions. Integrins are heterodimeric complexes of α and β subunits that function in cell adhesion to other cells or proteins. Platelets are

stabilized to the injury site by binding to collagen and VWF via GPVI (Moroi *et al.* 1989) and integrin $\alpha_2\beta_1$ (Santoro 1986) (Figure 1.1).

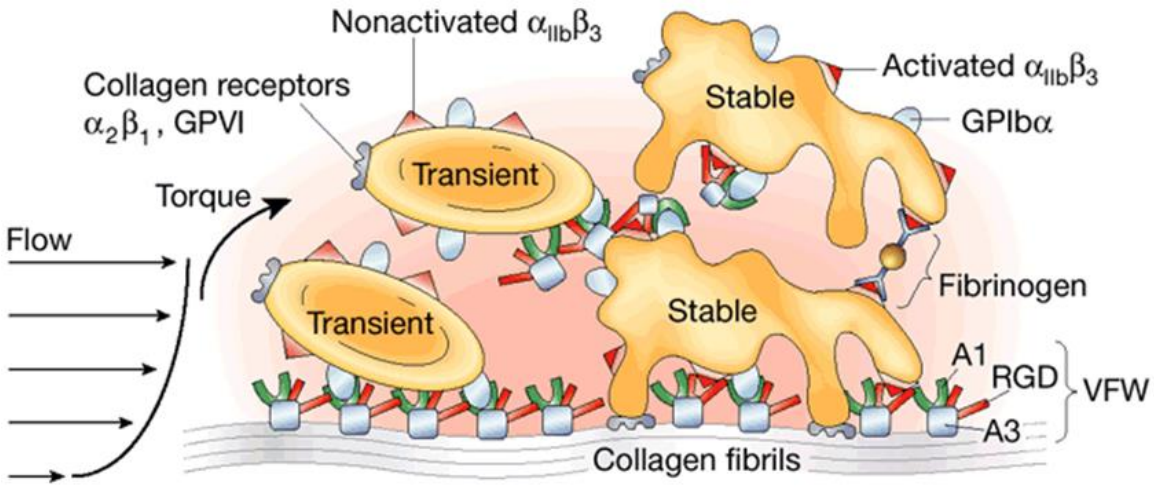

Figure 1.1 Platelet adhesion and aggregation under fluid shear. Upon vessel injury, VWF binds to exposed collagens in the ECM and platelets tether to and transiently interact with VWF via GPIb. Stable adhesion occurs when GPVI and $\alpha_2\beta_1$ interact with collagen at the site of injury. Figure reprinted with permission from ©Ruggeri, 2002, originally published in *Nature Medicine* (Ruggeri 2002).

1.3.2 Platelet activation and aggregation

Following platelet adhesion to the site of vessel injury, intracellular signaling results in platelet calcium mobilization, cytoskeletal reorganization, activation, and spreading. Initial GPIbα-VWF interactions induces weak intracellular signaling in platelets that leads to integrin activation (Du 2007). Platelet spreading is primarily mediated by integrin $\alpha_{IIb}\beta_3$ (GPIIb/IIIa; CD41/CD61) and is thought to be important for platelets withstanding the shear forces from blood flow (Weiss 1991). Moreover, platelets become activated via agonists thrombin and collagen that are present at the site of vessel injury. Thrombin binds GPIb and also cleaves the protease-activated receptors (PARs)-1 and -4

on the platelet surface. PAR-1/4 are part of the G protein-coupled receptor (GPCR) family that activate intracellular signaling pathways. PAR-1/4 initiate intracellular signaling through phospholipase C (PLC)-β to result in calcium mobilization and ultimately conversion of GPIIb/IIIa to its active state (Figure 1.2). PAR-1 is activated at low thrombin concentrations, while PAR-4 mediates activation at high thrombin concentrations (Leger *et al.* 2006).

Collagen induces intracellular signaling via interactions with the platelet immunoglobulin GPVI, which is part of the immunoreceptor tyrosine-based activation motif (ITAM)-coupled receptor family (Bergmeier and Stefanini 2013). The deeper layers of the ECM contain collagens type I, III, and V, while the upper layers primarily consist of type IV collagen, which has lower platelet activating activity than other collagens but is important in GPVI-dependent platelet activation in primary hemostasis (Jung *et al.* 2008). GPVI contains a short cytoplasmic tail that facilitates the association with the ITAM-containing Fc receptor γ (FcRγ) chain to initiate downstream signaling events through PLC-γ to mobilize calcium and ultimately activate GPIIb/IIIa (Watson *et al.* 2005; Boulaftali *et al.* 2014) (Figure 1.2).

A second wave of platelet activation occurs when proaggregatory compounds are released from platelet α- and δ-granules. Adult platelets contain 3 to 8 δ-granules per platelet that hold serotonin, polyphosphates, calcium, adenosine 5'-diphosphate (ADP), and adenosine triphosphate (ATP) (McNicol and Israels 1999). Upon initial platelet activation, ADP is released, which then binds to platelet GPCRs $P2Y_1$ and $P2Y_{12}$ for

second wave platelet activation. $P2Y_1$ is a G_q-coupled receptor and $P2Y_{12}$ is a G_i-coupled receptor and both receptors mediate activation of PLC-β in platelets (Offermanns 2006) (Figure 1.2). ADP-induced activation of platelets has a strong effect on activation of GPIIb/IIIa but only a minor effect on release of α- and δ-granule content (Cattaneo 2011). Platelets also contain 50 to 80 α-granules per platelet, which hold fibrinogen (FG), VWF, and coagulation factors V (FV) and VIII (FVIII) (Blair and Flaumenhaft 2009). The membranes of platelet α-granules contain GPIIb/IIIa and CD62P (P-selectin), which is the main receptor that binds leukocytes, and upon platelet activation, CD62P and GPIIb/IIIa are exposed on the platelet surface (Blair and Flaumenhaft 2009).

Thromboxane A_2 (TxA_2) synthesis and release from platelets contributes to the secondary wave of platelet activation. TxA_2 is generated when arachidonate is metabolized into TxA_2 by cyclooxygenase. Released TxA_2 binds to the TxA_2 receptors, which are G_q- and $G_{12/13}$-coupled, to further augment platelet activation (Stegner and Nieswandt 2011) (Figure 1.2). However, the half-life of TxA_2 in aqueous solutions is very short, limiting its duration of activation and impact. This has led to researchers using a stable TxA_2 analogue, such as U46619, when studying TxA_2-induced platelet activation (Gresele *et al.* 2012).

Platelet activation converts the GPIIb/IIIa complex into its high affinity state, which can bind to FG, VWF, and fibronectin (Kühne and Imbach 1998). Platelet aggregation occurs when FG and/or VWF binds GPIIb/IIIa and cross-links nearby activated platelets to form a platelet plug at the site of injury. GPIIb/IIIa is a calcium-dependent heterodimer

comprising of the type I transmembrane proteins GPIIb and GPIIIa (Xiao *et al.* 2004). The intracellular tail of the GPIIb/IIIa complex transmits signals bidirectionally either into the platelet cytoplasm after ligand binding, or from the cytosol to the GPIIb/IIIa extracellular domain (Gresele *et al.* 2012).

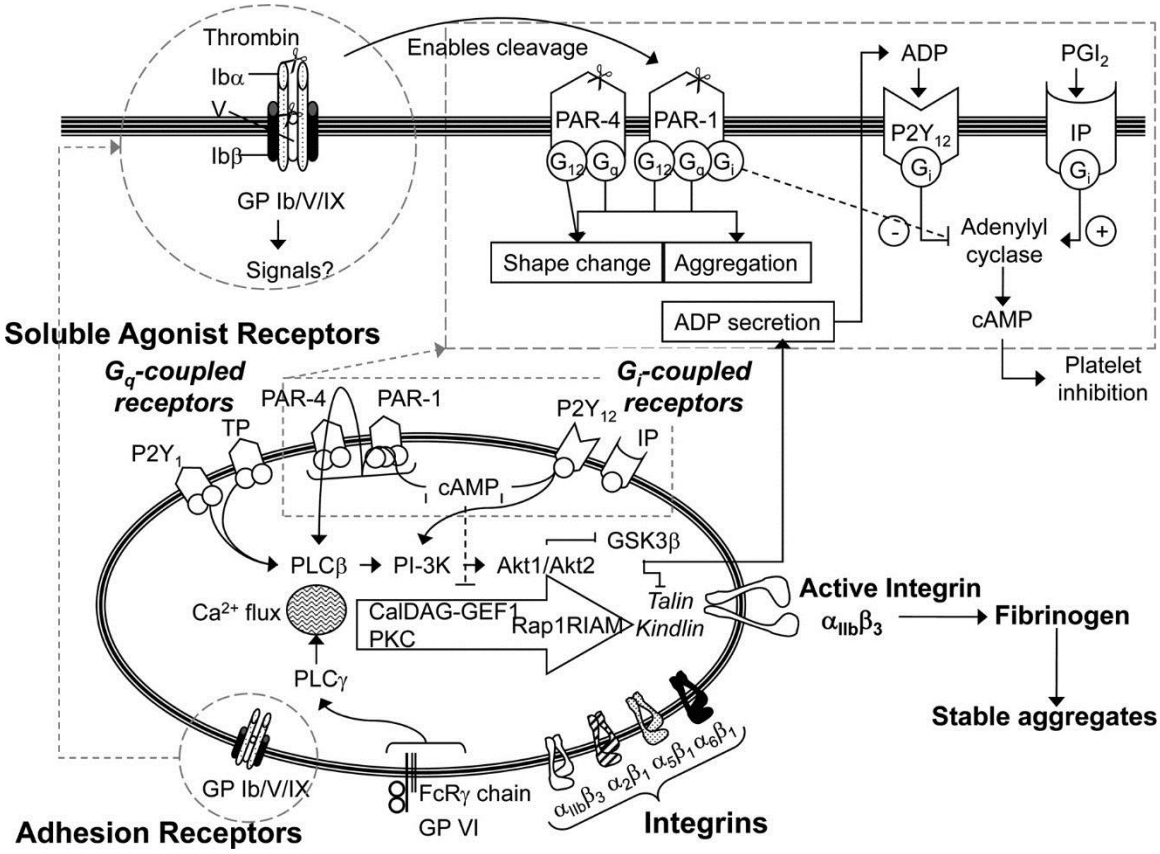

Figure 1.2 Platelet activation and aggregation. Platelets initially become activated from collagen, VWF, and thrombin interactions via GPVI, GPIb, and PAR-1/4 at the site of vessel injury. Release of ADP and TxA_2 from platelets results in a second wave of platelet activation. Conversion of GPIIb/IIIa ($\alpha_{IIb}\beta_3$) to its high affinity state allows for binding to fibrinogen to from platelet aggregates. Figure reprinted with permission from ©Smyth *et. al*., 2009, originally published in *Arteriosclerosis, Thrombosis, and Vascular Biology* (Smyth *et al.* 2009).

Agonist-induced platelet activation results in increased intracellular calcium mobilization (Figure 1.2). Cytosolic calcium disrupts the distribution of phopholipids in the platelet

outer membrane, promoting exposure of lipid phosphatidlyserine on the platelet surface (Keuren *et al.* 2005). The exposed negatively charged phosphatidylserine facilitates the assembly and activation of coagulation factors.

1.3.3 Dysfunction of primary hemostasis

Platelets are primarily associated with regulating primary hemostasis, but they also play a significant role in the pathophysiology of certain diseases. Dysfunction of platelet adhesion, activation, and/or aggregation is associated with von Willebrand disease, thrombocytopenia, and platelet function disorders. Von Willebrand disease is the most common inherited bleeding disorder and is classified into six different types: type 1, which is a partial deficiency of VWF; types 2A, 2B, 2M, and 2N are dysfunction of VWF; and type 3 is the total absence of VWF (Bowman *et al.* 2010). Thrombocytopenia is associated with a dramatic drop in platelet count below 50,000 cells/μL, which results in an impaired ability of patients to form adequate platelet aggregates (van Ommen and Peters 2012).

Platelet function disorders can be acquired or inherited, with a higher prevalence of platelet disorders being acquired. Often medication, such as aspirin, nonsteroidal anti-inflammatory drugs, and antibiotics, can result in acquired platelet dysfunction (Litalien and Jacqz-Aigrain 2001), but an underlying disease like liver failure, cancer metastasis, or cardiovascular disease can also result in dysfunction of primary hemostasis (Boccardo, Remuzzi and Galbusera 2004; Sharma and Berger 2011). Common inherited platelet disorders include defective or a deficiency of platelet GPIIb/IIIa (Glanzmann's

thrombasthenia), a defect in one of the components of the GPIb/IX/V complex (Bernard-Soulier Syndrome), and storage pool deficiency, which is a deficiency in platelet secretion granules (van Ommen and Peters 2012).

1.3.4 Common methodologies to study primary hemostasis

Platelet activation is most commonly assessed with the enzyme-linked immunosorbent assay (ELISA), gel electrophoresis and Western blotting, or flow cytometry. The use of ELISA for evaluating platelet function typically consists of the incubation of platelets with antibodies against platelet activation markers in the presence of agonists, and the degree of antibody binding is measured with a specialized ELISA plate reader. ELISAs have recently been modified to be high-throughput, fast techniques for assessing platelet function (Salles *et al.* 2010; Zhang *et al.* 2010), but they have yet to be widely incorporated into general clinics. Western blotting is a well characterized assay that has been extensively employed in platelet research to measure protein content in activated platelets. Nonetheless, gel electrophoresis and Western blotting requires large amounts of blood and translation of the technique into a diagnostic assay is complex, therefore this assay is typically not readily available for clinical applications (Zhang *et al.* 2010). Flow cytometry is a convenient and highly specific technique that can measure single-cell marker expression, as well as evaluate platelet aggregation in response to agonist stimulation (Michelson 1996). Recently, flow cytometry has become more commonplace in clinical laboratories, thus the development of assays that utilize this technology will be useful in studying primary hemostasis.

Platelet aggregation is traditionally evaluated with light transmission aggregometry (LTA), where the increase in light transmission through a suspension of platelets is measured after stimulation with an agonist (Harrison *et al.* 2011). Although LTA is a common technique used in the clinic, the test cannot be performed with whole blood, accuracy and reproducibility are very poor, and for samples from patients with thrombocytopenia, results are difficult to interpret (Ghoshal *et al.* 2014). Alternatively, impedance platelet aggregometry (IPA) utilizes anticoagulated whole blood stimulated with an agonist and measures the electrical impedance to assess platelet aggregation (Cardinal and Flower 1980). However, IPA is relatively new and still requires standardization for use in a clinical setting.

The bleeding time was the first test to assess primary hemostasis *in vivo*, which was performed by stabbing the patient with a lancet on the forearm and measuring the time until cessation of bleeding (Ivy, Nelson and Bucher 1941; Duke 1983). However, the inaccuracy, invasiveness, and lack of specificity with the bleeding time has made it unpopular, resulting in the development of devices that measure *in vitro* bleeding times. The most common whole blood, bleeding time device is the platelet function analyzer-100 (PFA-100). The PFA-100 utilizes only about 1 mL of citrated whole blood that is passed through a membrane coated with collagen and ADP or epinephrine and the time to occlusion (closure time) is measured (Kundu *et al.* 1995). The PFA-100 is widely used in clinical laboratories because it is a rapid technique that is easy to perform, however, it is not without limitations. It is highly sensitive for type 3 von Willebrand disease and the

more severe platelet defects, but it is insensitive for mild disorders, such as mild type 1 von Willebrand disease and storage pool deficiency (van Ommen and Peters 2012).

1.4 Secondary Hemostasis

1.4.1 Initiation phase of coagulation

Secondary hemostasis is initiated with the activation of the coagulation cascade to ultimately convert platelet-bound FG into a cross-linked fibrin meshwork that solidifies around platelet aggregates to form a thrombus. The coagulation cascade is a series of reactions in which coagulation factor zymogens circulating in the blood and glycoprotein cofactors are proteolytically activated to their serine protease forms. Coagulation is initiated at sites of vascular damage when subendothelial tissue factor (TF) is exposed to the blood. TF binds the coagulation factor VII (FVII) and acts as a cofactor to promote activation of FVII to activated FVII (FVIIa). It is thought that the miniscule amount of FVIIa that circulates in the blood plays a proteolytic role in the cleavage of FVII into FVIIa (Neuenschwander, Fiore and Morrissey 1993). Subsequently, the TF/FVIIa complex is capable of proteolytically activating small amounts of coagulation factor IX (FIX) into active FIX (FIXa) and factor X (FX) into active FX (FXa). FXa forms a prothrombinase complex with cofactor Va (FVa) on the subendothelium, which then converts prothrombin (factor II; FII) into thrombin (factor IIa; FIIa) (Monroe and Hoffman 2006) (Figure 1.3).

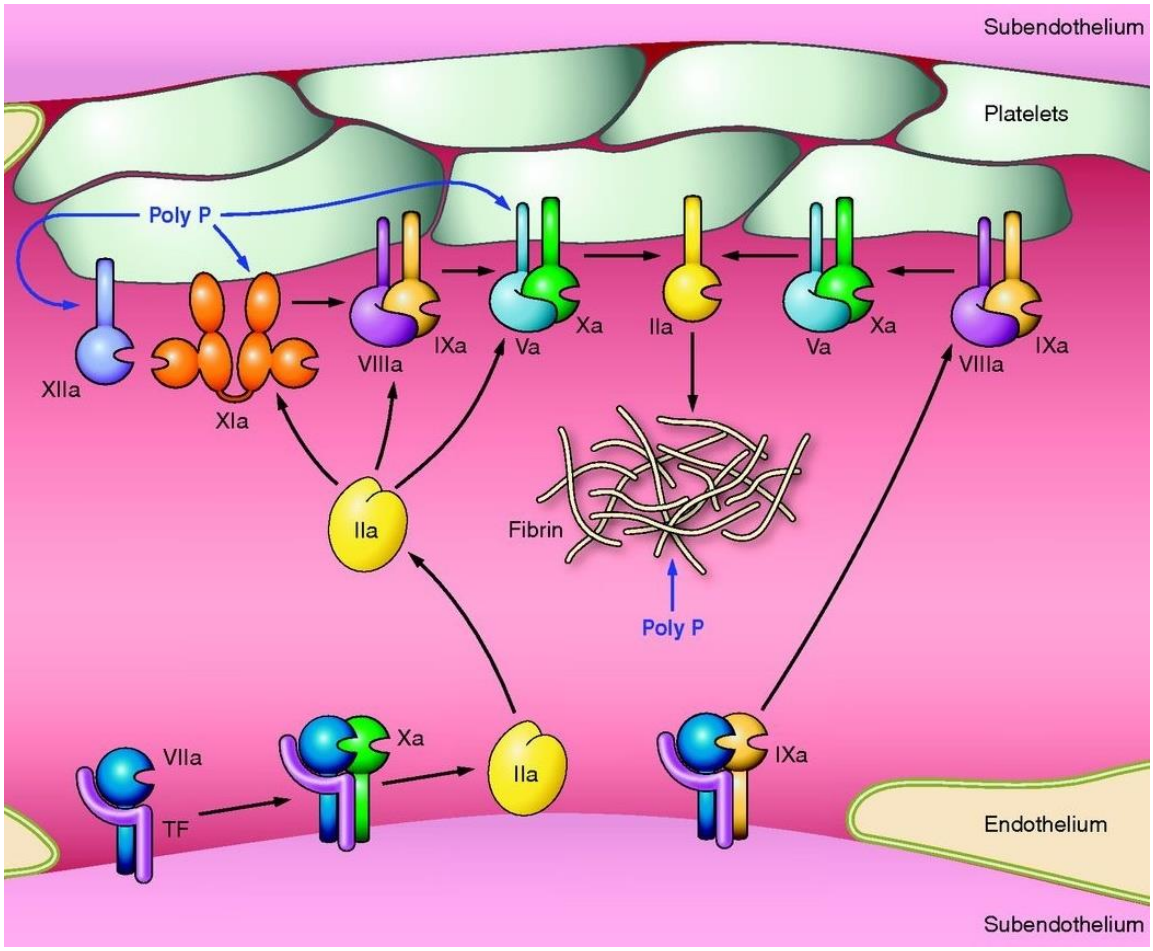

Figure 1.3 Coagulation cascade. Coagulation is initiated at sites of vascular injury when TF in the subendothelium is exposed to the blood and forms a complex with FVII, which is then activated to FVIIa. This complex activates FX to generate thrombin (FIIa). Thrombin activates FXI, FVIII, and FV to generate additional thrombin. Thrombin converts fibrinogen into fibrin around the platelet aggregates to form a thrombus. Simultaneously, polyphosphates (Poly P) released from platelets inhibit lysis of the thrombus and activate FXII, FV, and FXI. Figure adapted from ©Versteeg *et. al*., 2013, originally published in *Physiological Reviews* (Versteeg *et al.* 2013).

1.4.2 Amplification phase of coagulation

The amplification phase of coagulation consists of the slow accumulation of generated thrombin (Versteeg *et al.* 2013). In this phase, thrombin activates adhered platelets via PAR-1 and PAR-4, as previously described in section 1.3.2. Concurrently, thrombin converts coagulation factor XI (FXI) into activated FXI (FXIa) and converts FV that is

released from activated platelets into FVa to amplify the activity of prothrombinase complexes. Thrombin also converts FVIII into activated FVIII (FVIIIa), which in turn will bind to FIXa on the platelet surface and act as a cofactor for the conversion of FX into FXa (Figure 1.3).

1.4.3 Propagation phase of coagulation

The negatively charged phosphatidylserine exposed on the surface of activated platelets provides the platform for the propagation phase of coagulation. This phase consists of FXIa converting FIX into FIXa, which then forms the tenase complex with FVIII (Figure 1.3). Subsequently, the tenase complex activates FX and the FXa/FVa complex then produces enough thrombin to cleave the platelet-bound FG into insoluble fibrin chains around platelet aggregates. Thrombin binds to the Aα and Bβ polypeptide chains of FG to cleave and release the fibrinopeptides A and B to expose fibrin polymerization sites and initiate fibrin assembly (Crawley *et al.* 2007). Coagulation factor XIII (FXIII) is also activated by thrombin to form activated FXIII (FXIIIa), which then cross-links the formed fibrin chains into an insoluble, polymerized fibrin meshwork to form a thrombus (Ariëns *et al.* 2002).

Prothrombin, FVII, FIX, and FX are vitamin K-dependent coagulation factors that interact with phospholipid membranes (i.e., the activated platelet surface) via their amino-terminal domains that contain γ-carboxyglutamic acid (Dahlbäck 2000). Vitamin K acts as a cofactor in the post-translational carboxylation of 9-12 glutamic acid (Gla) residues of the amino-terminal domain (Gla domain) to γ-carboxyglutamate residues to

allow calcium binding and activation of the coagulation factors (van Herrewegen *et al.* 2012).

1.4.4 Intrinsic coagulation pathway

The intrinsic pathway of coagulation is activated to form thrombi without the aid of any external factors, such as TF. This pathway is thought to occur in parallel with TF-initiated coagulation (extrinsic pathway of coagulation) to aid in the amplification of thrombin generation. Activation of coagulation factors XII (FXII) and FXI has been found to be initiated by neutrophil extracellular traps (von Brühl *et al.* 2012; Itakura and McCarty 2013), collagen (van der Meijden *et al.* 2009), and polyphosphates (Renné and Gailani 2007; Puy *et al.* 2013). Polyphosphates produced by activated platelets bind to and activate FXII (FXIIa) and act as a cofactor for thrombin activation of FXI and FV (Choi, Smith and Morrissey 2011) (Figure 1.3). Activation of FXII cleaves plasma prekallikrein into kallikrein, resulting in subsequent activation of FXI, FIX, FX, and prothrombin (Müller *et al.* 2009). The activation of FXII by polyphosphates is thought to aid in fibrin clot stability (Ratnoff and Colopy 1955; Pauer *et al.* 2004) by acting to inhibit clot fibrinolysis (Smith *et al.* 2010).

1.4.5 Inhibition of secondary hemostasis

During secondary hemostasis, negative control proteins work to regulate thrombin generation and to prevent uncontrolled thrombus growth. The protease inhibitors antithrombin (AT), tissue factor pathway inhibitor (TFPI), heparin cofactor II, and C1 inhibitor circulate the blood and inactivate activated coagulation factors via binding to the

active site. TFPI is a Kunitz-type protease inhibitor present on the surface of endothelial cells, in platelets, and circulating in the plasma, and inhibits free FXa and transient TF/FVIIa/FXa complexes (Broze and Girard 2012). AT is a serine protease inhibitor and directly inhibits FIXa, FXa, and thrombin (Versteeg *et al.* 2013). Activated protein C (APC) in complex with protein S inactivates FVIIIa and FVa to diminish the prothrombotic actions of the tenase and prothrombinase complexes (Dahlback and Villoutreix 2005). APC is generated when thrombin binds thrombomodulin, which is expressed on endothelial cells, and thrombin proteolytically cleaves protein C into APC bound to endothelial protein C receptors (EPCRs) (Koutsi, Papapanagiotou and Papavassiliou 2008).

1.4.6 Secondary hemostasis dysfunction and thrombosis

Disorders involving the coagulation cascade are either inherited or acquired and can result in bleeding tendencies and/or thrombotic complications. The most common inherited coagulation disorders are hemophilia A and B, which results from deficiency of coagulation factors VIII (FVIII) and IX (FIX), and often manifests as muscle or joint hemorrhages (van Herrewegen *et al.* 2012). Hemophilia C, which is FXI deficiency, is a rare condition but bleeding tendency varies widely and is often unpredictable due to the FXI level not necessarily correlating with severity of bleeding (Rosenthal, Dreskin and Rosenthal 1953). Other rare congenital coagulation factor deficiencies that often result in bleeding are deficiencies in FV, FVII, FX, thrombin, or prothrombin (Bolton-Maggs *et al.* 2004). FXII deficiency is the most common factor deficiency; however, patients deficient in FXII often do not present any bleeding tendency (Lammle *et al.* 1991).

Acquired coagulation disorders are more common than inherited disorders and are often associated with disease or the use of pharmacological agents. Disseminated intravascular coagulation, which can result from disruption of the APC system due to diseases, such as sepsis, inflammation, cancer, trauma, or liver disease, is systemic activation of coagulation resulting in the widespread formation of microthrombi in blood vessels, reduced plasma levels of coagulation factors, and subsequent bleeding (Wada, Matsumoto and Yamashita 2014). Vitamin K deficiency is a common bleeding disorder in children with gastrointestinal disease (Sutor 1995) and results in reduced calcium binding of the γ-carboxyglutamic acid domains of coagulation factors and the loss of ability to bind to phospholipid membranes (Furie and Furie 1992). Liver disease is commonly associated with bleeding complications due to the inability of damaged parenchymal cells to synthesize coagulation factors, leading to factor deficiency (Mammen 1992). The use of the pharmacological agents heparin, which inhibits thrombin, or warfarin, which inhibits synthesis of vitamin K-dependent coagulation factors, abrogates the formation of occlusive thrombi, but can also lead to bleeding complications (Garcia, Libby and Crowther 2010).

In addition to hemorrhagic events, activation of the coagulation cascade in diseased blood vessels can lead to the formation of pathologic thrombi. Virchow's triad states that thrombosis is caused by alterations in the vessel wall, blood flow perturbations, and changes in blood composition (Naess *et al.* 2007). Venous thromboembolism, which is the formation of venous thrombi or pulmonary embolisms, is thought to occur from stasis of blood flow, low oxygen tension, endothelial cell activation, platelet activation, or

alterations in concentration or function of pro- or anticoagulant factors (Mackman 2012; Reitsma, Versteeg and Middeldorp 2012). Cancer metastasis is routinely associated with increased risk of occlusive thrombi formation, and thrombosis in cancer patients is a common cause of mortality (Trousseau 1865; Tesselaar *et al.* 2007). Tumor cells have been found to express elevated levels of TF, which can promote tumor growth, angiogenesis, and metastasis (Bromberg *et al.* 1995; Riewald and Ruf 2001). Currently, the role of TF-exposing extracellular vesicles produced by cancer cells (Dvorak *et al.* 1983) in potentiating occlusive thrombus formation is an active area of research. Additionally, it has been suggested that thrombus formation may facilitate tumor cell arrest in the vasculature during cancer metastasis (Dardik *et al.* 1997; McCarty *et al.* 2002; Bambace and Holmes 2011). Further investigations into the interactions between hemostasis and cancer is critical to ultimately improve diagnosis, prevention, and treatment of cancer.

1.4.7 Common methodologies to study secondary hemostasis

Typical screening tests for disorders of secondary hemostasis include the prothrombin time (PT), thrombin time (TT), activated partial thromboplastin time (aPTT), and activated clotting time (ACT) (van Herrewegen *et al.* 2012). The PT assay measures the time for citrated platelet poor plasma to clot after the addition of calcium and thromboplastin, which contains TF and phospholipids (Armand J. 1935). The PT assay will have prolonged clotting time of samples with deficiencies in FVII, FX, FV, prothrombin, or fibrinogen. Similar to the PT test, the TT assay is used to measure the time of clotting after administration of thrombin and calcium to citrated plasma (Kitchen

and Makris 2009). Prolonged TT may indicate reduced FG levels, FG dysfunction, disseminated intravascular coagulation, or abnormal fibrinolysis, but is most commonly due to contamination of the sample with the thrombin inhibitor heparin (Lee, Berntorp and Hoots 2008).

The aPTT assay assesses the intrinsic coagulation pathway by measuring the clotting time after adding partial thromboplastin (phospholipids), calcium, and a surface contact activator (e.g., celite, kaolin, silica, or ellagic acid) to citrated platelet poor plasma (Langdell, Wagner and Brinkhous 1953). Prolonged aPTT clotting time will occur with deficiencies in high molecular weight kininogen, prekallikrein, FXII, FXI, FIX, FVIII, FX, FV, prothrombin, or FG. The ACT test utilizes fresh, whole blood that is added to a tube containing a surface activator to induce activation of the intrinsic coagulation pathway, similar to the aPTT test, and the time to occlusion is measured (Horton and Augustin 2013). However, the ACT assay is less precise than the aPTT test and is influenced by numerous variables, such as platelet count, platelet function, factor deficiencies, heparin use, and blood temperature. These screening tests are limited in specificity and abnormal results typically require additional testing, such as performing individual coagulation factor activity assays, measuring FG levels, AT and APC assays, and genetic testing for inherited disorders (Favaloro, Funk and Lippi 2012).

One of the few assays that evaluates both primary and secondary hemostasis is thromboelastography (TEG). TEG measures the visco-elastic properties of a clot by inserting citrated whole blood, calcium, and TF or a surface contact activator into a cup

with a torsion wire suspending a pin connected to a mechanical-electrical transducer and the cup rotates to mimic sluggish venous flow and to activate coagulation (Salooja and Perry 2001). TEG measures the physical properties of the clot as it forms and provides global information on the dynamics of thrombosis and fibrinolysis (Luz, Nascimento and Rizoli 2013). TEG has been shown to be more sensitive to bleeding defects than the PT, TT, or aPTT assays, but typically further testing is required to elucidate the specific hemostatic dysfunction (Perry *et al.* 2010). TEG is currently a promising technique but additional studies are needed to further standardize the method and to increase specificity. As our understanding of secondary hemostasis progresses, new techniques will likely need to be developed to aid in the diagnosis of coagulation disorders and the evaluation of novel therapeutics.

1.5 Dissertation Overview

Hemostasis is a complex system of pro- and anticoagulant processes that work to cease bleeding at sites of vascular injury. Bleeding complications or thrombotic events are associated with various pathological states; however, the role of platelets and coagulation in many of these diseases remains ill-defined. Thus, the development of novel techniques for studying hemostasis and thrombosis will aid in elucidating underlying mechanisms of primary and secondary hemostasis and help with the development of new pharmacological therapeutic interventions for treating pathological conditions. This dissertation centers on the development and use of metrological assays to evaluate primary and secondary hemostasis in healthy adults and in early development, and to investigate the role of coagulation in cancer metastasis.

Currently available assays evaluate platelet aggregation or thrombus formation under static conditions, but few assess hemostasis and whole blood coagulation under the physiological condition of fluid shear. Moreover, few assays provide quantitative measurements of the biophysical properties underlying platelet aggregation and thrombus formation. Chapter 3 describes the development and application of label-free imaging techniques to evaluate the effect of shear rate and the activation of coagulation on the physical parameters of platelet aggregates and thrombi formed under fluid shear.

Although previous studies utilizing static platelet adhesion methods have characterized single platelet adhesion, activation, and spreading on protein-coated surfaces, the role of platelet concentration in the propagation of second wave activation and subsequent aggregation following adhesion to protein surfaces remains ill-defined. Chapter 4 presents a novel static platelet function assay that utilizes the label-free imaging methods developed in Chapter 3 and the physical parameter of platelet concentration to evaluate platelet adhesion, activation, and aggregation.

Development of the human hemostatic system is a dynamic process where neonatal hemostasis is functionally distinct from adult hemostasis. Currently available neonatal platelet function testing is limited due to difficulties obtaining adequate blood volume from neonates, lack of normal reference ranges, and an incomplete understanding of the neonatal platelet functional phenotype. Chapter 5 describes the development of four novel small volume, whole blood, platelet function assays for evaluating neonatal platelet adhesion, activation, and aggregation.

Cancer metastasis is commonly associated with increased risk of clot formation and formed thrombi can frequently be observed in histological samples of metastases (O'Meara 1958; O'Meara and Jackson 1958; Hiramoto *et al.* 1960); however, the role of tumor cells, blood cells, coagulation factors, and formed thrombi in metastasis is not well understood (Dardik *et al.* 1997; Bambace and Holmes 2011). Chapter 6 describes a method to evaluate cancer cell interactions with platelet aggregates and thrombi under fluid shear conditions and highlights a potential role of coagulation and polymorphonuclear leukocytes in facilitating metastatic cancer cell adhesion and arrest.

The methods and studies outlined in Chapters 3-6 provide insights into primary and secondary hemostasis in healthy adults, in early development, and in the pathologic state of cancer metastasis. In Chapter 7, the key findings from my dissertation research are summarized and areas of interest for future work are highlighted.

Chapter 2: Common Materials and Methods

2.1 Ethical Considerations

Studies in this dissertation were conducted using human blood. All human adult donors were healthy and gave full informed consent in accordance with the Declaration of Helsinki. For human neonate blood donations, parents gave full informed consent. Experiments using human adult and neonate donors were performed with approval of the Oregon Health & Science University Institutional Review Board.

2.2 Collection of Human Adult Blood

Human adult venous blood was collected via venipuncture from healthy male or female volunteers (age 18 or older) who had been aspirin-free for at least two weeks prior. Blood was collected directly into syringes containing the anticoagulant, trisodium citrate (NaCit; 0.38% w/v; Sigma-Aldrich, St Louis, MO) or D-phenylalanyl-L-prolyl-L-arginine chloromethyl ketone (PPACK, 40 μmol/L; Haematologic Technologies, Essex Junction, VT).

2.3 Flow Chamber Assays

2.3.1 Flow chamber protein coating

Glass capillary vitrotubes (0.2 × 2.0 × 50 mm or 0.4 × 4.0 × 50 mm; VitroCom, Mountain Lakes, NJ) were coated with a protein solution for 1 h at 25^{o}C, followed by washing with PBS. Protein-coated slides were then either blocked with BSA (5 mg/mL, 1 hr at 25°C; Sigma-Aldrich) or coated with a second protein coating solution for 1 hr, at 25^{o}C,

followed by washing with PBS and blocking with BSA. Protein-coated vitrotubes were assembled onto microscope slides and mounted onto the stage of an inverted microscope (Zeiss Axiovert 200 M, Carl Zeiss MicroImaging GmbH, Germany).

2.3.2 Platelet aggregation

A pulse-free syringe pump perfused NaCit-anticoagulated blood through coated vitrotubes for 5 min at physiologically relevant shear rates to form platelet aggregates (Figure 2.1). Vitrotubes containing platelet aggregates were washed for 5 min with modified HEPES-buffered Tyrode's solution (136 mmol/L NaCl, 2.7 mmol/L KCl, 10 mmol/L HEPES, 2 mmol/L $MgCl_2$, 2 mmol/L $CaCl_2$, 5.6 mmol/L glucose, 0.1% BSA; pH 7.45) at the same shear rate to remove unbound blood components. The samples were then fixed with paraformaldehyde (PFA, 4%) and capillary tubes were filled with Fluoromount-G (SouthernBiotech, Birmingham, AL) for image analysis.

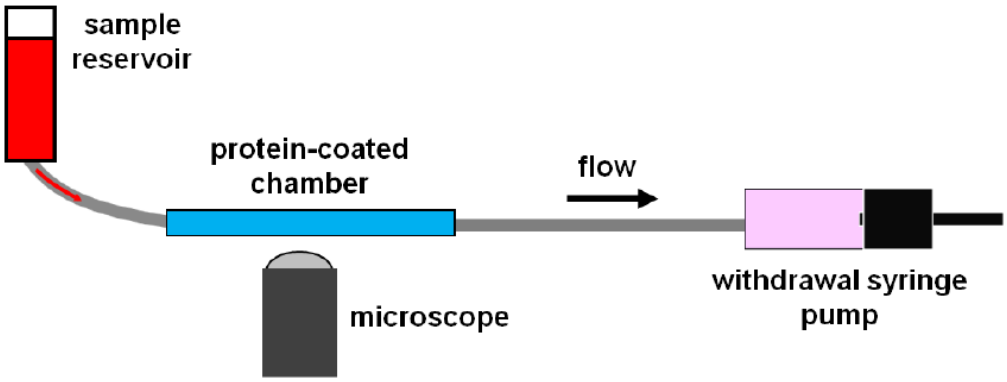

Figure 2.1 Schematic of platelet aggregation flow chamber system. Anticoagulated whole blood is pulled through a protein-coated chamber at the desired shear rate with a pulse-free syringe pump. The flow chamber is mounted above a microscope for imaging of platelet interactions and aggregate formation during and after perfusion. Figure was adapted from ©Michelle A. Berny-Lang Dissertation at Oregon Health & Science University (Berny-Lang 2010).

2.3.3 Thrombus formation

In order to trigger coagulation and drive fibrin formation under shear, a separate syringe pump mixed calcium flow buffer (75 mmol/L $CaCl_2$ and 37.5 mmol/L $MgCl_2$) with NaCit-anticoagulated venous blood immediately prior to perfusion through the protein-coated flow chamber (Figure 2.2) (White *et al.* 2007; Berny *et al.* 2010; White-Adams *et al.* 2010). Vitrotubes containing formed thrombi were washed for 5 min with modified HEPES-buffered Tyrode's solution at the same shear rate to remove unbound blood components. The samples were then fixed with 4% PFA and capillary tubes were filled with Fluoromount-G for image analysis.

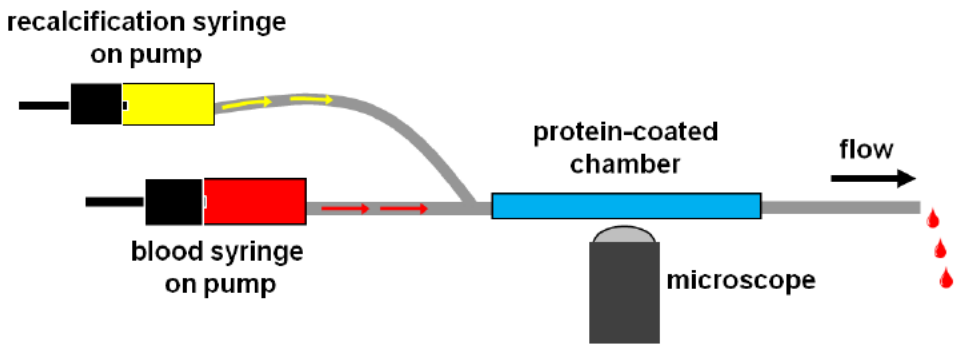

Figure 2.2 Schematic of the thrombus flow chamber system. Two syringe pumps co-perfuse sodium citrate-anticoagulated whole blood with calcium flow buffer to initiate coagulation and form thrombi in the protein-coated perfusion chamber. The flow chamber is mounted above an objective to image thrombus formation. Figure was adapted from ©Michelle A. Berny-Lang Dissertation at Oregon Health & Science University (Berny-Lang 2010).

2.4 Quantitative Imaging Methods

2.4.1 Hilbert transform differential interference contrast (HTDIC) method for volume measurements

Through-focus differential interference contrast (DIC) imaging of samples were performed at ×40 or ×63 magnification with an oil-coupled, numerical aperture (NA) of

1.4 objective lens on a Zeiss Axio Imager 2 microscope (Carl Zeiss MicroImaging GmbH). Three hundred through-focus transverse DIC images with an illumination condenser NA of 0.9 were separated by a 0.1 μm axial increment. Images were recorded with a charge-coupled device camera (12-bit AxioCam MRc5; Carl Zeiss). The microscope was operated under the control of SlideBook 5.5 software (Intelligent Imaging Innovations, Denver, CO).

The application of a Hilbert transform to DIC images, referred to as HTDIC, is a simple, non-iterative, fast-Fourier transform based image processing method that can quickly be applied to the imagery of biological specimens under high NA illumination conditions. High NA illumination enables enhanced sectioning of the specimen along the optical axis. Hilbert transform processing on the DIC image stacks significantly enhances edge detection for localization of the specimen borders in three dimensions by separating the gray values of the specimen intensity from those of the background. The HTDIC method is based on the work by Arnison *et. al.* (Arnison *et al.* 2000) but with the addition of Fourier filtering methods to enhance contrast and a Sobel-based edge detection method for automated volumetric analysis on the sample. The application of a high-pass Fourier filter was introduced to eliminate axial blurring and to facilitate edge detection of specimens in DIC image cubes (Figure 2.3). The cross-sectional planes of the DIC images were detected using a Sobel-based edge detection with the area computed in each plane and then added together using a custom program written in MATLAB (MathWorks, Natick, MA) (Baker, Phillips and McCarty 2012; Phillips, Baker-Groberg

and McCarty 2014). Area measurements were determined by outlining *en face* HTDIC images at the central focal position of the image cube.

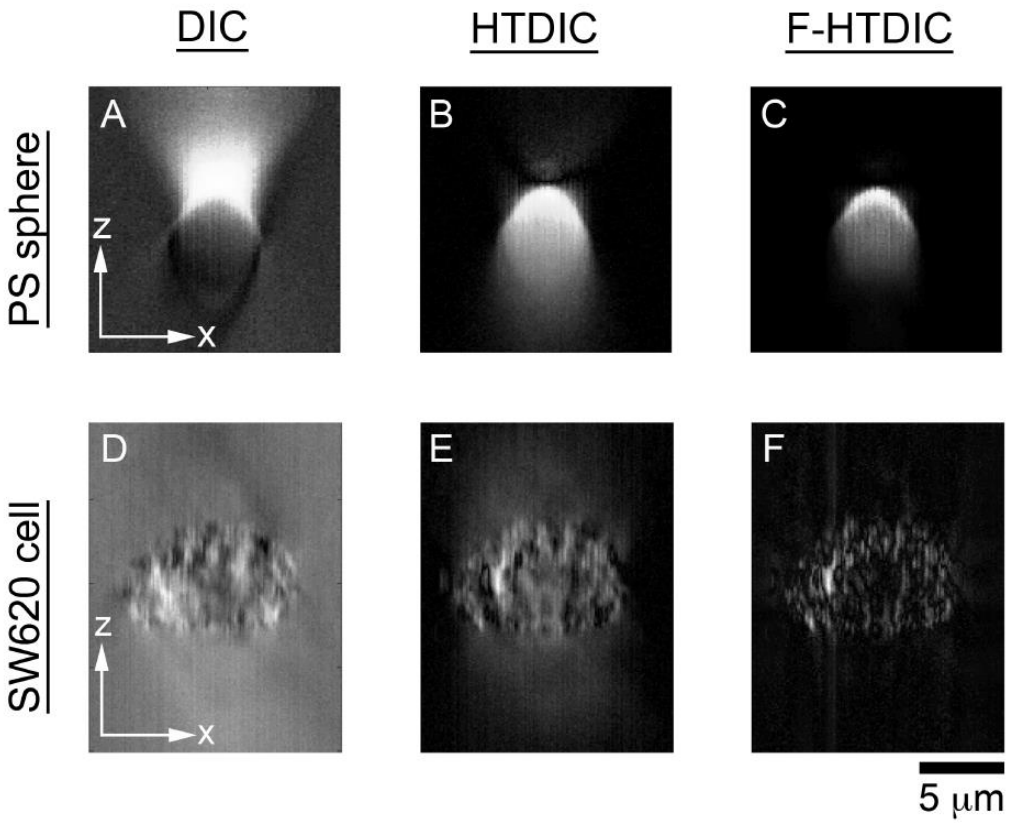

Figure 2.3 Optimal DIC contrast enhancement using HTDIC: polystyrene spheres and a SW620 cell. (A) Cross-sectional DIC imagery of a 4.8 μm polystyrene sphere, (B) corresponding HTDIC image, and (C) Fourier filtered HTDIC image. The axial dimension of the sphere images have been scaled to account for refractive index mismatch of the specimen (1.597) and the mounting media (1.4). (D-F) demonstrate the same image types for an SW620 cell, however, with no refractive index mismatch correction owing to the weak index contrast of the specimen. No thresholding has been performed on these images. Figure was adapted from ©Phillips *et. al.*, 2014, originally published in *JOVE* (Phillips, Baker-Groberg and McCarty 2014).

2.4.2 Non-interferometric quantitative phase microscopy (NIQPM) method for mass measurements

Through-focus, z-stack bright field imaging of the samples was performed at ×40 or ×63 magnification with an oil-coupled, 1.4 NA objective lens and an illumination condenser

NA of 0.1 with a green filter (λ = 540 ± 20 nm, Chroma Technology Corp., Bellows Falls, VT) on a Zeiss Axio Imager 2 microscope. Images were taken at 0.1 µm axial increments. Images were recorded with a charge-coupled device camera (12-bit AxioCam MRc5). The microscope was operated by SlideBook 5.5 software.

Mass measurements were acquired using the non-interferometric quantitative phase microscopy (NIQPM) technique. Cells often appear semi-transparent when imaged with standard bright field microscopes due to their weak scattering and absorption properties over the optical spectrum. NIQPM is based on a simplified model of wave propagation (paraxial approximation) assuming low NA illumination, weak scattering, and weak absorption by the specimen. Paganin and Nugent demonstrated that the phase profile of a cell could be reconstructed from through-focus bright field imagery of the sample (Paganin and Nugent 1998). The transport intensity equation relates axial intensity, denoted *I(x,y,z)*, variations to transverse phase variations by

$$(2.1): \quad -\frac{2\pi}{\lambda}\frac{\partial I(x,y,z)}{\partial z} = \nabla_{x,y}[I(x,y,z)\nabla_{x,y}\varphi(x.y.z)]$$

where $\nabla_{x,y}$ denotes the two dimensional gradient operator in the transverse *x,y* coordinates (perpendicular to optical, *z*-axis), φ denotes phase (radians), and λ is the wavelength of illumination light. Equation 2.1 was used to determine phase from bright field intensity measurements acquired with the Zeiss Axio Imager 2 microscope and charge coupled device camera. To solve for phase numerically, a Green function technique was applied to the measured phase values using a two-dimensional Fourier spectral method (Frank, Altmeyer and Wernicke 2010; Phillips *et al.* 2012).

The phase can also be defined as the sum of the refractive index of the sample, denoted n_{cell}, along the height of the sample, denoted *h(x,y)* (μm) (Barer 1953; Popescu *et al.* 2008), as described by the following equation:

$$(2.2): \quad \varphi(x,y) = \frac{2\pi}{\lambda}\int_0^{h(x,y)}[n_{cell}(x,y,z) - n_0]dz$$

Barer *et. al*. (Barer 1953) demonstrated that because the cellular refractive index is linearly proportional to the dry mass content of a cell, the dry mass content of a cell could be determined using quantitative measurements of phase. The refractive index is dependent on the dry mass density as given by

$$(2.3): \quad n_{cell}(x,y,z) = n_0 + \alpha C(x,y,z)$$

where *C* (g/mL) is the dry mass density of the cell and α is the specific refraction increment of the cell solids (~0.2 mL/g). By defining the projected mass density as

$$(2.4): \quad \rho(x,y) = \int_0^{h(x,y)} C(x,y,z)dz \quad [g/\mu m^2],$$

ρ was obtained from phase by substituting Equation 2.3 into Equation 2.2 to get

$$(2.5): \quad \rho = \frac{\lambda\varphi}{2\pi\alpha} \quad [g/\mu m^2]$$

Using a custom MATLAB program, total cellular mass was then determined by integrating over the area of the cell (Phillips and McCarty 2012).

The NIQPM method was validated for a range of sample sizes using polystyrene microspheres (Figure 2.4). The NIQPM reconstructed phase profile was compared to a theoretical phase profile for transmitted waves through a sphere, defined as

$$(2.6): \quad \varphi = \frac{4\pi(n_{sphere}-n_{FLG})}{\lambda}\sqrt{r^2-(x-x_0)^2}$$

where radius is denoted as *r*, and n_{FLG} is the refractive index of mounting media (1.4).

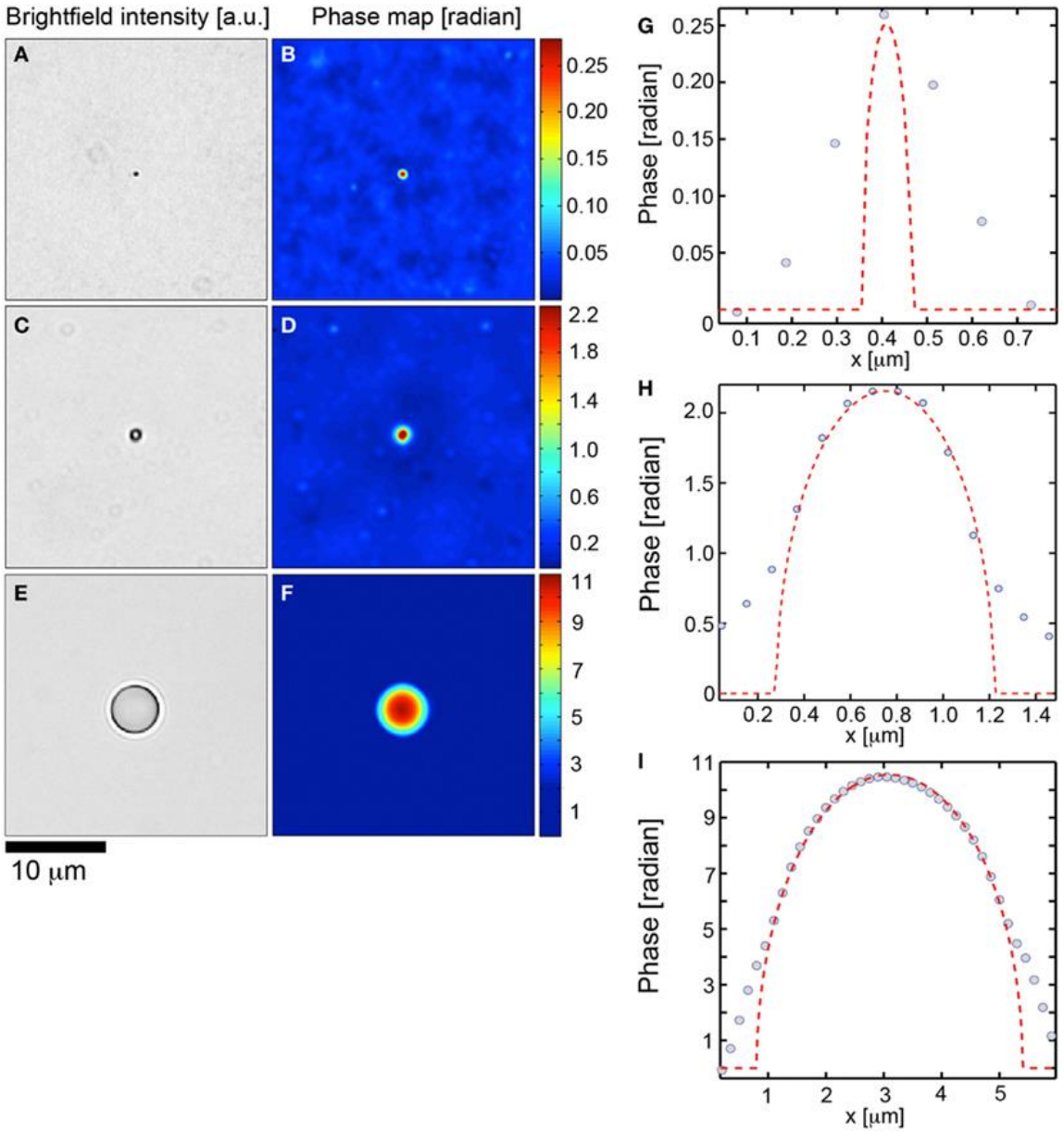

Figure 2.4 NIQPM validation over two orders of magnitude. (A,C,E) Bright field imagery of polystyrene microspheres (n = 1.597, λ = 540 nm) suspended in Fluoromount-G (n = 1.4) with diameters of 0.11, 0.95, and 4.8 μm, respectively. (B,D,F) Corresponding transport of intensity based quantitative phase maps. (G,H,I) demonstrate theoretical phase profiles (dashed) for each polystyrene sphere with corresponding data (circles) overlaid. Figure was adapted from ©Phillips *et. al*., 2012, originally published in *Frontiers in Oncology* (Phillips and McCarty 2012).

The general steps in the HTDIC and NIQPM protocols are illustrated in Figure 2.5.

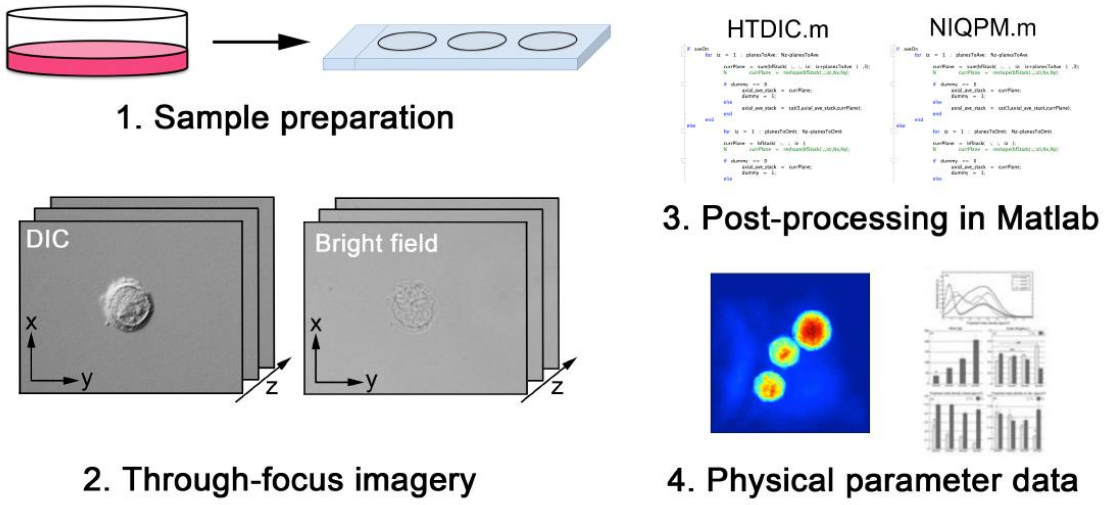

Figure 2.5 HTDIC and NIQPM workflow. (1.) Cells are mounted on microscope slides with cover glass affixed over the sample using Fluoromount-G. (2.) Through-focus DIC and bright field imaging with a standard microscope form the input to the image processing. (3.) Post-processing of images in MATLAB to determine cell volume from DIC and cellular mass distribution from bright field imagery. (4.) Quantitative endpoint metrics: heat maps and bar graphs. Figure was adapted from ©Phillips *et. al*., 2014, originally published in *JOVE* (Phillips, Baker-Groberg and McCarty 2014).

2.5 Statistical Analysis

All data are represented as mean ± standard error of the mean (SEM), unless noted otherwise. Each experimental condition was repeated at least 3 times. Statistical analysis was performed using paired Student's t-test. Significance for all statistical tests required $P \leq 0.05$, unless noted otherwise.

Chapter 3: Development of Label-free Imaging Techniques for the Quantification of Volume, Mass, and Density of Thrombus Formation

Sandra M. Baker, Kevin G. Phillips, and Owen J. T. McCarty

3.1 Abstract

Flow chamber assays, in which blood is perfused over surfaces of immobilized ECM proteins, are used to investigate the formation of platelet aggregates and thrombi under shear flow conditions. Elucidating the dynamic response of thrombi/aggregate formation to different coagulation pathway perturbations *in vitro* has been used to develop an understanding of normal and pathological cardiovascular states. Current microscopy techniques, such as differential interference contrast (DIC) or fluorescent confocal imaging, respectively, do not provide a simple, quantitative understanding of the basic physical features (volume, mass, and density) of thrombi/aggregate structures. The use of two label-free imaging techniques applied, for the first time, to platelet aggregate and thrombus formation are introduced: non-interferometric quantitative phase microscopy, to determine mass, and Hilbert transform DIC microscopy, to perform volume measurements. Together these techniques enable a quantitative biophysical characterization of aggregates and thrombi formed on three surfaces: fibrillar collagen, collagen + 0.1 nM tissue factor (TF), and collagen + 1 nM TF. It is demonstrated that label-free imaging techniques provide quantitative insight into the mechanisms by which thrombi and aggregates are formed in response to exposure to different combinations of procoagulant agonists under shear flow. Utilization of these imaging techniques can allow for insights into the kinetics and mechanisms by which thrombi are formed under various shear conditions in a label-free manner.

This work was originally published by Springer Cellular and Molecular Bioengineering 2012; Volume 5, Number 4, Pages: 488-492 and by Society of Photo-optical Instrumentation Engineers (SPIE) Journal of Biomedical Optics 2013; Volume 18, Number 1, Pages: 16014. Reprinted with permission

3.2 Introduction

Methods presented in this dissertation were designed to evaluate primary and secondary hemostasis under static and fluid shear conditions. This chapter presents two label-free, quantitative imaging techniques to define the biophysical parameters of volume and mass of platelet aggregates and thrombi formed on different procoagulant surfaces under fluid shear conditions. Our results indicate that the presence of coagulation restricts platelet aggregate/thrombi size at high arterial shear rates and fibrin formation increases thrombi mass while thrombi volume remains constant.

3.3 Background

Recent work has demonstrated the ability to utilize commercially available imaging platforms to perform quantitative investigations of cellular mass via low numerical aperture (NA) illumination bright field imagery (Phillips and McCarty 2012; Phillips, Jacques and McCarty 2012) and cellular volume (Baker, Phillips and McCarty 2012), using high NA illumination differential interference contrast (DIC) microscopy. Excitingly, these results demonstrate that key insights into the basic biophysical structure and composition of biological specimens are within reach using standard off-the-shelf optical microscopes employing label-free imaging modalities. To date, efforts to quantify

the basic physical features of platelet thrombi and aggregates in the context of hemostasis and thrombosis have relied on fluorescent probes and confocal microscopy to quantify protein biodistribution and perform sample volume measurements using surface markers. While instructive, some of the limitations of confocal microscopy stem from the potential for non-specific labeling by promiscuous antibodies and the lack of reagents or biomarkers for disease-specific applications. Moreover, confocal microscopy can provide only limited biophysical parameters – those dependent on the localization of the fluorescent label. DIC microscopy is commonly used to assess thrombi/aggregate surface area, but is limited to two-dimensional analyses of these complex structures. To provide a three-dimensional and label-free biophysical picture of these structures, we have developed a label-free imaging strategy consisting of Hilbert transform DIC microscopy (Arnison *et al.* 2000) and non-interferometric quantitative phase microscopy (NIQPM) (Paganin and Nugent 1998) to quantify the mass, volume, and density of platelet aggregates and thrombi formed *in vitro* using a flow chamber assay (McCarty *et al.* 2004). This platform is amenable to optical imaging to monitor both time-dependent and endpoint metrics associated with clot formation.

DIC microscopy is now a ubiquitous imaging modality due to its unique phase contrast enhancement ability. DIC image contrast is produced by phase gradients in transmitted waves through weak index contrast specimens, enabling high definition imaging of unstained samples that otherwise would appear semi-transparent using traditional bright field microscopy techniques (Arnison *et al.* 2000; Lee *et al.* 2007). Phase gradients in the transmitted field through the sample arise from either height changes, mass density

variations, or the product of the two along the optical path taken by waves through the sample (Preza *et al.* 1998; Gramatikov 2012; Phillips *et al.* 2012). DIC images are not amenable to thresh-holding due to the overlap of gray level intensities of the imaged specimen with the background substrate upon which the sample is mounted. This failure to isolate details of the sample from the background makes additional processing of the image necessary in order to extract quantitative information (Arnison *et al.* 2000).

The Hilbert transform is a spatial frequency space multiplier operator that creates symmetric image features through the maintenance of positive frequency components and the reversal of negative frequency components (van Munster, van Vliet and Aten 1997; Arnison *et al.* 2000). The utility of the transform lays in its ability to remove the *bas relief* of DIC images, thus enabling the ability to threshold the background intensity values out of the image (Figure 3.1a). The application of a Hilbert transform to DIC images, referred to as HTDIC, is a simple non-iterative fast-Fourier transform based image processing method that can quickly be applied to the imagery of biological specimens.

The ability to threshold the image comes with the artificial introduction of low frequency noise components which give rise to axial blurring (Figure 3.1a, top right). We introduce the application of a high-pass Fourier filter to eliminate this axial blurring to facilitate edge detection of specimens in DIC image cubes (Figure 3.1a, bottom right). Using this high-pass filtered HTDIC post processing procedure we investigated the geometric parameters of platelet aggregates and thrombi formed under conditions of shear.

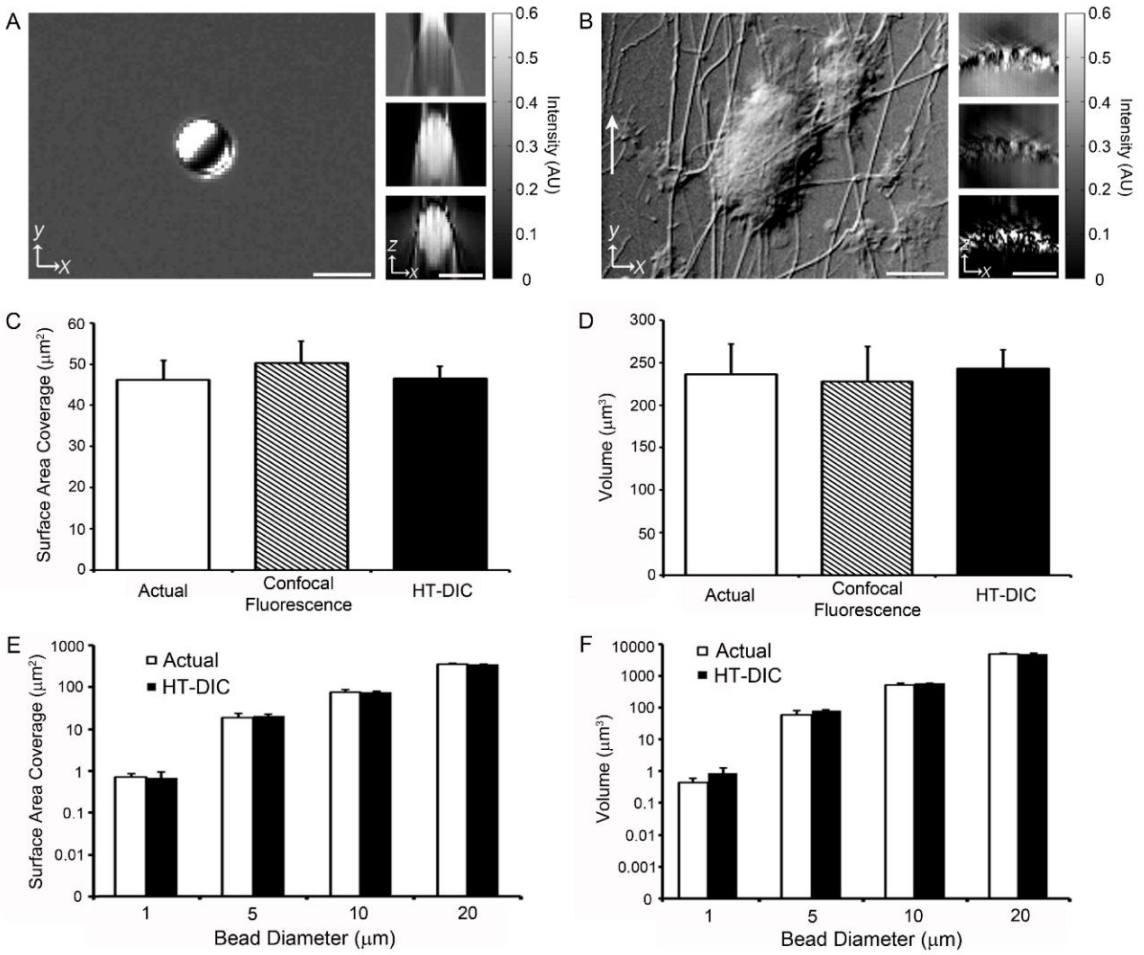

Figure 3.1 Validation of HTDIC imaging technique. (a) Sagittal ×40 DIC image of a 4.82 ± 0.59 μm diameter polystyrene microsphere bead (left). Cross-sectional view of the DIC z-stack images (top right), Hilbert transformed DIC z-stack (middle right), and high-pass filtered Hilbert transformed DIC z-stack (bottom right) of the microsphere. (b) Sagittal DIC image of a platelet aggregate formed at 200 s^{-1} shear rate (left). Cross-sectional view of the DIC z-stack images (top right), Hilbert transformed DIC z-stack (middle right), and high-pass filtered Hilbert transformed DIC z-stack (bottom right) of the platelet aggregate. The direction of flow is indicated by the white arrow. Intensity values are in arbitrary units. Scale bars represent 5 μm. (c and d) Mean surface area coverage and volume of ten 7.67 ± 0.38 μm diameter fluorescein polystyrene microspheres calculated using confocal fluorescence microscopy and the HTDIC technique. The actual surface area coverage and volume of the spheres using the manufacturer specifications are also plotted. Error bars are ± standard deviation. (e and f) Mean surface area coverage and volume for ten 0.95 ± 0.10 μm, 4.82 ± 0.59 μm, 9.86 ± 0.65 μm, and 20.92 ± 0.64 μm diameter uniform polystyrene microspheres calculated using the HTDIC technique. Results are plotted against the actual values for the spheres according to the manufacturer. Error bars are ± standard deviation.

NIQPM is carried out using standard bright field imagery. Bright field images of weak index contrast specimens, such as cells, appear semi-transparent due to the weak scattering and low absorption of the illuminating light. The amplitude of transmitted waves thus remains relatively unchanged during propagation through the sample. However, thickness and density fluctuations within the sample create phase lags in the transmitted waves. Under the paraxial approximation to the full wave dynamics, the phase of the transmitted waves can be related to the axial variation of the intensity of these waves via the transport of intensity equation (Paganin and Nugent 1998). To satisfy the assumptions of the paraxial approximation, low (NA = 0.1) trans-illumination combined with through-focus bright field imaging form the basis of the input to the transport of intensity equation to perform phase measurements of the transmitted field through the sample. We have recently validated the NIQPM method on polystyrene spheres ranging in size from 0.11 to 4.8 μm in diameter, which produce phase shifts ranging from 0.25 to 11 radians (Phillips and McCarty 2012). To determine mass, phase is then mapped to the axially integrated mass density of the specimen (Barer 1953) to produce a projected mass density image. Summation of the area of the projected mass density image gives the total mass of the specimen (Popescu 2008).

Collagen is a protein found in connective tissues, and when exposed to whole blood in circulation, such as in damaged endothelium, platelets bind to collagen via the adhesive protein VWF (McCarty *et al.* 2006). The process of platelet recruitment, adhesion, activation and aggregate formation is termed primary hemostasis. Tissue factor (TF) is a protein expressed on the surface of subendothelial cells and when bound to coagulation

factor VIIa, can activate factor X to initiate thrombin generation, resulting in fibrin formation (Berny *et al.* 2010). As collagen-bound platelets become activated, they provide a surface for the activation of the coagulation cascade. This process of leads to local generation of fibrin on the growing platelet plug, termed thrombus formation or secondary hemostasis.

The combination of the NIQPM method with the HTDIC post processing procedure is a powerful image analysis technique that enables the determination of sample mass, volume, and density fluctuations in different regions of interest within a sample. In the current study, we utilize the HTDIC/NIQPM method to analyze the geometric parameters of platelet aggregates and thrombi formed under conditions of shear.

3.4 Materials and Methods

3.4.1 Confocal microscopy validation of the HTDIC technique

To validate the HTDIC method (described in Chapter 2), average surface area coverage and volume of ten 7.67 ± 0.38 μm diameter fluorescein polystyrene microspheres (Bangs Laboratory, Inc., Fishers, IN) were measured using both confocal fluorescence microscopy and our HTDIC technique (Figures 3.1c and 3.1d). Confocal fluorescent microscopy was performed on a Zeiss Elyra PS.1/LSM 710 microscope (Carl Zeiss MicroImaging GmbH) and microspheres were imaged and analyzed using the Zen 2011 imaging software (Carl Zeiss MicroImaging GmbH). The confocal fluorescence microscopy software calculated mean surface area coverage to be 50.3 ± 5.3 μm^2 and mean volume to be 228.0 ± 40.7 μm^3 for the ten microspheres. The HTDIC technique

calculated mean surface area coverage to be 46.6 ± 2.9 μm^2 and mean volume to be 243.3 ± 21.5 μm^3 for the microspheres. According to the manufacturer specifications, actual surface area coverage and volume of the microspheres was 46.2 ± 4.6 μm^2 and 236.3 ± 35.5 μm^3. This validation demonstrates that the HTDIC technique is equivalent to confocal fluorescence microscopy in estimating geometric sample parameters.

3.4.2 Determination of valid sample size range for the HTDIC technique

To investigate the range of validity of the HTDIC method to measure volume, 10 different (0.95 ± 0.10 μm, 4.82 ± 0.59 μm, 9.86 ± 0.65 μm, and 20.92 ± 0.64 μm diameter; Bangs Laboratory, Inc., Fishers, IN) polystyrene microspheres were analyzed. The actual manufacturer surface area coverage and volume of the microspheres were compared to values calculated using the HTDIC technique (Figures 3.1e and 3.1f). The HTDIC method was determined to be within the manufacturing variation of the microspheres in the range of 1– 20 μm diameter samples. As expected, the HTDIC method failed for 0.1 μm polystyrene microspheres (data not shown), as they are below the diffraction limit of optical microscopy (~0.25 μm) (de Lange *et al.* 2001).

3.4.3 Blood collection and flow chamber preparation

To investigate and characterize the physical parameters of platelet aggregation and thrombus formation, human whole blood was perfused over three different surfaces containing immobilized procoagulant agonists: fibrillar collagen, fibrillar collagen with relipidated human recombinant TF at a concentration of 0.1 nM, or fibrillar collagen with TF at 1 nM. Calcium ions present in whole blood are essential for the activation of

coagulation factors. Experimental chelation of calcium ions in whole blood by the anticoagulant, sodium citrate (NaCit), prevents the activation of coagulation factors, thus allowing for only platelet aggregation to occur. Recalcification of sodium citrate-anticoagulated whole blood with excess molar calcium and magnesium results in thrombin generation and thrombus formation.

With the purpose of generating platelet aggregates under flow (Figures 3.1b), whole blood was collected into NaCit or PPACK, as described in Chapter 2. Blood collected into PPACK was supplemented with 10 μmol/L PPACK every hour to maintain inactivation of coagulation factors, resulting in only platelet-collagen adhesion and platelet–platelet aggregations. Glass capillary vitrotubes (0.2 × 2.0 × 50 mm) were coated with fibrillar equine Type I collagen (100 μg/mL, Chrono-Log, Havertown, PA) or collagen and TF (Dade Innovin, Siemens Healthcare Diagnostics, Deerfield, IL) at 0.1 nM or 1 nM, as described in Chapter 2. PPACK- or NaCit-anticoagulated blood was perfused through the flow chamber for 5 min to form platelet aggregates at physiologically relevant shear rates of either 200 s^{-1} or 1000 s^{-1} (De Clerck *et al.* 1994; Berny *et al.* 2010).

In order to form thrombi under shear in the presence of coagulation, venous blood was collected into NaCit and perfused through glass capillary vitrotubes (0.2 × 2.0 × 50 mm) coated with fibrillar collagen (100 μg/mL) or collagen and TF at 0.1 nM or 1 nM in the presence of calcium flow buffer, as described in Chapter 2. All experiments were repeated using blood from three different donors.

3.4.4 Platelet aggregate and thrombus image acquisition

Through-focus, z-stack images performed at ×63 magnification from three random fields of view (215 μm × 160 μm) were processed for each sample, resulting in a total of nine z-stack images for each treatment. Z-stack images were taken from the surface of the slide to 5 μm above the platelet aggregate or thrombi, which ranged in height from 2 – 15 μm, in accord with previous studies (McCarty *et al.* 2005). The HTDIC and NIQPM imaging methods described in Chapter 2 were used to obtain sample volume and mass. Volume and mass calculations were used to calculate the mean density of platelet aggregates and thrombi formed over the three surfaces.

3.5 Results

3.5.1 Surface area and volume of platelet aggregates and thrombi

Figures 3.2c, 3.2d, 3.2e, and 3.2f show the histograms of surface area coverage and volume of individual platelet aggregates and thrombi formed at 200 s^{-1} and 1000 s^{-1} shear rates. Table 3.1 displays the range for the greatest frequency (peak) for surface area coverage and volume of individual platelet aggregates and thrombi.

Table 3.1 Range of greatest frequency for surface area coverage and volume of individual platelet aggregates and thrombi at 200 s^{-1} and 1000 s^{-1}.

	Platelet aggregates		Thrombi	
Shear rate	Surface area coverage (μm^2)	Volume (μm^3)	Surface area coverage (μm^2)	Volume (μm^3)
200 s^{-1}	140 - 180	150 - 250	80 - 120	50 - 150
1000 s^{-1}	140 - 160	300 - 400	60 - 100	300 - 400

Figures 3.2c and 3.2d display mean total surface area coverage of platelet aggregates and thrombi formed at 200 s^{-1} and 1000 s^{-1} for a 215 µm by 160 µm field of view, while Figures 3.2e and 3.2f show mean total volume of platelet aggregates and thrombi for the field of view formed at 200 s^{-1} and 1000 s^{-1}.

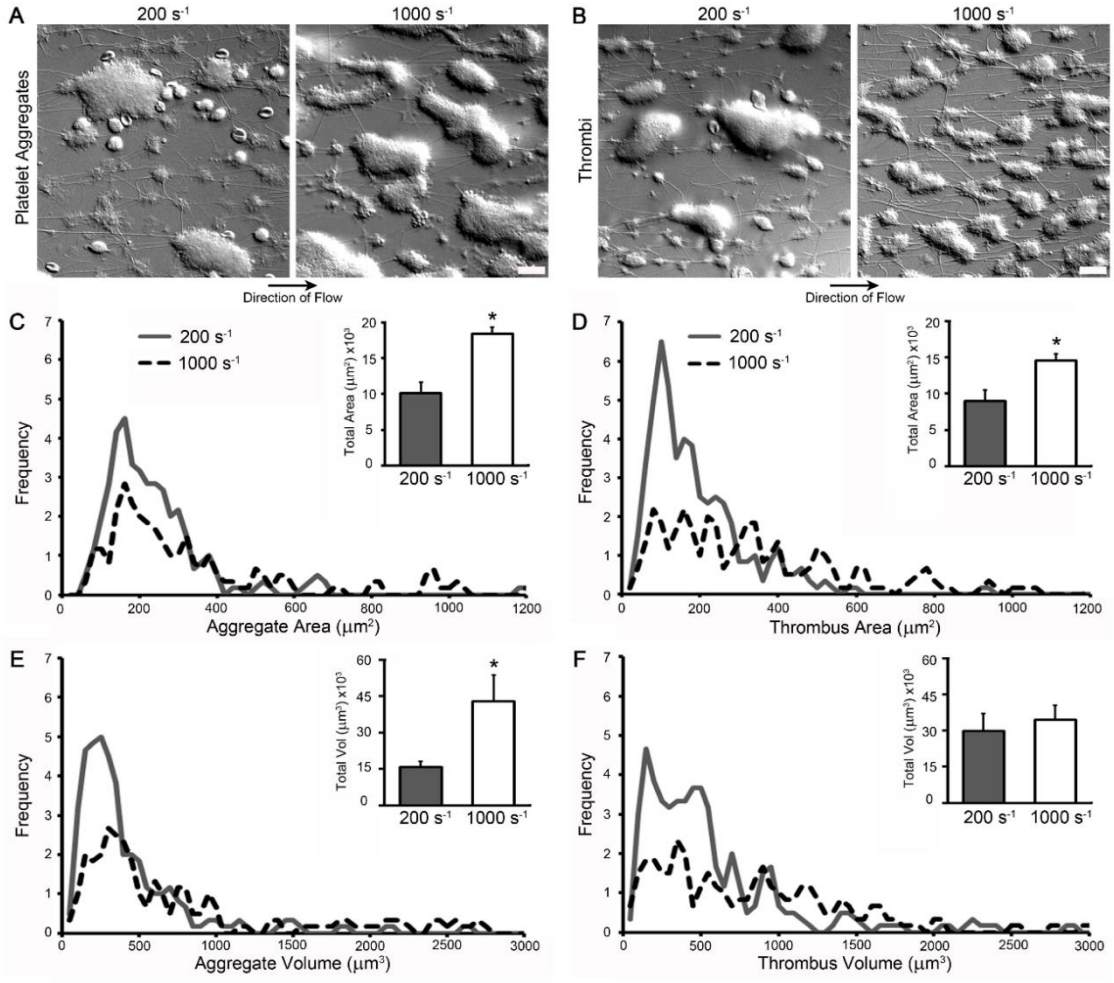

Figure 3.2 Platelet aggregate and thrombi surface area coverage and volume. (a) DIC image of platelet aggregates formed at 200 s^{-1} and 1000 s^{-1} shear rates. (b) DIC images of thrombi formed at 200 s^{-1} and 1000 s^{-1} shear rates. All scale bars represent 20 µm. (c, d, e, and f) Histograms of aggregate and thrombus surface area coverage and volume for 200 s^{-1} and 1000 s^{-1} shear rates collected over three trials. The surface area coverage histograms used 20 μm^2 size bins, while the volume histograms used 50 μm^3 bins. Inlaid bar graphs display mean total aggregate and thrombus surface area coverage and volume for a 215 µm by 160 µm field of view. Error bars are ± SEM. Asterisks denote a $P \leq 0.05$ in comparison to 200 s^{-1} shear rate values.

Platelet aggregate mean total surface area coverage for the 215 μm by 160 μm field of view increased from 10,091 ± 531 μm^2 at 200 s^{-1} to 18,393 ± 2040 μm^2 at 1000 s^{-1}, with a *P* of 0.017. Platelet aggregate mean total volume for the field of view increased from 15,948 ± 2146 μm^3 at 200 s^{-1} to 42,937 ± 10,672 μm^3 at 1000 s^{-1}, with a *P* of 0.036. Thrombi mean total surface area coverage for the same size field of view increased from 8,982 ± 1,567 μm^2 at 200 s^{-1} to 14,527 ± 909 μm^2 at 1000 s^{-1}, with a *P* of 0.038. Thrombi mean total volume for the field of view increased from 29,761 ± 7235 μm^3 at 200 s^{-1} to 34,349 ± 5,991 μm^3 at 1000 s^{-1}, with a *P* of 0.651.

3.5.2 Volume, mass, and density of platelet aggregates and thrombi formed on three different surfaces

Whole blood collected into sodium citrate resulted in only platelet-collagen adhesion and platelet-platelet aggregations (Figure 3.3), while the addition of calcium and magnesium to citrated-anticoagulated whole blood activated coagulation factors to form fibrin (Figure 3.3) and create thrombi.

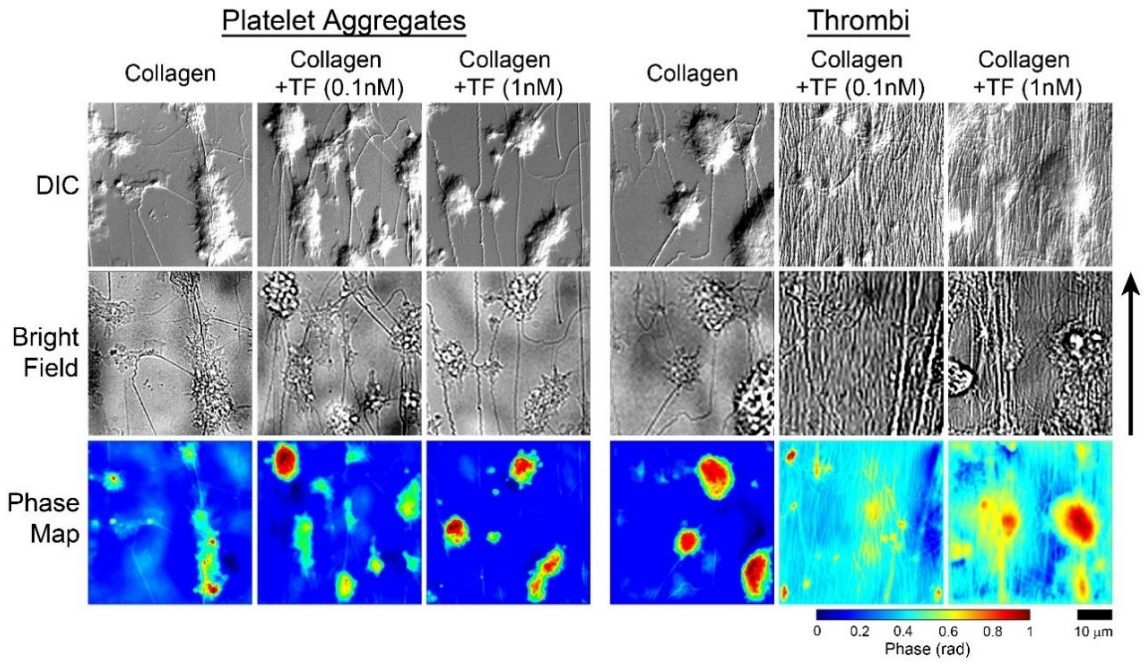

Figure 3.3 Phase maps of aggregates and thrombi formed on a collagen surface. Differential interference contrast (top row), bright field (middle row), and corresponding NIQPM phase map images (bottom row) for platelet aggregates and thrombi formed on three surfaces: fibrillar collagen, fibrillar collagen + 0.1 nM TF, and fibrillar collagen + 1 nM TF. The arrow indicates direction of flow. The scale and color bars are common to all images.

Mean volume of platelet aggregates and thrombi did not significantly differ between the three surfaces (fibrillar collagen, fibrillar collagen + 0.1 nM TF, or fibrillar collagen + 1 nM TF) (Figure 3.4a). However, mean mass (Figure 3.4b) and density (Figure 3.4c) of thrombi significantly increased from 122.8 ± 14.1 pg and 0.03 ± 0.002 pg/μm^3 to 325.0 ± 10.7 pg and 0.07 ± 0.003 pg/μm^3 ($P \leq 0.01$) on fibrillar collagen + 1 nM TF compared with fibrillar collagen alone.

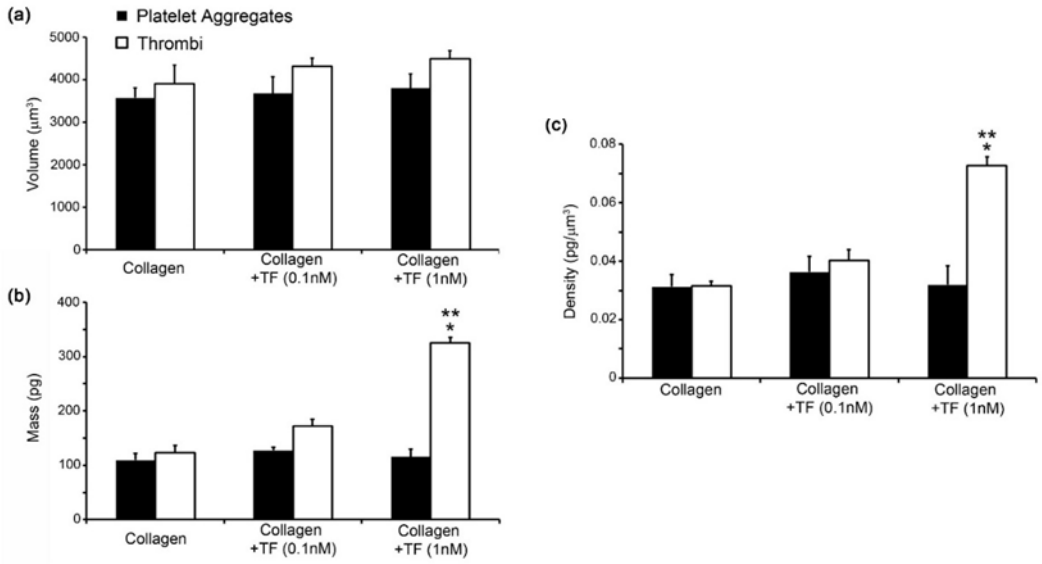

Figure 3.4 Volume, mass, and density of platelet aggregates and thrombi. (a) Mean volume, (b) mass, and (c) density of platelet aggregates and thrombi for a 50 μm by 50 μm field of view. Error bars are ± SEM. * denotes a $P \leq 0.01$ in comparison to platelet aggregate values and ** indicates a $P \leq 0.01$ compared with collagen-coated slides.

3.6 Discussion

Evaluation of the physical features of thrombi and platelet aggregates can be carried out using specific fluorescent probes imaged under confocal microscopy to quantify volume (Falati *et al.* 2002). However, fluorescent labels have been suspected to affect platelet function and structural quantitative information, such as density, cannot be investigated with confocal microscopy. We have developed two label-free imaging techniques (HTDIC and NIQPM) to characterize the volume, mass, surface area coverage, and density of platelet aggregates and thrombi formed under shear.

Our data indicates that the surface area coverage and volume of platelet aggregates increases with shear. However, under conditions of coagulation, the surface area

coverage of thrombi increases with shear while the volume appears to remain constant. Two dimensional analysis of thrombi and aggregates imaged under DIC demonstrate TF-dependent fibrin formation in the presence of calcium and magnesium, though the quantification of the biophysical changes among thrombi is confined to area alone. These two dimensional images cannot reveal the three dimensional organization of platelet aggregates and fibrin formation. Interestingly, NIQPM and HTDIC revealed that although the volume of formed thrombi on a surface of collagen +1 nM TF was similar to the other treatments, the mass and density of the thrombi formed with 1 nM TF increased significantly, presumably due to an increased degree of fibrin formation for the same equivalent number of platelets. This parallels confocal-based observations of fluorescent fibrin reporters, which indicate the presence of TF increases the number of fibrin cross-links in thrombi (Campbell *et al.* 2009).

Our results demonstrate the effectiveness of label-free imaging modalities to measure the basic physical features of platelet aggregates and thrombi structures. Utilization of these imaging techniques can allow for insights into the kinetics and mechanisms by which thrombi are formed under various shear conditions in a label-free manner. Having the capability of determining clot density in a fast, accurate, and technologically-accessible manner will provide investigators a quantitative means to characterize the efficacy of novel antithrombotics and treatment strategies to inhibit pathologic thrombus formation.

Chapter 4: Development of a Method to Quantify Platelet Adhesion and Aggregation under Static Conditions

Sandra M. Baker-Groberg, Flor A. Cianchetti, Kevin G. Phillips, Owen J.T. McCarty

4.1 Abstract

Platelets are important players in hemostasis and thrombosis. Thus, accurate assessment of platelet function is crucial for identifying platelet function disorders and measuring the efficacy of antiplatelet therapies. We have developed a novel platelet aggregation technique that utilizes the physical parameter of platelet concentration in conjunction with volume and mass measurements to evaluate platelet adhesion and aggregation. Platelet aggregates were formed by incubating purified platelets on fibrinogen- or fibrillar collagen-coated surfaces at platelet concentrations ranging from 20,000 to 500,000 platelets/μL. Platelets formed aggregates under static conditions in a platelet concentration-dependent manner, with significantly greater mean volume and mass at higher platelet concentrations (≥ 400,000 platelets/μL). We show that a platelet glycoprotein (GP) IIb/IIIa inhibitor abrogated platelet-platelet aggregation, which significantly reduced the volume and mass of the platelets on the collagen surface. This static platelet aggregation technique is amenable to standardization and represents a useful tool to investigate the mechanism of platelet activation and aggregation under static conditions.

This work was originally published by Springer
Cellular and Molecular Bioengineering 2014; Volume 7, Number 2, Pages: 285-290
Reprinted with permission

4.2 Introduction

Chapter 3 described the development of label-free, quantitative imaging modalities used to investigate platelet aggregation and thrombus formation under fluid shear conditions. The method presented in this chapter utilizes the developed imaging assays to evaluate platelet function by assessing the physical parameters of platelet aggregation under static conditions with varying platelet concentration. The technique described in Chapter 4 provides a novel method to evaluate platelet function and study the effect of novel antiplatelet therapeutics.

4.3 Background

Platelets are anucleate blood cells that are critical to the process of hemostasis and thrombosis. During hemostasis, the endothelium produces inhibitory factors that keep platelets in a resting state. However, during vascular injury, the ECM is exposed to blood, resulting in local platelet adhesion and activation to initiate platelet aggregation and thrombus formation (Michelson 2004). Platelets bind the exposed ECM proteins collagen and von Willebrand factor through integrin $\alpha_2\beta_1$ and glycoprotein (GP) Ib, respectively, allowing for rapid activation via GPVI (Shattil, Kashiwagi and Pampori 1998; Roberts, McNicol and Bose 2004). Upon platelet activation, GPIIb/IIIa (integrin $\alpha_{IIb}\beta_3$) changes conformation to its active form on the platelet surface and binds the blood plasma protein fibrinogen to help meditate platelet-platelet adhesion. Activated platelets release platelet

agonists (e.g., ADP and TxA_2) that activate other platelets in the blood stream, further augmenting the platelet aggregation process (Michelson 2004; Maloney, Brass and Diamond 2010). Vessel injury also exposes tissue factor to the blood, which activates the coagulation cascade to generate thrombin. Thrombin converts the platelet-bound fibrinogen into fibrin to create a fibrin meshwork that solidifies around the platelet aggregate to form a thrombus. However, in the conditions of disease, normal platelet hemostasic function is often disrupted, resulting in bleeding and/or thrombotic complications (Ruggeri 2002; Michelson 2004).

We introduce a platelet function technique that utilizes the physical parameter of platelet concentration in conjunction with volume and mass quantification to assess platelet adhesion and aggregation. Purified platelets are incubated on protein coated glass coverslips under static conditions at physiologically low, normal, or high platelet concentrations to form platelet aggregates. Platelet-substrate and platelet-platelet interactions are visualized using a basic laboratory microscope, and platelet aggregate mass and volume are measured using the HTDIC/NIQPM imaging technique. We have previously used the HTDIC/NIQPM imaging technique to quantify the volume and mass of red blood cells, platelet aggregates, and thrombi (Baker, Phillips and McCarty 2012; Phillips and McCarty 2012, 2012; Phillips, Jacques and McCarty 2012; Baker-Groberg, Phillips and McCarty 2013). Combining HTDIC/NIQPM imaging with static platelet aggregation provides a quantitative platelet aggregation technique that can be used to study platelet function and evaluate the efficacy of antiplatelet therapies.

4.4 Materials and Methods

4.4.1 Human blood collection and platelet purification

Human venous blood was drawn from healthy donors into NaCit and acid citrate dextrose (85 mmol/L sodium citrate, 111 mmol/L glucose, 78 mmol/L citric acid), as previously described (McCarty *et al.* 2005). Platelet-rich plasma was prepared by centrifugation of anticoagulated blood at 200 g for 10 min. Platelets were further purified from platelet-rich plasma by centrifugation at 1000 g in the presence of prostacyclin (0.1 μg/mL). Purified platelets were resuspended in modified HEPES-buffered Tyrode's solution containing 0.1 μg/mL prostacyclin and washed once by centrifugation and resuspension in HEPES-buffered Tyrode's solution at indicated concentrations (Aslan *et al.* 2013).

4.4.2 Static adhesion assay

Glass coverslips (32 mm diameter) were placed in 24 well-plates and coated with 50 μL of fibrinogen (FG; 50 μg/mL; Kordia Laboratory Supplies, Leiden, NL) or fibrillar collagen (100 μg/mL) for 1 hr at 25^{o}C, followed by washing with PBS and blocking with BSA (5 mg/mL, 1 hr at 25^{o}C). Purified platelets were incubated with the FG- or collagen-coated coverslips for 45 min at 37^{o}C at the physiologically low (20,000 platelets/μL), normal (100,000 to 400,000 platelets/μL), or high (500,000 platelets/μL) platelet concentrations (Hanke *et al.* 2010). The coverslips were washed with modified HEPES-buffered Tyrode's solution and fixed with 4% PFA. The samples were mounted onto glass microscope slides with Fluoromount-G. Experiments were repeated using blood from three different donors.

4.4.3 Image acquisition and processing

DIC and bright field z-stack images were taken from the surface of the slide to 5 µm above the platelet aggregates with ×63 magnification. HTDIC and NIQPM analysis was performed to determine volume, mass, and density of platelet aggregates for each region (32 µm by 32 µm; 12 regions per field of view; three fields of view per sample), as described in Chapter 2.

4.5 Results

It was observed that under static conditions, platelets aggregated at the higher platelet concentrations of 400,000 and 500,000 platelets/µL, while platelets only formed microaggregates or single platelet monolayers at the lower concentrations of 20,000 and 100,000 platelets/µL (Figure 4.1 and 4.2).

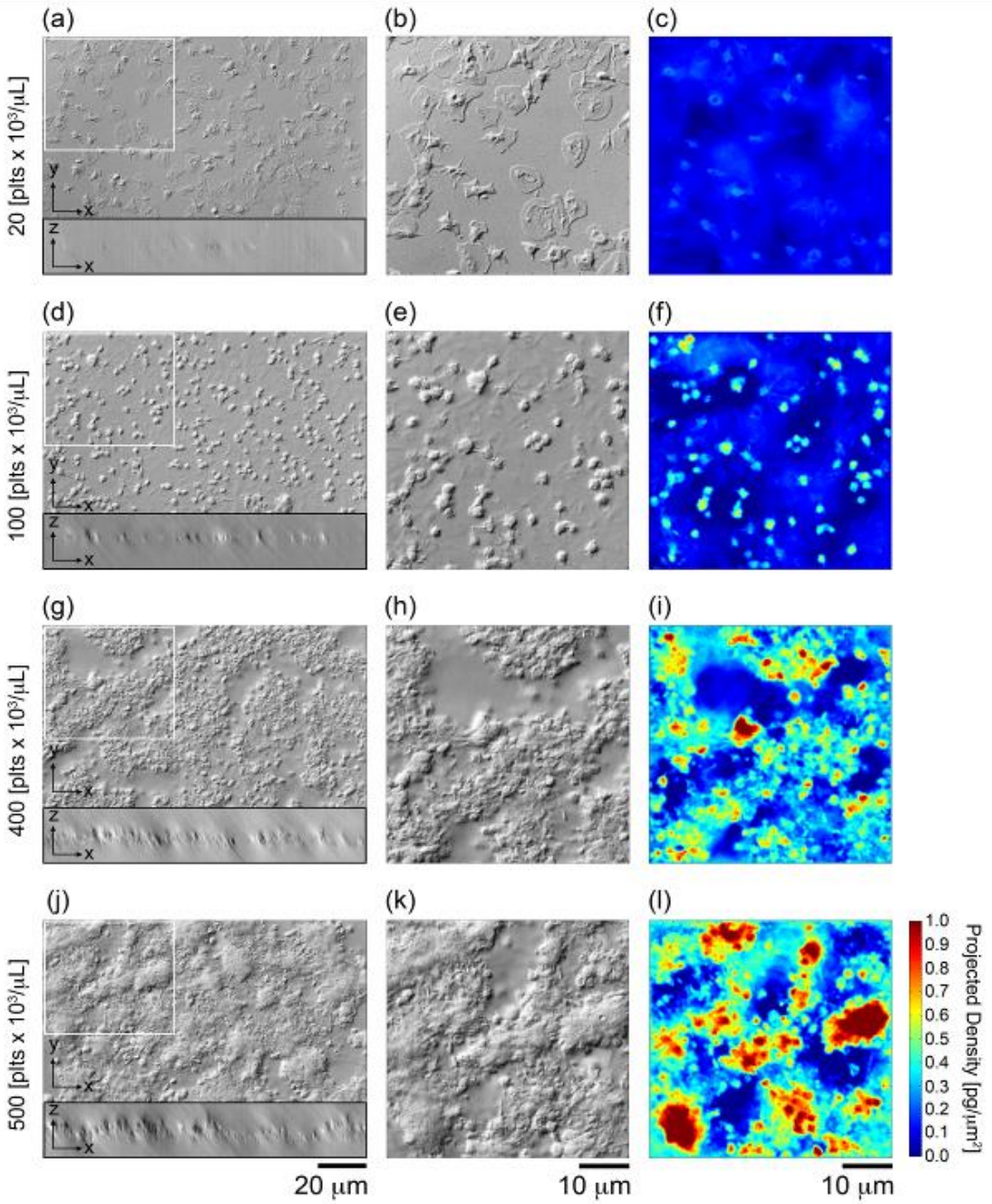

Figure 4.1 Platelet aggregation on fibrinogen-coated surfaces. (a,d,g,j) XY and XZ DIC projections of platelet aggregates formed on fibrinogen-coated coverslips at 20,000, 100,000, 400,000, or 500,000 platelets/μL, respectively. Representative image from 3 independent experiments. (b,e,h,k) Magnified image of region within the white box in (a,d,g,j). (c,f,i,l) Projected density of the white box in (a,d,g,j) determined with the NIQPM technique.

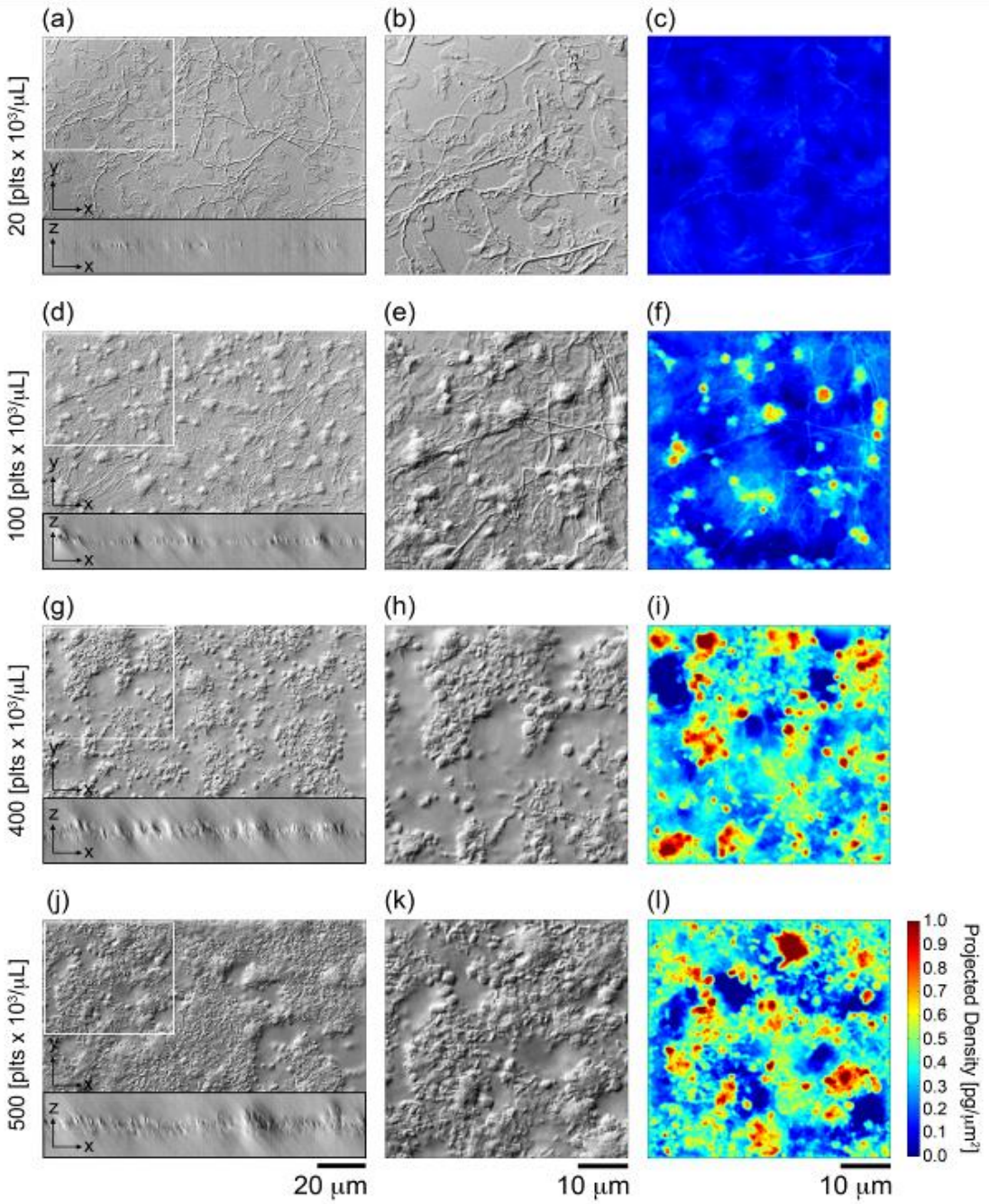

Figure 4.2 Platelet aggregation on collagen-coated surfaces. (a,d,g,j) XY and XZ DIC projections of platelet aggregates formed on fibrillar collagen-coated coverslips at 20,000, 100,000, 400,000, or 500,000 platelets/μL. Representative image from 3 independent experiments. (b,e,h,k) Magnified image of region within the white box in (a,d,g,j). (c,f,i,l) Projected density of the white box in (a,d,g,j) determined with the NIQPM technique.

The mean region volume and mass of platelet aggregates increased with platelet concentration on both the fibrinogen and collagen surfaces (Figure 4.3).

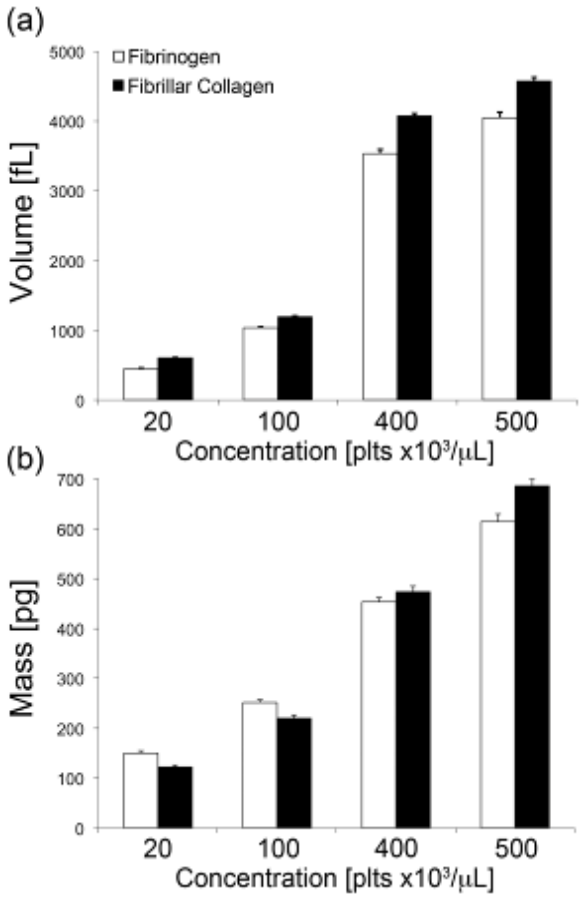

Figure 4.3 Platelet aggregate formation under static conditions as a function of platelet count. Mean platelet aggregate (a) volume and (b) mass for a 32 μm by 32 μm region collected over three trials. Error bars are ± standard error of the mean.

To determine whether our technique could be used to evaluate antiplatelet therapies, platelets were incubated with the GPIIb/IIIa inhibitor, eptifibatide (20 μg/mL; Millennium Pharmaceuticals, Cambridge, MA) for 10 min at 25^{o}C prior to platelet incubation on collagen-coated glass coverslips at platelet concentrations of 400,000 and 500,000 platelets/μL. We found that inhibition of GPIIb/IIIa abrogated platelet

aggregation, resulting in only a monolayer of platelets remaining, accompanied by a significant decrease in the mean region volume and mass as compared to vehicle treatment (Figure 4.4).

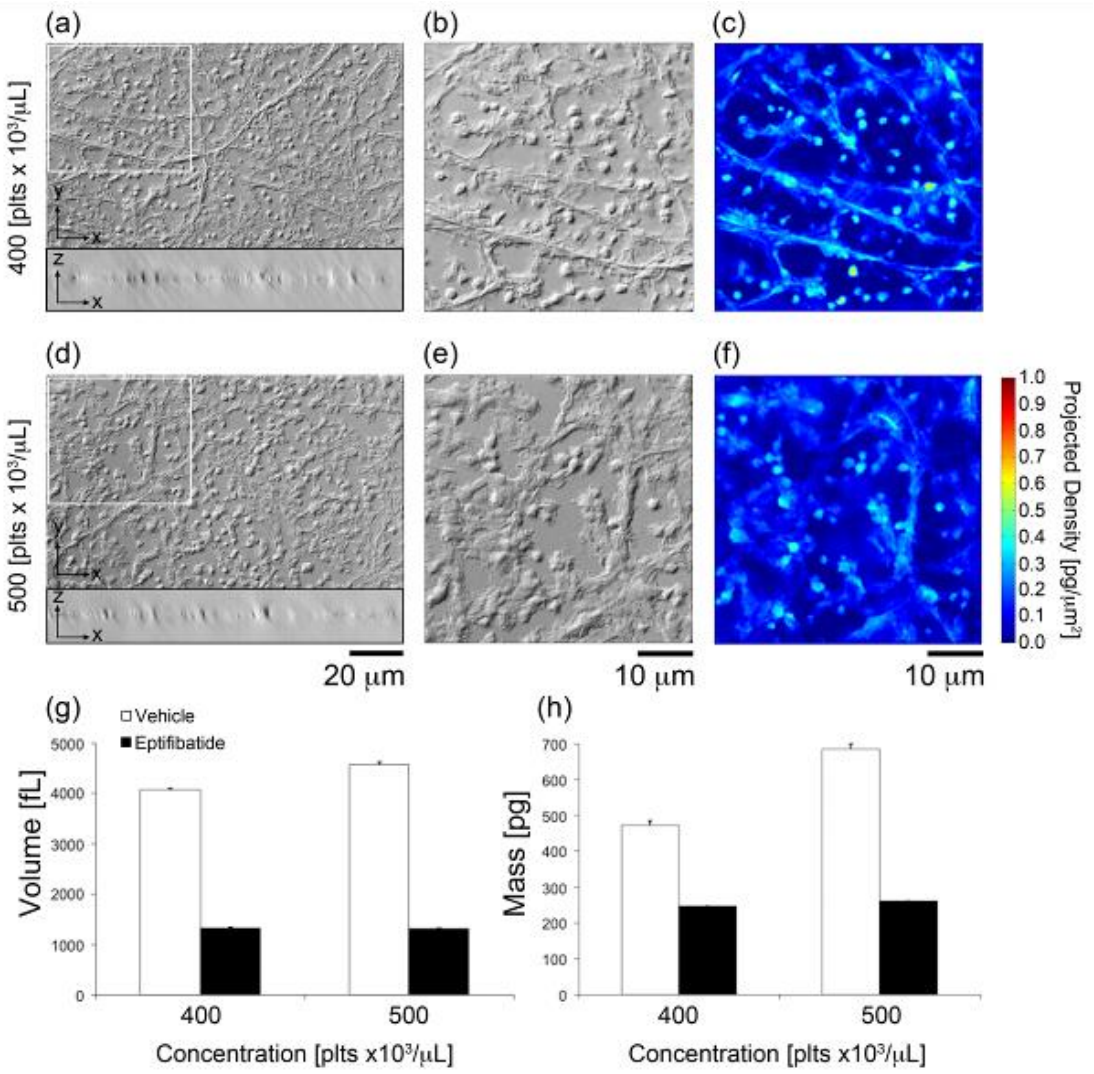

Figure 4.4 Platelets treated with a GPIIb/IIIa inhibitor form platelet monolayers on collagen-coated surfaces. Platelets were incubated with the GPIIb/IIIa inhibitor, eptifibatide (20 µg/mL; 10 min at 25°C), followed by incubation on fibrillar collagen-coated glass coverslips at platelet concentrations of (a,b,c) 400,000 or (d,e,f) 500,000 platelets/µL. (a,d) XY and XZ DIC projections of GPIIb/IIIa-treated platelet aggregates. Representative image from 3 independent experiments. (b,e) Magnified image of region within the white box in (a,d). (c,f) Projected density of the white box in (a,d) determined with the NIQPM technique. Mean platelet aggregate (g) volume and (h) mass for a 32 µm by 32 µm region collected over three trials. Error bars are ± standard error of the mean.

For both the conditions utilizing 400,000 and 500,000 platelets/μL, it is noteworthy that the mean volume and mass of platelets on collagen in the presence of the GPIIb/IIIa inhibitor were comparable to the mean volume and mass of platelets on collagen for 100,000 platelets/μL, where only a confluent monolayer of platelets was observed.

4.6 Discussion

This study describes the use of a novel static platelet aggregation method to quantify platelet aggregation on the single cell level. To the best of our knowledge, this is the first report of the role of platelet count in the induction of platelet-platelet aggregation under static conditions. This method could be used to investigate the mechanisms of platelet-platelet interactions as a function of platelet count in a closed system, where the ADP and TxA_2 feedback pathways may dominate platelet activation. Utilization of our method could provide a quantitative assay to evaluate the efficacy of platelet antagonists that target the ADP and TxA_2 pathways.

Chapter 5: Assessment of Neonatal Platelet Adhesion, Activation, and Aggregation

Sandra M. Baker-Groberg, Susan Lattimore, Michael Recht, Owen J.T. McCarty, and Kristina M. Haley

5.1 Abstract

Both acquired and inherited bleeding disorders may present in the neonatal period and have devastating lifelong effects. Diagnosing bleeding disorders in the neonatal population could aid in providing treatment for bleeding complications. However, currently available platelet function testing is limited in neonates owing to difficulties obtaining adequate blood volume, lack of normal reference ranges, and an incomplete understanding of the neonatal platelet functional phenotype. We aim to develop small-volume, whole blood platelet function assays to quantify and compare neonatal and adult platelet function. Peripheral blood was obtained from healthy, full-term neonates at 24-hours of life. Platelet activation, secretion, and aggregation were measured via flow cytometry. Platelet adhesion and aggregation were assessed under static and flow conditions. As compared to adult platelets, peripheral neonatal platelet P-selectin expression and integrin GPIIb/IIIa activation was significantly reduced in response to the G protein-coupled receptor (GPCR)-agonists thrombin receptor activator peptide (TRAP-6), ADP, and U46619 and the immunoreceptor tyrosine-based activation motif (ITAM)-signaling pathway agonists CRP and rhodocytin. Neonatal platelet aggregation was markedly reduced in response to TRAP-6, ADP, U46619, CRP, and rhodocytin as compared to adult platelets. The extent of neonatal and adult platelet adhesion and

aggregate formation under static and shear conditions on collagen and von Willebrand factor (VWF) were similar. As compared to adult platelets, we found that peripheral neonatal platelet activation and secretion were blunted in response to either GPCR- or ITAM-agonists, while the extent of neonatal platelet adhesion and aggregate formation was similar to adult platelets.

This work is currently under review in the *Journal of Thrombosis and Haemostasis.*

5.2 Introduction

The methods developed in Chapters 3 and 4 were utilized to study primary and secondary hemostasis in healthy adults. However, there are few metrological techniques currently available that can be used to assess platelet function in the neonate population due to blood volume limitations. The lack of functional assays that can be used with neonates hinders the evaluation of platelets in this population as well as the understanding of physiological differences between neonatal and adult platelets. Chapter 5 presents four small volume, whole blood, platelet function assays developed to evaluate neonatal platelet adhesion, activation, and aggregation under static and fluid shear conditions.

5.3 Background

Maintenance of the highly regulated human hemostatic system is dependent on the delicate balance of the pro- and anticoagulant systems of primary and secondary hemostasis and fibrinolysis. At sites of vascular injury, primary hemostasis is initiated

when platelets are recruited to extracellular matrix proteins in the basement membrane through binding of the platelet glycoprotein (GP) Ib complex to collagen-bound von Willebrand factor (VWF), allowing for adhesion via platelet $\alpha_2\beta_1$ and GPIIb/IIIa integrins (Wei *et al.* 2009). Following platelet adhesion, intracellular signaling downstream of the immunoreceptor tyrosine-based activation motif (ITAM) containing receptor, GPVI, results in rapid calcium mobilization, granule release, cytoskeletal reorganization, platelet spreading to increase surface area, and release of the secondary mediators, adenosine 5'-diphosphate (ADP) and thromboxane A_2 (TxA_2), which activate platelets downstream of the G-protein coupled receptors (GPCRs) $P2Y_{12}$ and $P2Y_1$ and TxA_2 receptor, respectively (Del Vecchio, Motta and Romagnoli). Upon platelet activation, the GPIIb/IIIa complex undergoes a conformational change into its high affinity state, allowing for binding of fibrinogen, VWF, and fibronectin (Kühne and Imbach 1998). Platelets aggregate together via GPIIb/IIIa-fibrinogen interactions to form a platelet plug. Furthermore, phosphatidylserine is exposed on the platelet surface following activation, facilitating the assembly and activation of coagulation factors. Concomitant with primary hemostasis is the activation of the coagulation cascade, resulting in the generation of thrombin, which in turn activates platelets via the GPCRs PAR1/4 and cleaves fibrinogen into fibrin around the platelet plug to firmly establish a hemostatic plug.

The neonatal hemostatic system is developmentally regulated, and significant differences exist between the adult and neonatal hemostatic system. Discrepancies in the secondary hemostatic system have been fairly well-defined. Age-specific reference values for the pro- and anticoagulant proteins are available. Delineating whether differences exist

between the neonatal and adult primary hemostatic system has been problematic. Neonatal platelet number and structure does not differ from adult platelet number and structure (Israels, Rand and Michelson 2003; Haley, Recht and McCarty 2014). Yet, neonatal platelet function is thought to be distinct from adult platelet function (Ferrer-Marin *et al.* 2013). The neonatal platelet functional phenotype has largely been inferred from studies with samples derived from cord blood. However, it is unclear whether platelets isolated from cord blood are functionally similar to platelets derived from peripheral blood (Saxonhouse *et al.* 2010). Currently available evidence indicates that neonatal platelets have decreased response to platelet agonists, decreased granule secretion, decreased fibrinogen binding, and decreased platelet aggregation (Del Vecchio, Motta and Romagnoli; Israels *et al.* 1999; Sola-Visner 2012). This hypo-reactivity is believed to persist for up to several weeks after delivery (Strauss, Sidlik-Muskatel and Kenet 2011). Despite these differences, bleeding times and PFA-100 closure times in healthy full-term neonates have been reported as shorter than in adults, suggesting more effective primary hemostasis (Roschitz *et al.* 2001).

Despite the characterization of their hemostatic system as immature, healthy full-term newborns are functionally hemostatic. However, premature and sick newborns often present with comorbid disruptions in their hemostatic system, with a relatively high incidence of thrombocytopenia and coagulopathy leading to potentially life-threatening bleeding (Sola-Visner 2012). Improved understanding of the functional phenotype of neonatal platelets is needed in order to determine age-based reference values as well as the role of potential platelet hypo-reactivity in pathological bleeding. New platelet

function tests are needed that can be easily employed in the neonatal population. Currently, the blood volume required to perform platelet aggregation testing presents challenges and the role of the other hemostatic components on platelet function has not been assessed. We have developed four small-volume, whole blood, platelet function assays to allow for the assessment of the functional phenotype of neonatal platelets in their natural milieu, allowing for comparison to adult platelets.

5.4 Materials and Methods

5.4.1 Adult and neonate whole blood collection

Adult venous blood was collected from healthy volunteers in accordance with an Oregon Health & Science University Institutional Review Board approved protocol into trisodium citrate (0.38% w/v; Sigma-Aldrich, St Louis, MO). 500 - 1000 µL of blood from healthy, full-term (> 38 weeks gestation) neonates who were in the newborn nursery and receiving no medications was collected via heel stick into trisodium citrate (0.38% w/v) at 24-hours of life in accordance with an Oregon Health & Science University Institutional Review Board approved protocol. Neonates in the newborn intensive care unit were excluded from participation.

5.4.2 Platelet and white blood cell (WBC) quantification assay

2.5 µL of adult or neonatal citrated whole blood was diluted 1:10 with HEPES-buffered Tyrode's solution (136 mM NaCl, 2.7 mM KCl, 10 mM HEPES, 2 mM $MgCl_2$, 2 mM $CaCl_2$, 5.6 mM glucose, 0.1% bovine serum albumin; pH 7.45), added to a fluorescence-activated cell sorting (FACS) tube containing antibodies CD41-FITC (1:100; BioLegend,

San Diego, CA) and CD45-APC (1:100; BD Biosciences, San Jose, CA), and incubated at 25˚C for 20 min. BD Cytofix Fixation Buffer (1:3; BD Biosciences) was added to the FACS tube and incubated for 5 min at 25˚C. The sample was then diluted 1:100 with PBS, measured by FACS (BD FACSCanto II Flow Cytometer; BD Biosciences), and analyzed using Flowing 2.5.1 software (Perttu Terho and Turku Bioimaging, Turku, Finland). The percentage of events positive for CD41-FITC or CD45-APC was quantified by FACS to enumerate platelets and white blood cells (WBCs).

5.4.3 Platelet activation assay

A volume of 2.5 µL of adult or neonatal citrated whole blood was diluted 1:10 with HEPES-buffered Tyrode's solution, added to FACS tubes containing the antibodies PAC-1-FITC (1:100; BD Biosciences) or CD62P-APC (1:100; Acris Antibodies, Herford, Germany) and either thrombin receptor activator 6 (TRAP-6; 10 µM; Tocris Bioscience, Bristol, UK), ADP (10 µM; Sigma-Aldrich), TxA_2 receptor agonist (U46619; 10 µM; Tocris Bioscience), collagen-related peptide (CRP; 10 µg/mL; kind gift from Dr. Richard Farndale, Cambridge, UK), epinephrine (10 µM; Chrono-Log, Havertown, PA), rhodocytin (300 nM; kindly provided by Dr. Johannes Eble, Muenster, Germany), calcium ionophore A23187 (10 µM; Sigma-Aldrich), or vehicle, and incubated for 20 min at 25˚C. BD Cytofix Fixation Buffer (1:3) was added to each FACS tube and incubated at 25˚C for 5 min. Samples were diluted 1:100 with PBS, measured by FACS (BD FACSCanto II Flow Cytometer), and analyzed using Flowing 2.5.1 software. The platelet gate was determined by CD41-FITC positive events measured in the platelet and WBC quantification assay. This assay required a total of 25 µL whole blood.

5.4.4 Platelet aggregation assay

A volume of 150 µL of adult or neonatal citrated whole blood was treated with D-phenylalanyl-L-prolyl-L-arginine chloromethyl ketone (PPACK; 40 µM; Haematologic Technologies, Essex Junction, VT) and split evenly into two aliquots. Each aliquot was centrifuged at 1000 g for 5 min. Plasma was removed and stored at 25˚C. Each sample was re-suspended with 75 µL of HEPES-buffered Tyrode's solution and incubated with antibodies CD45-APC (1:100) and either CD31-eFluor 450 or CD31-FITC (1:100; eBioscience, San Diego, CA) for 15 min at 25˚C, followed by centrifugation at 1000 g for 5 min. The supernatants were discarded and the pelleted blood samples were re-suspended in reserved plasma in order to maintain donor plasma fibrinogen levels. The aliquots were combined and 10 µL of the sample was added to microfuge tubes containing TRAP-6 (10 µM), ADP (10 µM), U46619 (10 µM), CRP (10 µg/mL), epinephrine (10 µM), ristocetin (1 mg/mL; Chrono-Log), rhodocytin (300 nM), calcium ionophore (10 µM), or vehicle in a BioShake iQ shaker plate (Quantifoil Instruments GmbH, Jena, Germany) rotating at 1000 rpm and heated to 37˚C. In select experiments, blood samples were pretreated with a GPIIb/IIIa inhibitor (eptifibatide; 20 µg/mL; Millennium Pharmaceuticals, Cambridge, MA), a monoclonal antibody directed against GPIb (6D1; 20 µg/mL; kindly provided by Dr. Barry Coller, New York, NY), or vehicle for 10 min at 25˚C prior to agonist incubation. At 0, 0.5, 1, 2, and 5 min after agonist treatment, 1 µL of the sample was removed and diluted 1:200 with 12.5% BD Cytofix Fixation Buffer in PBS. Samples were measured by FACS (BD FACSCanto II Flow Cytometer) and analyzed using Flowing 2.5.1 software. The rate and degree of platelet aggregation was determined by quantifying double-colored CD31 events at each time

point, as adapted from the method used by De Cuyper *et. al.* (De Cuyper *et al.* 2013). In order to distinguish platelet-platelet interactions from platelet-WBC interactions, CD45 positive events were excluded from the platelet aggregation analysis. This assay required 150 µL of whole blood.

5.4.5 Static platelet adhesion and aggregation assay

5 mm diameter circles were drawn on rectangular glass coverslips (No. 1.5, 22 × 50 mm; Corning Inc., Corning, NY) using a PAP pen (Life Technologies, Eugene, OR). Coverslips were coated with fibrillar equine Type I collagen (100 µg/mL; Chrono-Log) or human VWF (100 µg/mL; Haematologic Technologies) for 1 hr at 25˚C, followed by washing with PBS. Protein-coated coverslips were then blocked with fatty acid free bovine serum albumin (BSA; 5 mg/mL; Sigma-Aldrich) for 1 hr at 25˚C and washed with PBS. 10 µL of citrated whole blood was incubated with TRAP-6 (10 µM), ADP (10 µM), U46619 (10 µM), CRP (10 µg/mL), epinephrine (10 µM), ristocetin (1 mg/mL), rhodocytin (300 nM), calcium ionophore (10 µM), or vehicle for 10 min at 25˚C. In select experiments, blood samples were pretreated with eptifibatide (20 µg/mL), 6D1 (20 µg/mL), or vehicle for 10 min at 25˚C prior to agonist treatment. 5 µL of agonist-treated blood was added to VWF- or collagen-coated coverslip circles and incubated for 30 min at 25˚C. Coverslips were washed with HEPES-buffered Tyrode's solution and treated with a staining solution containing antibodies CD41a-PE (1:100; eBioscience) and CD62P-FITC (1:100; BioLegend) for 10 min at 25˚C. Coverslips were washed and fixed with 4% PFA and Hoechst 33342 (1:1000; Life Technologies) for 10 min at 25˚C. Coverslips were washed again and mounted onto glass slides using Fluoromount-G

(SouthernBiotech, Birmingham, AL). Slides were imaged using a ×63 oil-coupled, 1.4 numerical aperture objective and an upright Zeiss Axio Imager.M2 microscope (Carl Zeiss MicroImaging GmbH, Gottingen, Germany). Through-focus transverse differential interference contrast (DIC) images of the samples were separated by a 0.1 μm axial increment while the microscope was operated under the control of SlideBook 5.5 software (Intelligent Imaging Innovations, Denver, CO). Volume measurements were obtained using the custom Hilbert transform DIC (HTDIC) program written in MATLAB (MathWorks, Natick, MA), as previously described (Baker, Phillips and McCarty 2012; Baker-Groberg *et al.* 2015). This assay required 100 μL of whole blood.

5.4.6 Flow chamber assay

Small-volume flow chambers (μ-Slide VI0.1; Ibidi GmbH, Munich, Germany) were coated with fibrillar collagen (100 μg/mL) or VWF (100 μg/mL) for 1 hr at 25˚C, followed by washing with PBS. Protein-coated flow chambers were blocked with BSA (5 mg/mL) for 1 hr at 25˚C and washed with PBS. Coated flow chambers were assembled onto the stage of an inverted Zeiss Axiovert 200M microscope (Carl Zeiss MicroImaging GmbH). Citrated whole blood was perfused through collagen- or VWF-coated flow chambers at shear rates of 200 s^{-1} (9.4 μL of blood per chamber) or 1500 s^{-1} (70.3 μL of blood per chamber) for 30 sec using a pulse-free syringe pump. In select experiments, blood samples were pretreated with eptifibatide (20 μg/mL), 6D1 (20 μg/mL), or vehicle for 10 min at 25˚C prior to perfusion. Flow chambers were washed with HEPES-buffered Tyrode's solution for 5 min to remove unbound blood components and stained with antibodies CD41a-PE and CD62P-FITC (1:100) for 5 min at the same shear rate.

Samples were fixed with 4% PFA and stained with Hoechst 33342 (1:1000) for 5 min at the same shear rate, followed by washing with HEPES-buffered Tyrode's solution. DIC and fluorescent images were acquired using SlideBook 5.5 software. Percent surface area coverage of CD41a positive cells in a 140 × 105 μm field of view was analyzed using ImageJ 1.48v software (National Institutes of Health, Bethesda, MD). This assay required 200 μL of whole blood.

5.5 Results

5.5.1 Quantification of neonatal platelets and white blood cells

The mean percentage of events positive for CD41-FITC (binds GPIIb) or CD45-APC for neonatal and adult samples are listed in Table 5.1. Neonatal samples contained a higher percentage of CD45-APC positive events (white blood cells) as compared with adult samples. Equivalent percentages of CD41-FITC positive events (platelets) were observed for neonatal and adult samples.

Table 5.1 Percentage of events positive for CD41-FITC or CD45-APC of adult and neonate whole blood samples measured by fluorescence-activated cell sorting (FACS).

Antibody	Adult (%)	Neonate (%)
CD41-FITC	2.3 ± 1.07	2.9 ± 1.09
CD45-APC	0.6 ± 0.14	2.0 ± 0.83*
Unlabeled (RBCs)	97.1 ± 1.16	95.2 ± 1.90

Data are represented as mean ± SEM, n ≥ 3; *denotes $P < 0.05$ with respect to adult samples

5.5.2 Measurement of neonatal platelet activation and secretion

In order to evaluate platelet activation, a small-volume, whole blood, platelet activation assay was utilized to assess the binding of PAC-1-FITC (binds to activated GPIIb/IIIa) or CD62P-APC (P-selectin antibody) to adult or neonatal platelets in response to platelet agonists. We first used adult platelets in order to standardize our assays. Consistent with previous reports, adult platelets expressed significantly increased levels of P-selectin and activated GPIIb/IIIa in response to the GPCR-agonists TRAP-6, epinephrine, ADP (binds receptors $P2Y_1$ and $P2Y_{12}$), U46619 (TxA_2 receptor agonist), a combination of ADP and U46619, the ITAM-mediated signaling pathway agonists CRP (GPVI ligand) or rhodocytin (CLEC-2 ligand), or a calcium ionophore (Figure 5.1G&H).

We next investigated the responsiveness of neonatal platelets to platelet agonists. Our results show that neonatal platelets increased their expression of the active form of GPIIb/IIIa in response to ADP, U46619, the combination of ADP and U46619, epinephrine, CRP, rhodocytin, or a calcium ionophore (Figure 5.1G). However, the degree of GPIIb/IIIa activation was markedly blunted for neonatal platelets as compared to adult platelets at equimolar agonist concentrations, with neonatal platelets being unresponsive to stimulation with TRAP-6.

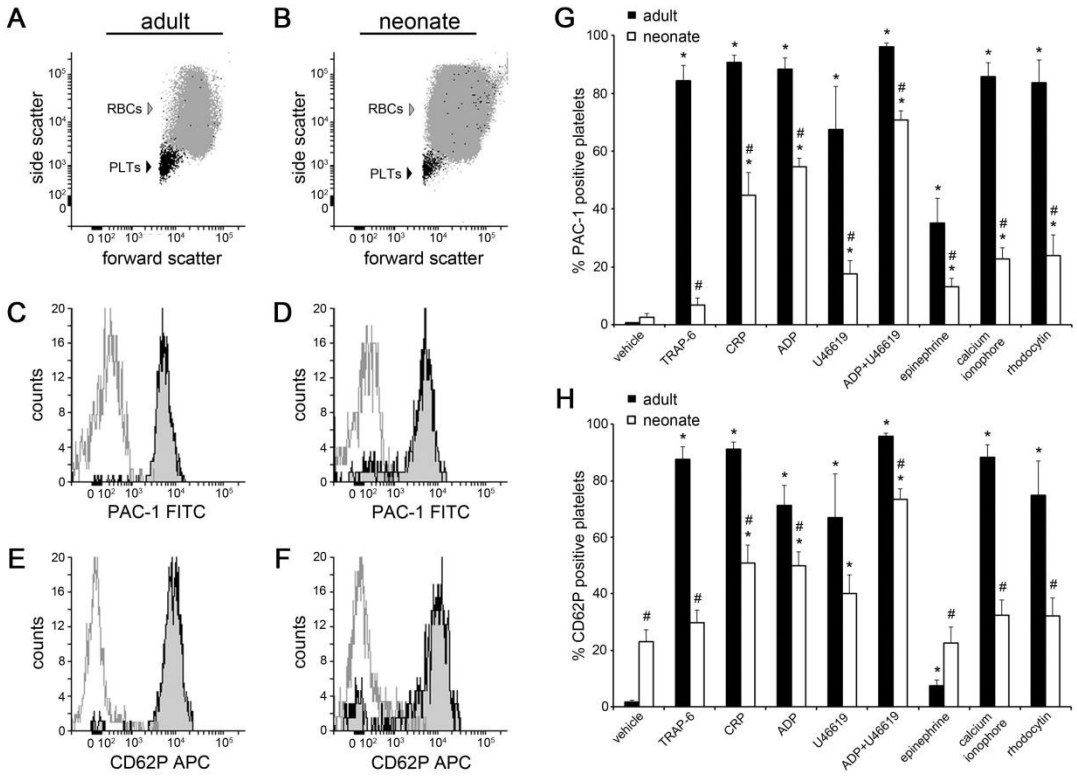

Figure 5.1 Adult and neonatal whole blood platelet activation. Representative flow cytometry forward and side scatter dot plots of a whole blood sample from an adult (A) and a neonate (B). Representative histograms of PAC-1-FITC (C and D) and CD62P-APC (E and F) fluorescence intensity of adult and neonatal whole blood treated with ADP + U46619 (10 µM; black line) or vehicle (gray line). Percent of platelets positive for PAC-1-FITC (G) and CD62P-APC (H) in response to TRAP-6 (10 µM), CRP (10 µg/mL), ADP (10 µM), U46619 (10 µM), ADP+U46619 (10 µM), epinephrine (10 µM), calcium ionophore (10 µM), rhodocytin (300 nM), or vehicle treatment. Data are represented as mean ± SEM, n ≥ 3. *denotes $P < 0.05$ compared with vehicle treated samples. #denotes $P < 0.05$ compared with adult samples.

We next examined the ability of agonists to induce neonatal platelet secretion, as measured by P-selectin expression. Our results show that the basal expression of P-selectin was significantly higher for neonatal platelets as compared to adult platelets. The expression levels of neonatal platelet P-selectin significantly increased in response to ADP, U46619, the combination of ADP and U46619, and CRP (Figure 5.1H). Similar to the trend observed for GPIIb/IIIa activation, the increase in P-selectin expression was

markedly blunted for neonatal platelets as compared to adult platelets at equimolar agonist concentrations. Moreover, stimulation of neonatal platelets with TRAP-6, epinephrine, a calcium ionophore, or rhodocytin failed to increase the P-selectin expression levels above baseline.

5.5.3 Quantification of neonatal platelet aggregation and agglutination

We next employed a small-volume, whole blood, platelet aggregation and agglutination assay to measure and compare adult and neonatal platelet aggregation in response to GPCR- and ITAM-agonists. Two populations of platelets that had been labeled with a red or green fluorescent anti-CD31 antibody in whole blood were mixed together, and the degree of double-labeled events was quantified as a function of time following stimulation. Our results show that both adult and neonatal platelets aggregated in response to the GPCR-agonists TRAP-6, ADP, U46619, the combination of ADP and U46619, and the ITAM-signaling pathway agonist CRP (Figure 5.2). However, it is noteworthy that the degree of platelet aggregation, as measured by the percent of double-labeled events and reported as fold-change relative to baseline, was dramatically reduced for neonatal samples as compared to adult samples for these agonists. Moreover, only adult platelets were observed to aggregate in response to either epinephrine or rhodocytin. In contrast, equivalent levels of adult and neonatal platelet agglutination were observed in response to ristocetin (Figure 5.2E). For both adult and neonatal samples, platelet aggregation in response to TRAP-6, CRP, and the combination of ADP and U46619 was eliminated in the presence of a GPIIb/IIIa-function blocking antibody, while an anti-GPIb blocking antibody blocked ristocetin-induced agglutination (Table 5.2).

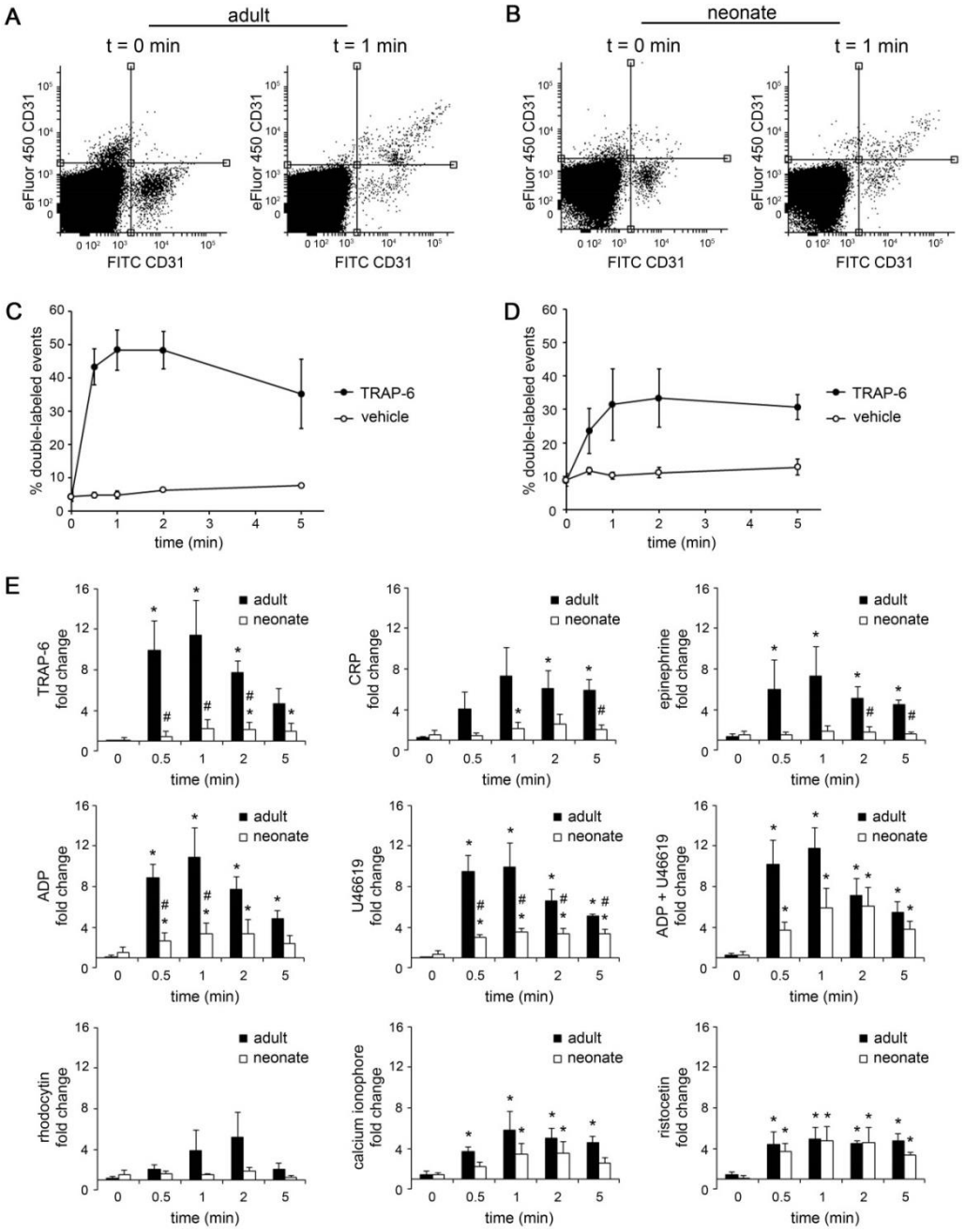

Figure 5.2 Adult and neonatal whole blood platelet aggregation. Representative CD31-FITC and CD31-eFluor 450 dot plots of adult (A) and neonate (B) blood at t = 0 (left) and t = 1 min (right) after treatment with TRAP-6 (10 µM). Double-labeled events (platelet aggregates) are shown in the upper right quadrant. Representative graph of percent double-labeled events of adult (C) and neonate (D) platelets stimulated with TRAP-6 (10 µM) or vehicle at 0, 0.5, 1, 2, and 5 min. (E) Fold change of percent double-labeled events normalized to vehicle treatment of adult and neonate blood stimulated with TRAP-6 (10 µM), CRP (10 µg/mL), epinephrine (10 µM), ADP (10 µM), U46619 (10 µM), ADP+U46619 (10 µM), rhodocytin (300 nM), calcium ionophore (10 µM), or ristocetin (1 mg/mL). Data are represented as mean ± SEM, n ≥ 3. *denotes $P < 0.05$ compared with vehicle treated samples. #denotes $P < 0.05$ compared with adult samples.

Table 5.2 Effect of GPIIb/IIIa and GPIb inhibition on adult and neonate platelet aggregation.

Agonist	Antagonist	Adult	Neonate
TRAP-6	vehicle	4.6 ± 1.55	1.9 ± 0.83**
	eptifibatide	0.8 ± 0.12*	0.6 ± 0.37*
	6D1	6.4 ± 3.71	2.3 ± 0.75**
CRP	vehicle	5.9 ± 1.08	2.0 ± 0.48**
	eptifibatide	2.2 ± 1.33*	0.7 ± 0.26*,**
	6D1	7.3 ± 3.86	3.4 ± 1.71**
ADP + U46619	vehicle	5.5 ± 0.99	3.8 ± 0.84**
	eptifibatide	3.1 ± 1.82*	0.8 ± 0.46*,**
	6D1	6.0 ± 1.76	5.4 ± 1.90
Ristocetin	vehicle	4.7 ± 0.74	3.3 ± 0.32
	eptifibatide	4.1 ± 1.36	4.5 ± 1.75
	6D1	1.3 ± 0.19*	2.3 ± 0.87*,**

Blood samples were treated with agonists for 5 min at 37°C. Data are represented as mean fold change of percent double-labeled events normalized to vehicle ± SEM, $n \geq 3$; *denotes $P < 0.05$ with respect to vehicle; **denotes $P < 0.05$ with respect to adult samples.

5.5.4 Measurement of neonatal platelet adhesion and aggregate formation under static conditions

A small-volume, whole blood, static platelet adhesion and aggregation assay was developed to quantify neonatal platelet adhesion. Our results show that both adult and neonatal platelets bound to immobilized VWF (Figure 5.3A) or collagen (Figure 5.3B). When whole blood was treated with the agonists TRAP-6, ADP, U46619, the combination of ADP and U46619, CRP, or a calcium ionophore, both adult and neonatal platelets were observed to form aggregates on immobilized VWF and collagen, as observed by both DIC imaging (Figure 5.3A&B) and quantified as the volume per platelet aggregate (Figure 5.3C&D).

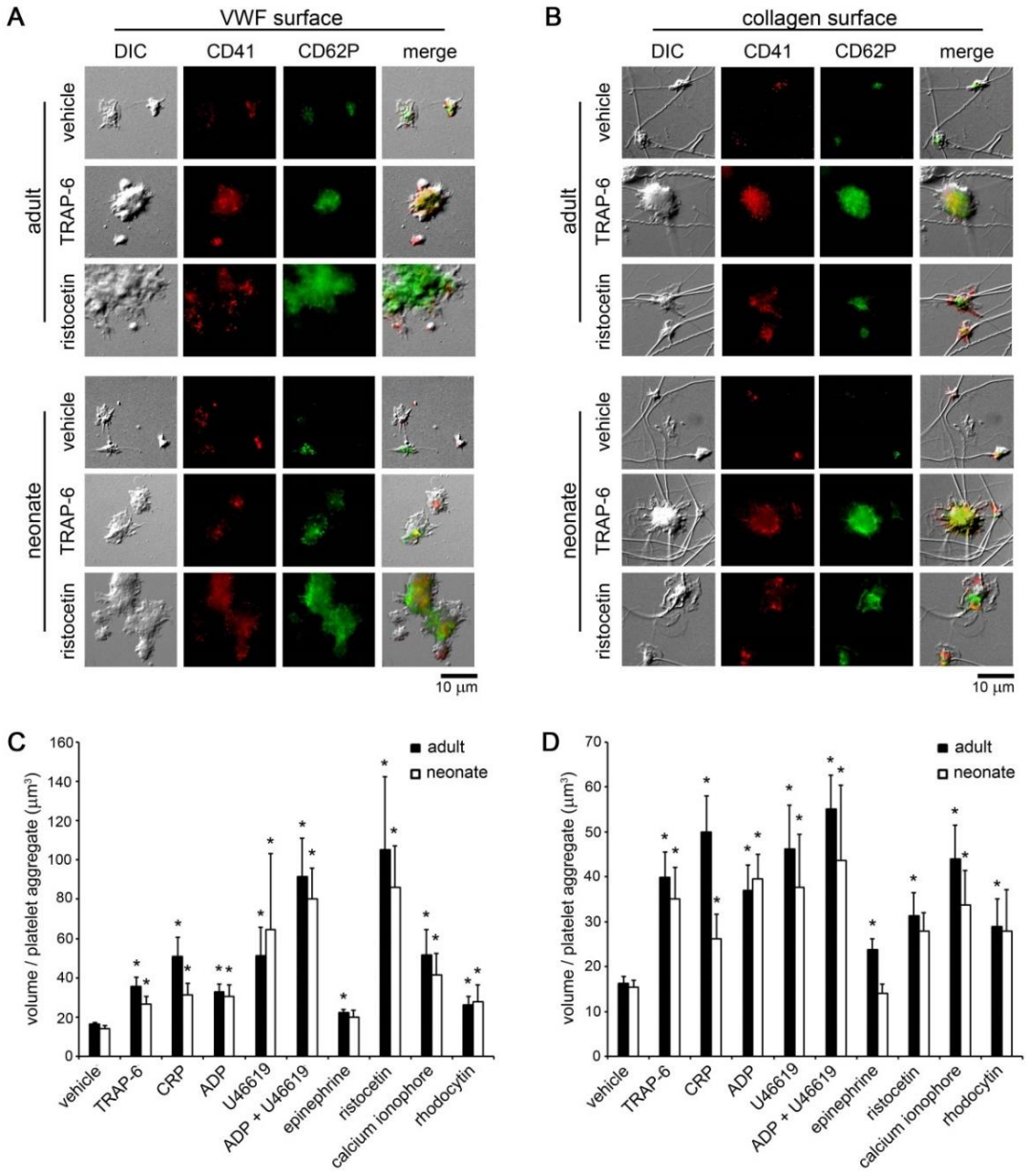

Figure 5.3 Adult and neonate platelet adhesion and aggregation under static conditions. Representative DIC images and corresponding fluorescent CD41a-PE and CD62P-FITC images of adult and neonate platelet aggregates formed on coverslips coated with 100 µg/mL VWF (A) or 100 µg/mL fibrillar collagen (B). Adult and neonate citrated whole blood were pretreated with vehicle, TRAP-6 (10 µM), CRP (10 µg/mL), ADP (10 µM), U46619 (10 µM), ADP+U46619 (10 µM), epinephrine (10 µM), ristocetin (1 mg/mL), calcium ionophore (10 µM), or rhodocytin (300 nM) for 10 min prior to coverslip incubation. Mean volume of adult and neonate platelet aggregates positive for CD62P-FITC formed on coverslips coated with VWF (C) or fibrillar collagen (D). Data are represented as mean ± SEM, n ≥ 3. *denotes $P < 0.05$ compared with vehicle treated samples.

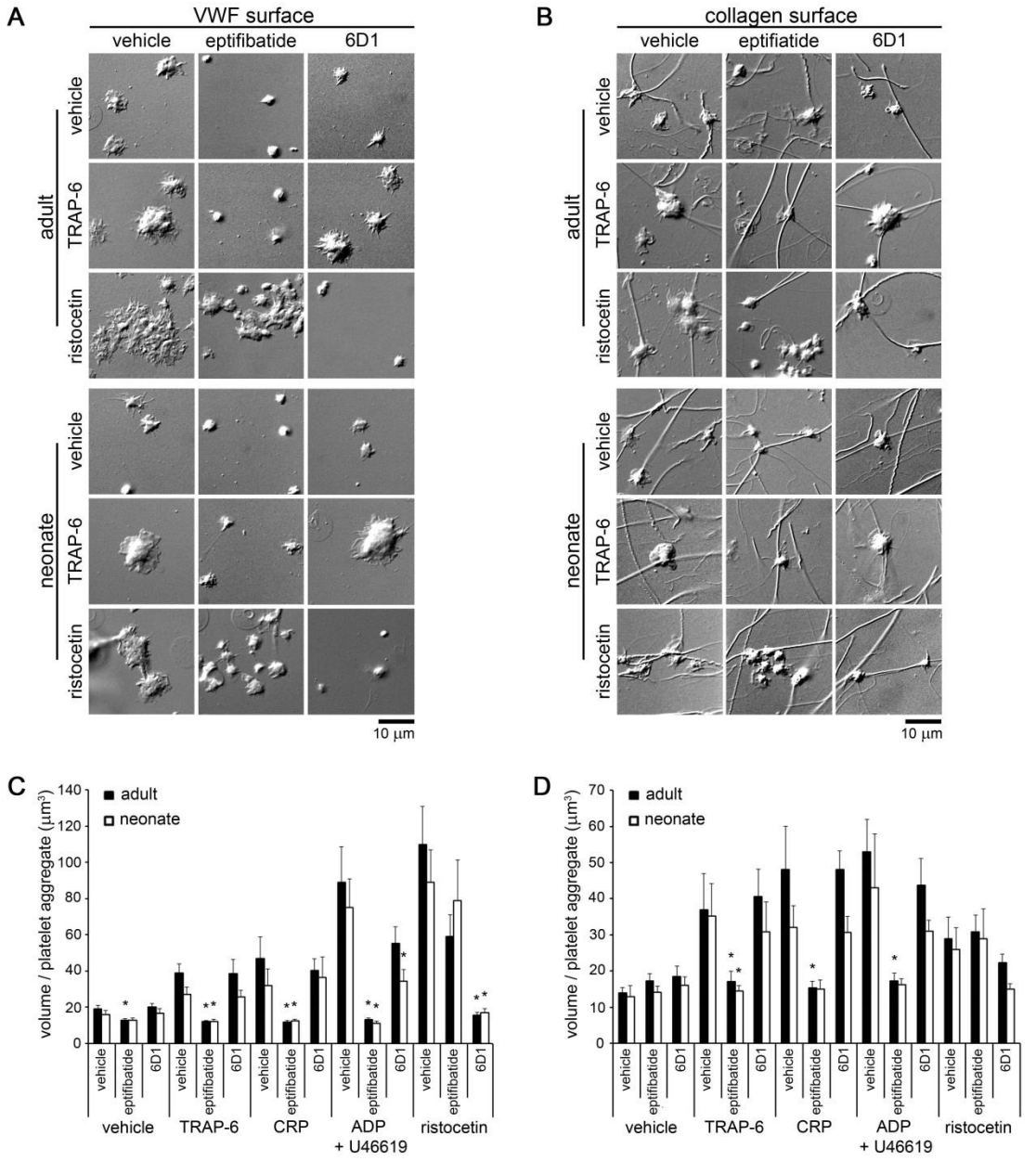

Figure 5.4 Effect of GPIIb/IIIa and GPIb inhibition on adult and neonate platelet adhesion and aggregation under static conditions. Representative DIC images of adult and neonate platelet aggregates formed on coverslips coated with 100 µg/mL VWF (A) or 100 µg/mL fibrillar collagen (B). Adult and neonate citrated whole blood were incubated with a GPIIb/IIIa inhibitor (eptifibatide; 20 µg/mL), a GPIb function blocking antibody (6D1; 20 µg/mL), or vehicle for 10 min at 25°C and then treated with TRAP-6 (10 µM), CRP (10 µg/mL), ADP+U46619 (10 µM), ristocetin (1 mg/mL), or vehicle for 10 min. Mean volume of adult and neonate platelet aggregates positive for CD62P-FITC formed on coverslips coated with VWF (C) or fibrillar collagen (D). Data are represented as mean ± SEM, n ≥ 3. *denotes $P < 0.05$ compared with vehicle treated samples.

Moreover, both adult and neonatal platelet aggregates were observed to increase their P-selectin expression levels. Equivalent levels of platelet adhesion, P-selectin expression, and aggregate formation in response to either GPCR- or ITAM-signaling pathway agonists were observed for both adult and neonatal samples, with the exception of a reduction in neonatal platelet aggregation formation on collagen following stimulation with either epinephrine or CRP as compared to adult platelets. Both adult and neonatal platelet aggregate formation on VWF and collagen in response to TRAP-6, CRP, or the combination of ADP and U46619 was eliminated in the presence of a function-blocking anti-GPIIb/IIIa antibody, whereas the robust ristocetin-induced platelet agglutinate formation observed on VWF was eliminated by a GPIb-blocking antibody (Figure 5.4).

5.5.5 Measurement of neonatal platelet aggregate formation under shear

We next developed a small-volume assay to study and compare adult or neonatal platelet aggregate formation on collagen and VWF under both venous and arterial shear rates. We observed that both adult and neonatal platelets bound to and aggregated on VWF or collagen surfaces in a shear rate-dependent manner, with an increased degree of aggregate formation observed at the higher shear rate (Figure 5.5). Both the rate and extent of aggregate formation were equivalent for adult and neonatal samples. Adult and neonatal platelet aggregate formation on collagen was eliminated in the presence of a function-blocking anti-GPIIb/IIIa antibody, whereas a GPIb-blocking antibody eliminated platelet adhesion to VWF under shear (Figure 5.6).

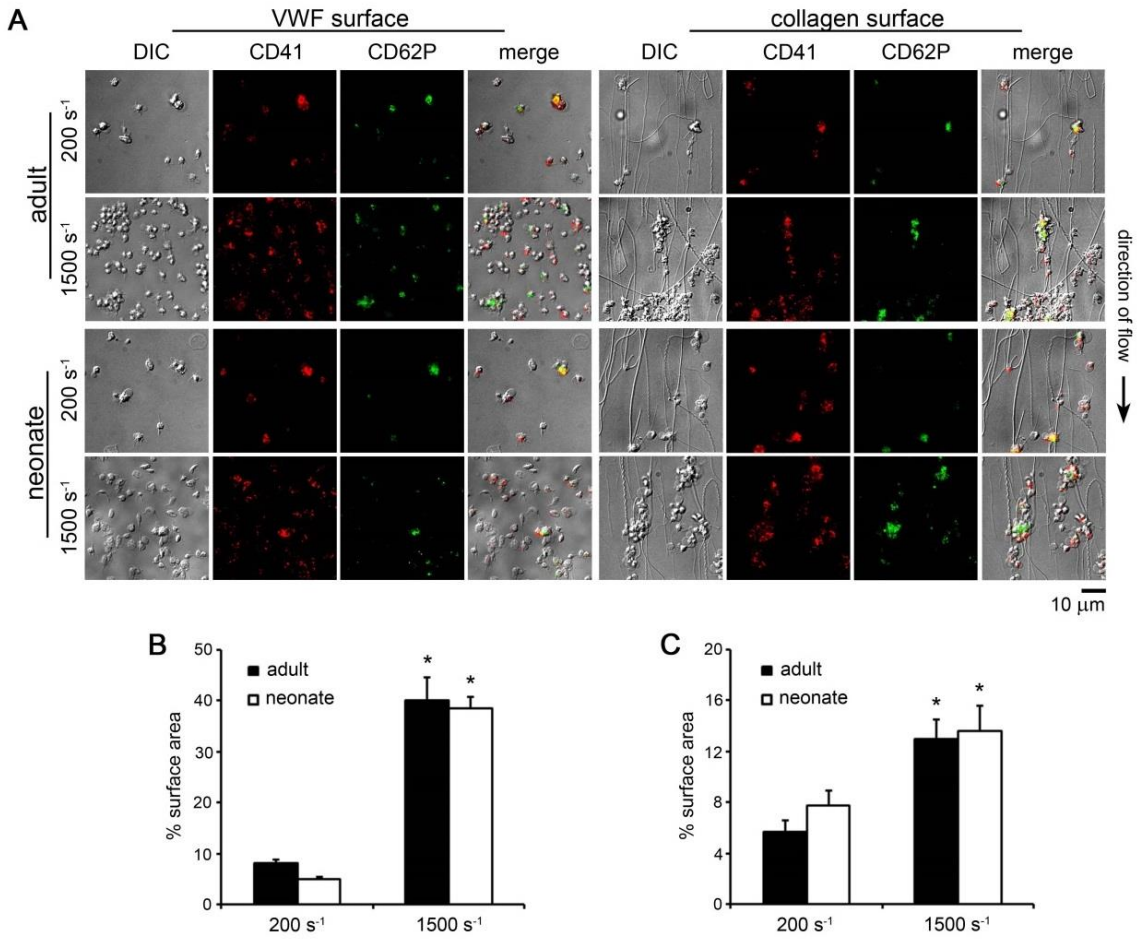

Figure 5.5 Adult and neonatal platelet adhesion and aggregation under fluid shear conditions. (A) Representative DIC images and corresponding fluorescent CD41a-PE and CD62P-FITC images of adult and neonate platelet aggregates formed in a small volume flow chamber coated with 100 µg/mL VWF or 100 µg/mL fibrillar collagen at 200 or 1500 s^{-1} shear rate for 30 sec. The black arrow denotes direction of blood flow. Mean percent surface area coverage of a 140 × 105 µm field of view of adult and neonate platelet aggregates positive for CD41a-PE formed in flow chambers coated with VWF (B) or collagen (C). Data are represented as mean ± SEM, n ≥ 3. *denotes $P < 0.05$ compared with 200 s^{-1} shear rate.

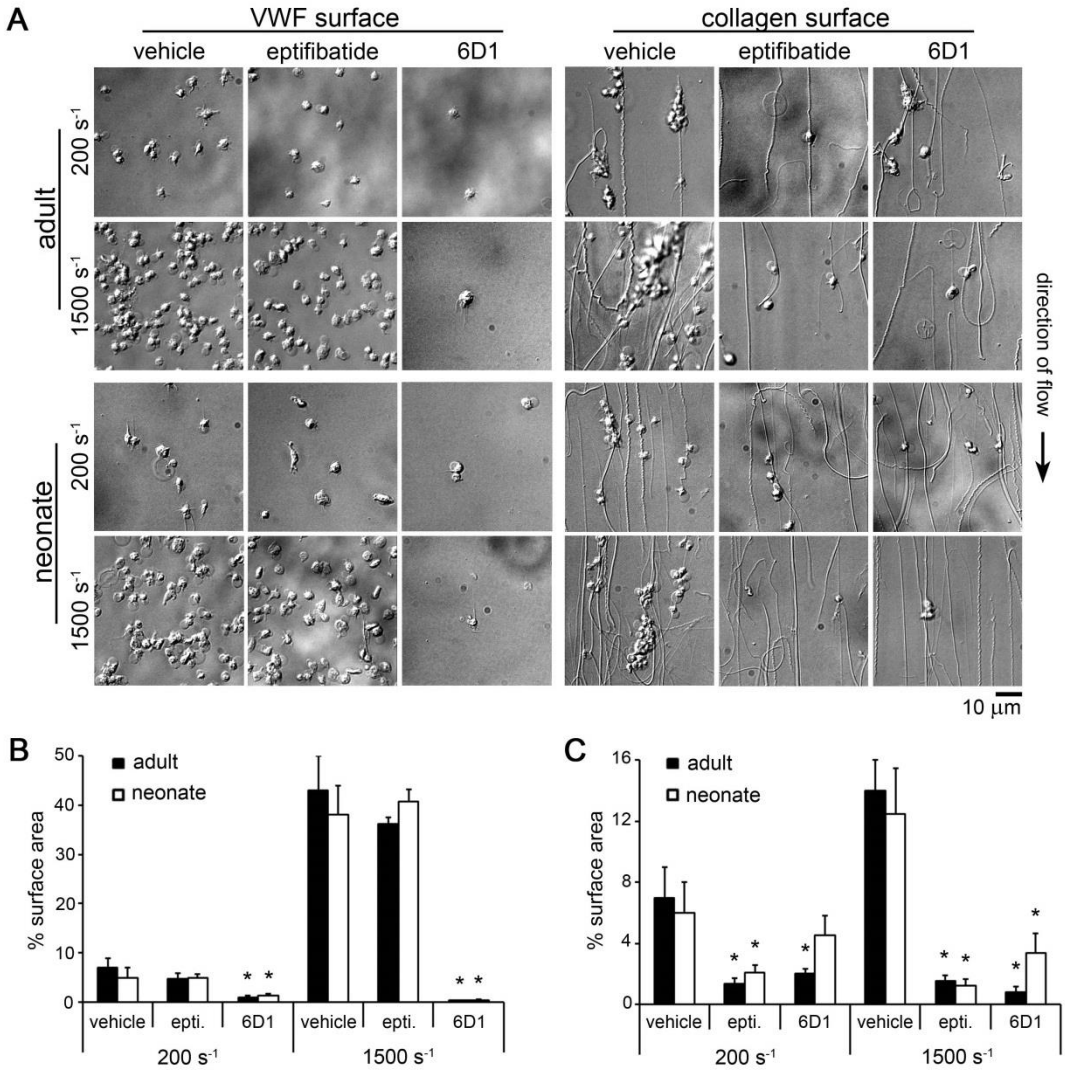

Figure 5.6 Effect of GPIIb/IIIa and GPIb inhibition on adult and neonate platelet adhesion and aggregation under fluid shear conditions. (A) Representative DIC images of adult and neonate platelet aggregates formed in a small volume flow chamber coated with 100 µg/mL VWF or 100 µg/mL fibrillar collagen at 200 or 1500 s^{-1} shear rate for 30 sec. Adult and neonate citrated whole blood were incubated with a GPIIb/IIIa inhibitor (eptifibatide; 20 µg/mL), a GPIb function blocking antibody (6D1; 20 µg/mL), or vehicle for 10 min at 25^{o}C prior to perfusion through flow chambers. Mean percent surface area coverage of a 140 × 105 µm field of view of adult and neonate platelet aggregates positive for CD41a-PE formed in flow chambers coated with VWF (B) or collagen (C). Data are represented as mean ± SEM, n ≥ 3. *denotes $P < 0.05$ compared with vehicle treated samples.

5.6 Discussion

The hemostatic system is developmentally regulated, characterized by age-dependent qualitative and quantitative differences in both primary and secondary hemostasis. Determining the presence of an acquired or inherited coagulation defect in the neonatal population is dependent upon the availability of assays which can be carried out in patients with limited venous access and limited blood volume as well as the availability of reference values that accurately reflect the dynamic changes within this developmentally regulated system. This is particularly challenging when evaluating the primary hemostatic system. Available platelet function data have demonstrated that neonatal platelets obtained from cord blood are hypo-reactive compared to adult platelets when evaluating platelet response to agonists in terms of granule secretion, receptor conformational changes, intracellular calcium changes, and aggregation (Israels, Rand and Michelson 2003; Haley, Recht and McCarty 2014). However, primary hemostasis as measured by bleeding time and PFA-100 closure times is shortened in neonatal blood compared to adult blood (Israels *et al.* 2001). Further, healthy newborns do not have a primary hemostatic defect clinically. Our understanding of the functional phenotype of neonatal platelets and the implications of the differences from the functional phenotypes of adult platelets is limited by the lack of assays that can be utilized in the neonatal population. The challenges are at least three fold: 1) improved diagnostic tool(s) are needed to accurately determine the presence or absence of inherited or acquired primary hemostatic defects, 2) reference ranges for platelet function in neonates at various gestational ages must be established; and 3) understanding how normal neonatal platelet

function mediates primary hemostasis and how those differences can be capitalized upon to improve care in the neonatal population and beyond.

In order to address these challenges, we developed four small-volume, whole blood, platelet function assays that can be applied to neonatal samples to assess platelet adhesion, activation, and aggregation. In total, the four assays require only 500 µL of whole blood, which can be safely obtained from even extremely low birth weight infants. Importantly, we ensured that our assays used whole blood in order to more closely mimic the interactions between each of the blood components that occur *in vivo* and minimize the handling and manipulation of the neonatal blood samples. Neonatal platelet activation and aggregation were evaluated with FACS-based methods and platelet adhesion and aggregation were visualized and quantified with static and flow chamber assays.

Platelet activation results in granule secretion, which promotes primary hemostasis by activating nearby platelets and strengthening platelet adhesion. P-selectin expression is significantly enhanced when α-granules are released, making antibodies directed to P-selectin valid markers for granule release and general platelet activation (Furie, Furie and Flaumenhaft 2001). Studies using flow cytometry analysis have reported that neonatal platelets from peripheral blood in the first days of life are hypo-responsive to ADP (binds the G-protein-coupled receptors $P2Y_1$ and $P2Y_{12}$), TRAP-6, which binds protease-activated receptor 1 (PAR-1), CRP (GPVI ligand), and U46619 (TxA_2 receptor agonist) (Kühne and Imbach 1998; Israels 2009; Schlegel *et al.* 2010; Strauss, Sidlik-Muskatel and Kenet 2011; Sola-Visner 2012), have reduced P-selectin expression following

agonist stimulation (Rajasekhar *et al.* 1994; Sitaru *et al.* 2005; Wasiluk *et al.* 2008), and have less α-granules (Saving, Mankin and Gorman 2002) relative to adult platelets. At 24-hours of life, we determined that neonatal platelets expressed significantly less P-selectin in response to both GPCR- and ITAM-signaling pathway agonists as compared to adult platelets. The lack of response to epinephrine may be explained by the reported decrease in α2-adrenergic receptors on neonatal platelets as compared to adults (Corby and O'Barr 1981). The fact that we did not observe platelet secretion in response to TRAP-6 is in line with previous studies demonstrating reduced calcium mobilization upon PAR-1 activation in neonatal platelets as compared to adults (Gelman *et al.* 1996). Along these lines, the lack of neonatal platelet P-selectin expression in response to calcium ionophore A23187 in our study further suggests reduced levels or mobilization of intracellular calcium in neonatal platelets as compared to adult platelets.

Our study demonstrates that neonatal platelets expressed an increased baseline level of P-selectin as compared to adult platelets, whereas neither adult nor neonatal platelets expressed the activated form of GPIIb/IIIa at rest. Along these lines, Schmugge *et. al.* reported that platelets from 2-3 day old neonates collected peripherally by dripping blood from the end of a needle into a tube were found to have increased P-selectin, annexin V, microparticles, and CD41 (inactive GPIIb/IIIa) levels, but not activated GPIIb/IIIa when compared with adult samples collected via venipuncture (Schmugge *et al.* 2003). They tested five adult samples collected with the same method used with neonates and found no difference in platelet baseline P-selectin expression levels compared with collection by venipuncture, suggesting that the different expression levels of P-selectin observed in

the neonatal samples were likely not due to a collection artifact. Future studies are required to understand the mechanisms by which P-selectin expression levels are developmentally regulated, and to understand whether this plays a physiological role in neonatal hemostasis.

Upon platelet activation, GPIIb/IIIa is converted into its high-affinity state, which binds plasma fibrinogen to initiate platelet aggregation. It has been shown that neonatal and adult platelet baseline expression levels of GPIIb/IIIa are equivalent (Sitaru *et al.* 2005); however, neonatal platelets have been shown to have reduced PAC-1 binding (which only binds the active form of GPIIb/IIIa) following agonist stimulation relative to adult platelets (Rajasekhar *et al.* 1994; Sitaru *et al.* 2005; Wasiluk *et al.* 2008). Our data support this paradigm in that we found that neonatal platelets expressed less active GPIIb/IIIa in response to both GPCR- and ITAM-mediated agonists as compared to adult platelets. These results indicate that signaling pathways regulating GPIIb/IIIa activation may be differently regulated in neonatal platelets compared with adult platelets. Additionally, it has been previously reported that neonatal platelets from cord blood or peripheral blood have a reduced aggregation response compared to adult platelets (Uçar *et al.* 2005; Ferrer-Marin *et al.* 2011). Interestingly, while we observed a decrease in platelet aggregation for neonatal platelets relative to adult platelets in response to both GPCR- and ITAM-signaling pathway agonists, we did find that the extent of platelet agglutination in response to ristocetin was equivalent between neonatal and adult platelets. Ristocetin has been shown to bind plasma VWF and open the A1 loop, exposing the GPIbα binding site to initiate platelet agglutination (Sadler 2010). As

expected, we found that the inhibition of GPIb reduced adult and neonatal platelet agglutination or aggregate formation on VWF in response to ristocetin in a GPIIb/IIIa-independent manner. Although neonatal platelet activation and aggregation are reduced relative to adults *in vitro*, full-term neonates do not clinically display a bleeding tendency (Sola-Visner 2012). This may be attributed in part to enhanced platelet/vessel wall interactions due to the presence of higher molecular weight VWF, higher concentrations of VWF, higher hematocrits, and higher red blood cell mean corpuscular volumes in neonates than older children and adults (Andrew, Paes and Johnston 1990; Israels *et al.* 2001; Saxonhouse *et al.* 2010).

New platelet function assays are needed to aid in the diagnosis of platelet dysfunction in the neonatal population, to guide treatment decisions in the event of clinically significant bleeding, as well as to understand the physiological differences between neonatal and adult platelets. Defining the functional phenotype of neonatal platelets may eventually provide guidance in diagnosing disease states in the neonatal population. Future work will assess differences in platelet function at varying gestational ages and in pre-term neonates.

Chapter 6: Role of Coagulation in the Recruitment of Colon Adenocarcinoma Cells to Thrombus under Shear

Sandra M. Baker-Groberg, Asako Itakura, András Gruber, and Owen J. T. McCarty

6.1 Abstract

Colorectal cancer metastases can appear on the peritoneum and in lymph nodes, liver, and lungs, suggesting both hematogenous and lymphatic spreading of the primary tumor. While antithrombotic agents have been shown to reduce both long-term incidence and metastasis, the role of coagulation in facilitating metastasis is ill defined. We investigated the kinetics and molecular mechanisms of metastatic colon adenocarcinoma cell recruitment to thrombi under shear flow, *ex vivo*. Platelet aggregates were formed by perfusing citrated anticoagulated whole blood over immobilized fibrinogen or fibrillar collagen. Thrombi were formed by perfusing recalcified whole blood over fibrinogen or fibrillar collagen in the presence of coagulation. Cultured colon adenocarcinoma cells (SW620) were perfused either during or following platelet aggregate or thrombus formation. The degree of transient tumor cell interactions (recruitment, rolling, and release) and the number of firmly adhered tumor cells were quantified using fluorescence microscopy. Platelet aggregates and thrombi formed on both fibrinogen- or fibrillar-collagen supported SW620 cell interactions and adhesion under shear. Thrombi or fibrin supported a greater degree of SW620 cell interactions and adhesion compared with platelet aggregates or fibrinogen, respectively, demonstrating that coagulation promoted SW620 cell recruitment under shear. Interestingly, in the absence of anticoagulation, we observed SW620 preferentially binding to thrombus-bound polymorphonuclear

leukocytes (PMNs). The addition of purified PMNs to thrombi resulted in a doubling of the number of interacting and bound SW620 cells. Since thrombi often accumulate and activate leukocytes, our findings suggest that leukocytes may play a role in localizing metastases to sites of thrombogenesis.

This work was originally published by the American Physiological Society
American Journal of Physiology: Cell Physiology 2013;
Volume 305, Number 9, Pages: C951-9
Reprinted with permission

6.2 Introduction

The methods presented in Chapters 3-5 were developed to study primary and secondary hemostasis in healthy donors. However, thrombotic complications can occur in various pathological states, such as cancer. During cancer metastasis, tumor cells can traverse the vasculature and arrest at a distal site to form secondary tumors; however, the role of coagulation in cancer metastasis remains ill-defined. In this chapter, methods to investigate the interactions of metastatic colon adenocarcinoma cells with platelet aggregates and thrombi under fluid shear were developed. Here, results indicate that the activation of coagulation promotes metastatic cancer cell recruitment and adhesion under physiological fluid shear. Additionally, the presence of PMNs facilitated cancer cell adhesion to formed thrombi under shear.

6.3 Background

There is a clear association between cancer mortality and metastasis. Cancer metastasis involves the separation of cancer cells from a primary tumor, entrance of tumor cells into

the blood or lymphatic circulation, adhesion to or entrapment at a distal site, and proliferation to form a secondary tumor (Konstantopoulos and Thomas 2009; Wirtz, Konstantopoulos and Searson 2011). Successful hematogenous metastasis would require tumor cells to survive in the blood environment and transit of large cells through small vessels that exposes tumor cells to shear forces, all of which could influence tumor cell survival, arrest, and extravasation (Felding-Habermann *et al.* 1996; Valastyan and Weinberg 2011). There has been considerable progress in decoding molecular features of cancer cells; however, the interactions between tumor cells and blood during transit through the vasculature remain ill defined. Local thrombotic blood vessel occlusions are commonly observed on histological evaluation of metastases (Trousseau 1865; O'Meara 1958; O'Meara and Jackson 1958; Hiramoto, Yagi and Pressman 1959; Heisig 1967). The aim of this study was to investigate tumor cell recruitment and arrest to thrombi in the presence of coagulation under fluid shear.

The key components of coagulation, platelet activation and fibrinogen, have been implicated in facilitating cancer metastasis (Gay and Felding-Habermann 2011). For decades, researchers examining tumor cell arrest in capillaries have observed close relationships between activated platelets and tumor cells.(Mannucci *et al.* 1989) In a pioneering experiment, Gasic et al. (Gasic, Gasic and Stewart 1968) demonstrated that thrombocytopenia inhibited metastasis, while platelet activation and infusion restored metastatic potential. More recently, researchers have found that growth factors produced by platelets promote growth of metastatic colon adenocarcinoma cells (Honn, Tang and Crissman 1992; Bockhorn, Jain and Munn 2007; Friedl and Alexander 2011; Labelle,

Begum and Hynes 2011). In addition to platelet interactions, elevated fibrinogen and soluble fibrin levels have been documented in the blood of many cancer patients (Luzzatto and Schafer 1990; Iversen and Thorlacius-Ussing 2003), and fibrinogen deficiency significantly reduced spontaneous metastases in mice (Palumbo *et al.* 2000, 2002, 2005; Camerer *et al.* 2004). Intimate interactions among platelets, fibrinogen, and tumor cells have been observed in the lung vasculature of mice where tumor cells were densely coated with platelets and fibrin clots (Dardik *et al.* 1997; Borsig *et al.* 2001; Läubli *et al.* 2006; Icli *et al.* 2007). Platelet and fibrin adhesion to tumor cells may provide a protective barrier against immune defenses, in particular, defense against the cytotoxicity of natural killer cells (Honn, Tang and Crissman 1992; Nieswandt *et al.* 1999). Other studies have suggested tumor cell arrest and formation of a secondary tumor are aided by platelets and fibrin clots providing a mechanism of adhesion and extravasation (Honn, Tang and Crissman 1992; Felding-Habermann *et al.* 1996; Dardik *et al.* 1997; McCarty *et al.* 2000; Bambace and Holmes 2011). However, experimental or clinical evidence for direct inhibition of the progression of metastatic cancer by antithrombotic therapy and consequential improvement in survival is limited, possibly in part because current antithrombotic prophylaxis carries bleeding risks that may counterbalance its benefits.

Elevated levels of circulating leukocytes (leukocytosis) have frequently been observed in cancer patients (McKee 1985; Shoenfeld *et al.* 1986; Ascensao *et al.* 1987); however, how polymorphonuclear leukocytes (PMNs) directly influence cancer progression and metastasis remains unclear. PMNs have been shown to have a cytotoxic effect on tumor

cells (Di Carlo *et al.* 2001) by maintaining intimate contact with tumor cells and producing reactive oxygen species, membrane-perforating agents, and mediators of cell killing (Jadhav, Bochner and Konstantopoulos 2001). However, PMNs have also been shown to enhance cancer progression and metastasis (Aeed, Nakajima and Welch 1988; Welch *et al.* 1989). Studies have demonstrated that PMNs can arrest tumor cells in the microvasculature of organs (Orr and Mokashi 1985; Ishikawa *et al.* 1986) and facilitate their extravasation (Starkey *et al.* 1984; Wu *et al.* 2001). Other studies have shown a fluid shear dependence on the kinetics, dynamics, and molecular mechanisms of PMN-tumor cell adhesion and arrest (Kitayama *et al.* 2000; Jadhav, Bochner and Konstantopoulos 2001; Jadhav and Konstantopoulos 2002; Hanley *et al.* 2003). These data support the notion that PMNs interact with tumor cells while traversing the vasculature and that this interaction may play a significant role in metastasis.

Prior studies investigating tumor cell interactions with blood cells have largely been performed in purified systems (Dardik *et al.* 1997; McCarty *et al.* 2000; Haier and Nicolson 2001; Alves *et al.* 2008). We aimed to extend these studies to characterize tumor cell-blood cell interactions in the presence of coagulation *ex vivo* under venous shear rates. We found that thrombi supported tumor cell recruitment and adhesion under shear. Importantly, the presence of thrombus-bound PMNs significantly increased the degree of tumor cell adhesion and arrest, suggesting that thrombus-bound PMNs may recruit circulating tumor cells *in vivo* as well.

6.4 Materials and Methods

6.4.1 SW620 cell culture

SW620 colon adenocarcinoma cells from lymph node were cultured in Dulbecco's Modified Eagle Medium (DMEM; Invitrogen, Carlsbad, CA) with fetal bovine serum (FBS; 10% w/v; Invitrogen) and penicillin-streptomycin (10% w/v; Invitrogen). Cells were detached with TrypLE Select (Invitrogen) for 20 min at 37^{o}C, pelleted at 150 g for 5 min, resuspended to a concentration of 1x10^{6} cells/mL in serum-free DMEM with Cell Tracker Orange 5-(and-6)-(((4-Chloromethyl)Benzoyl)Amino)Tetramethylrhodamine (CMTMR; 1 μM; 30 min at 37^{o}C; Invitrogen), pelleted at 150 g for 5 min to remove excess dye, and resuspended in serum-free DMEM.

6.4.2 Whole blood collection and capillary tube preparation

Venous blood was collected into NaCit, as described in Chapter 2. Glass rectangular capillary vitrotubes (0.4 × 4.0 × 50 mm) were coated with either fibrillar collagen (100 μg/mL) or FG (50 μg/mL), as described in Chapter 2.

6.4.3 Polymorphonuclear leukocyte (PMN) purification

Human venous blood was collected from healthy volunteers into citrate phosphate dextrose (7:1 v/v) and PMNs were purified as described previously (Itakura and McCarty 2013). Purified PMNs were incubated with Cell Tracker Blue 7-Amino-4-Chloromethylcoumarin (CMAC; 1 μM; 30 min at 37^{o}C; Invitrogen) at a concentration of 1x10^{6} PMNs/mL, pelleted at 400 g for 10 min, and resuspended in PMN leukocyte buffer.

6.4.4 SW620 cell perfusion experiments

NaCit-anticoagulated blood was perfused through fibrillar collagen- or fibrinogen-coated vitrotubes for 5 min at a shear rate of 265 s^{-1} to form platelet aggregates. To form thrombi and allow for activation of the coagulation cascade, citrated blood was mixed with calcium flow buffer, as described in Chapter 2. In selected experiments, calcium flow buffer supplemented with 50 pM TF, as previously described (Berny *et al.* 2010), was mixed with purified pooled plasma from three separate donors before perfusion through fibrinogen-coated vitrotubes. Subsequently SW620 cells at 1×10^6 cells/mL were perfused at 25, 35, 75, 100, or 150 s^{-1} shear rate for 1 min over a surface of BSA, fibrin(ogen), or the formed platelet aggregates or thrombi. The number of transiently interacting cells (recruitment, rolling, and release) or firmly adhered cells was quantified through fluorescent video capture with SlideBook 5.5 software (×20 magnification).

In some experiments, citrated anticoagulated blood was incubated with fluorescent CMTMR SW620 cells at 1×10^6 cells/mL for 5 min, followed by perfusion over fibrillar collagen- or fibrinogen-coated vitrotubes for 5 min at a shear rate of 25, 35, 75, 100, or 150 s^{-1} to form platelet aggregates. The rates of transiently interacting cells or firmly adhered cells were quantified using fluorescent video capture. In selected experiments, citrated anticoagulated blood was treated with a coagulation factor Xa inhibitor (rivaroxaban; 10 μM; Bayer Healthcare, Leverkusen, Germany), a thrombin inhibitor (hirudin; 20 μg/mL; CIBA-Geigy Pharmaceuticals, Horsham, West Sussex, United Kingdom), or a coagulation factor XIIa inhibitor [corn trypsin inhibitor (CTI); 20 μg/mL; Enzyme Research Laboratories, South Bend, IN] for 10 min before recalcification.

6.4.5 PMN-SW620 cell flow perfusion

Platelet aggregates or thrombi were formed at 265 s^{-1} over a fibrinogen-coated surface, followed by the perfusion of purified fluorescent CMAC PMNs ($1x10^6$ PMNs/mL) for 1 min at the same shear rate. SW620 cells were then perfused over the formed aggregates or thrombi with PMNs at 25, 35, 75, 100, or 150 s^{-1} for 1 min. Cell interaction rates were quantified through fluorescent video capture.

6.5 Results

6.5.1 SW620 cells interact with aggregates and thrombi in a shear dependent manner

Initial experiments were designed to analyze the rate of tumor cell interactions (recruitment, rolling, and release or firm adhesion) with platelets and thrombi under flow. Tumor cells were perfused in a parallel plate flow chamber either during or following platelet aggregate of thrombus formation. Platelet aggregates were formed by perfusing citrated whole blood over surfaces of fibrinogen or fibrillar collagen. Thrombi were formed by coperfusing calcium flow buffer with citrated anticoagulated whole blood over surfaces of fibrinogen or fibrillar collagen. Recalcification with calcium flow buffer allows the coagulation cascade to be triggered to generate thrombin and fibrin formation (termed thrombi). Fluorescent CMTMR SW620 cells were perfused either during or following platelet aggregate or thrombus formation at shear rates ranging from 25 to 150 s^{-1} (Figure 6.1, A–D). Transiently interacting and firmly adherent cells were defined as SW620 cells that were recruited and either released in < 60 s or remained bound for > 60 s, respectively.

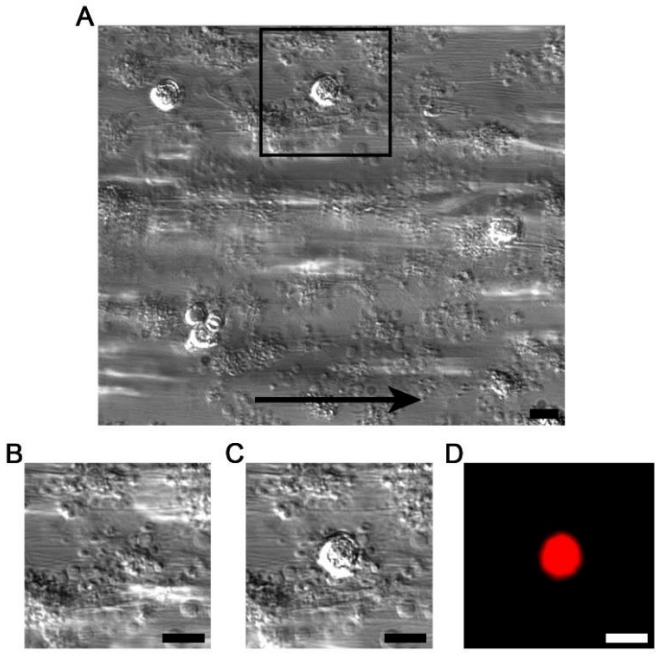

Figure 6.1 Recruitment of SW620 adenocarcinoma cells to thrombi under shear. Fluorescently labeled SW620 cells were perfused at shear rates ranging from 25 to 150 s^{-1} during or following platelet aggregate or thrombus formation. Platelet aggregates were formed by perfusing citrated anticoagulated blood over fibrinogen- or fibrillar collagen-coated surfaces. Thrombi were formed by perfusing blood with calcium flow buffer over surfaces of fibrinogen or fibrillar collagen. A: representative ×40 DIC image of SW620 cells [phase bright object in region of interest (ROI) outlined by the black box] adherent to thrombi formed on a fibrinogen-coated surface. Flow is from left to right, as denoted by the black arrow. B: ROI of thrombus before tumor cell adhesion. C: ROI following the arrest of a SW620 cell. D: corresponding fluorescent image of C, showing a fluorescently-labeled SW620 cell. Rates of transiently interacting and adhering SW620 cells were quantified using fluorescent video capture. All scale bars are 10 μm.

Transiently interacting and firmly adherent SW620 cells on platelet aggregates or thrombi were highly dependent on shear rate (Figure 6.2). A maximal rate of SW620 cell recruitment and adhesion to platelet aggregates or thrombi was observed at 25 s^{-1}, while no interactions were observed > 100 s^{-1}.

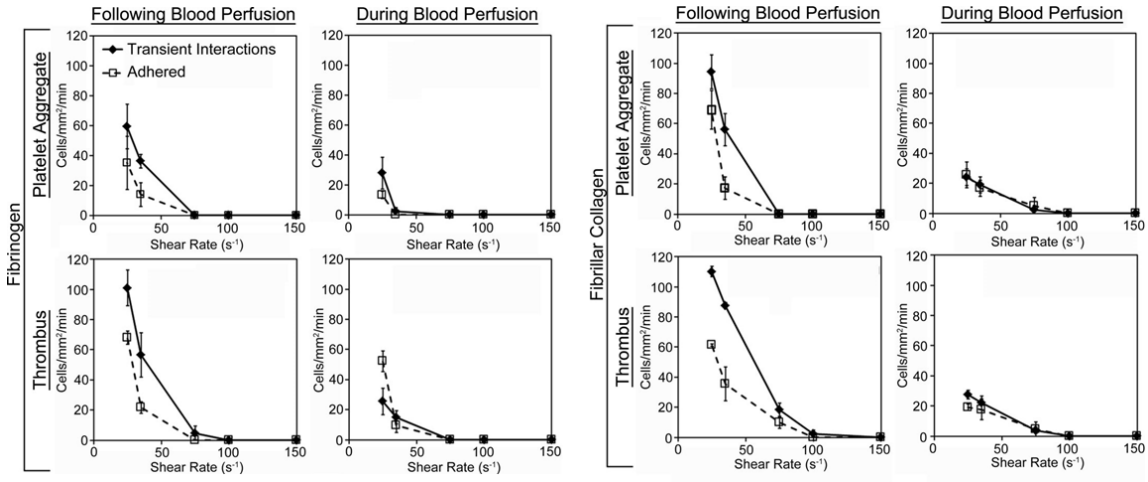

Figure 6.2 SW620 adenocarcinoma cells interact with platelet aggregates and thrombi in a shear-dependent manner. For tumor cell adhesion experiments following platelet aggregation or thrombus formation, platelet aggregates or thrombi were formed over a fibrinogen- (left) or fibrillar collagen-coated surface (right) at 265 s^{-1}. Fluorescent SW620 cells (1×10^6 cells/ml) were perfused over platelet aggregates or thrombi at shear rates of 25, 35, 75, 100, or 150 s^{-1}. To study tumor cell adhesion during platelet aggregation or thrombus formation, fluorescent SW620 cells were added to whole blood and perfused over fibrinogen- or fibrillar collagen-coated surface at 25, 35, 75, 100, or 150 s^{-1}. Rates of transiently interacting (recruitment, rolling, and release) and firmly adhered cells were quantified using fluorescent video capture. Data are represented as means ± SEM of 3 individual experiments.

Total interacting cells were calculated by adding the rates of transiently interacting and firmly adherent cells. As shown in Figure 6.3, A and B, on a fibrinogen surface, the rate of total interacting SW620 cells with thrombi was nearly double compared with the rate of total interacting SW620 cells with platelet aggregates at 25 s^{-1}, regardless of whether SW620 cells were perfused with the blood or following aggregate or thrombus formation. An equivalent rate of total interacting SW620 cells with platelet aggregates or thrombi formed on collagen was observed at 25 s^{-1}; however, thrombi formed on collagen supported a significantly greater degree of SW620 cell interactions at both 35 and 75 s^{-1} compared with platelet aggregates when SW620 cells were perfused following aggregate or thrombus formation (Figure 6.3, A and B).

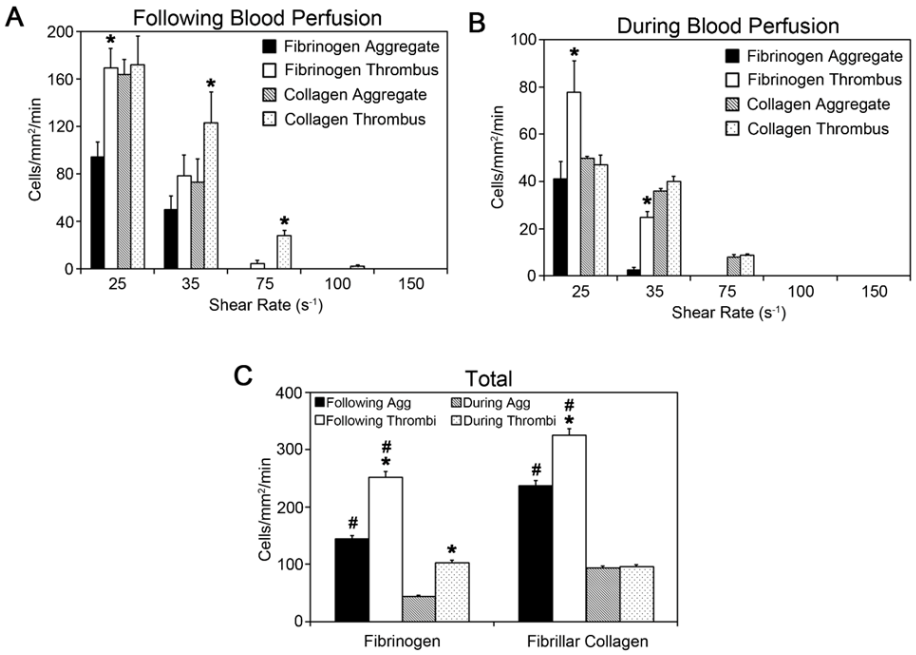

Figure 6.3 Cumulative rate of SW620 adenocarcinoma cell interactions with thrombi and platelet aggregates. Total rates of interacting SW620 cells (summation of transiently interacting and firmly adherent) for each shear rate for tumor cell adhesion experiments (A) following or (B) during platelet aggregation or thrombus generation. C: total rates of interacting SW620 cells across all shear rates were calculated for tumor cell adhesion experiments following or during platelet aggregation or thrombus formation. Data are represented as means ± SEM of 3 individual experiments. *$P < 0.05$ for thrombi compared with platelet aggregates. #$P < 0.05$ for following blood perfusion experiments compared with during blood perfusion experiments.

To compare the extent of SW620 cell interactions with platelet aggregates and thrombi under shear, we calculated the total rate of interacting cells by cumulating the transiently interacting and firmly adherent across all shear rates. When SW620 cells were perfused over platelet aggregates or thrombi, the presence of coagulation significantly increased the total level of cell interactions for both fibrinogen and collagen surfaces (Figure 6.3C). Under these conditions, platelet aggregates or thrombi formed on collagen surfaces supported increased levels of total interactions compared with fibrinogen (Figure 6.3C).

Previous studies have demonstrated that the conversion of fibrinogen to fibrin enhanced tumor cell recruitment under flow in a purified system (Alves *et al.* 2009). We next designed experiments to compare the recruitment of SW620 cells to a surface of fibrin or fibrinogen. Perfusion of SW620 cells over fibrinogen surfaces resulted in a mean interaction rate of 65 cells/mm^2, while recruitment rates of SW620 cells over the fibrin surface resulted in a significantly greater mean adhesion rate of 228 cells/mm^2 (Figure 6.4). In contrast, SW620 cells failed to bind to a surface of BSA (Figure 6.4).

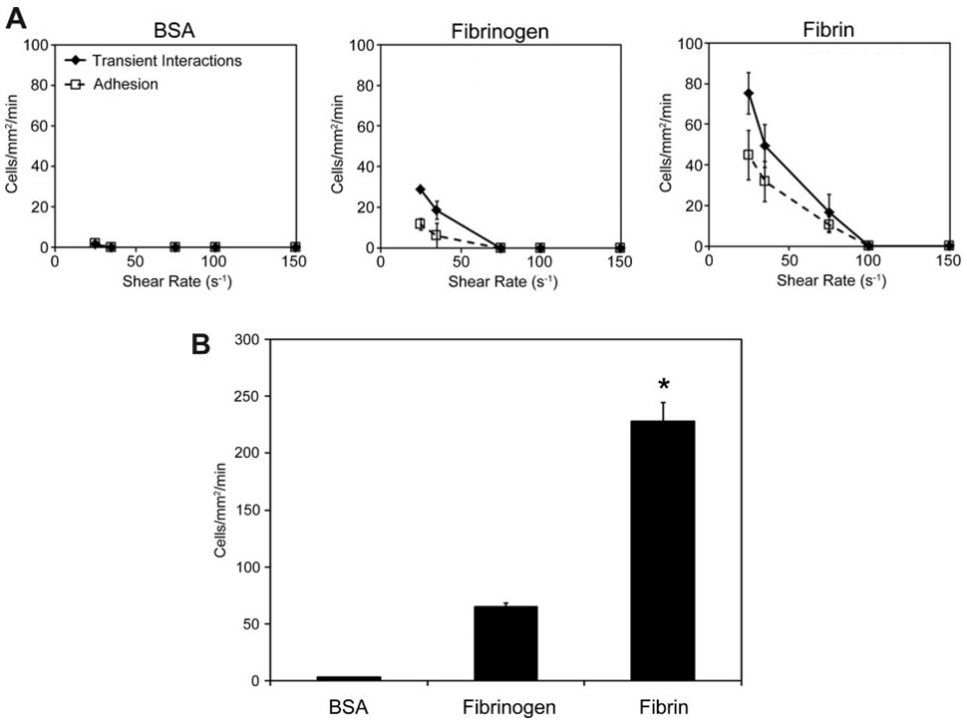

Figure 6.4 Fibrin surfaces increase SW620 adenocarcinoma cell transient interactions and adhesion rates. Fluorescent SW620 cells were perfused over a BSA, fibrinogen, or fibrin surface at 25, 35, 75, 100, or 150 s^{-1}. In selected experiments, purified pooled plasma from 3 donors was coperfused with calcium flow buffer supplemented with 50 pM tissue factor at 265 s^{-1} over a fibrinogen-coated surface to generate fibrin. A: rates of transiently interacting (recruitment, rolling, and release) and firmly adhered cells were quantified using fluorescent video capture. Solid lines indicate transient interactions and dashed lines represent firm adhesion. B: total rates of interacting SW620 cells across all shear rates were calculated for BSA, fibrinogen, and fibrin coated surfaces. Data are represented as means ± SEM of 3 individual experiments. *$P < 0.05$ for fibrin compared with fibrinogen.

6.5.2 Role of coagulation factors in SW620 cell recruitment and adhesion to thrombi under shear

Subsequent experiments focused on defining the role of the contact activation pathway of blood coagulation in SW620 cell recruitment and adhesion to thrombi under shear. When recalcified blood was pretreated with a thrombin inhibitor (hirudin), a factor Xa (FXa) inhibitor (rivaroxaban), or a factor XIIa (FXIIa) inhibitor (CTI) before perfusion over fibrinogen or collagen, the rate of SW620 recruitment and adhesion was significantly reduced (Figure 6.5).

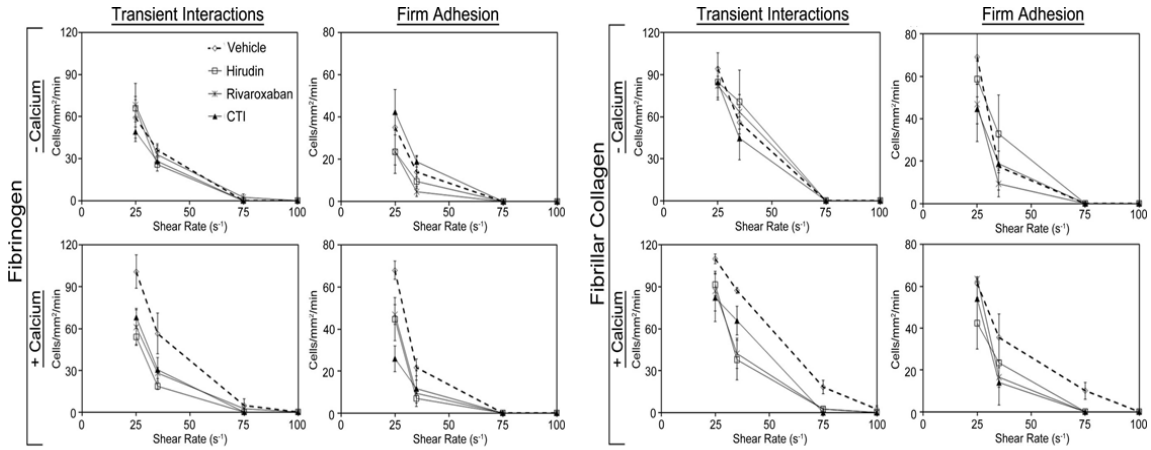

Figure 6.5 Coagulation inhibitors decrease SW620 adenocarcinoma cell transient interactions and adhesion rate to thrombi under shear. Sodium citrated anticoagulated human whole blood was incubated with a thrombin inhibitor (hirudin; 20 μg/mL), a coagulation factor Xa inhibitor (rivaroxaban; 10 μM), or a coagulation factor XIIa inhibitor (corn trypsin inhibitor, CTI; 20 μg/mL) for 10 min at 25°C. Blood was then perfused over a fibrinogen- (left) or fibrillar collagen-coated surface (right) at 265 s^{-1} (−Calcium). In selected experiments, whole blood was co-perfused with calcium flow buffer (+Calcium). Fluorescent SW620 cells were perfused over formed platelet aggregates or thrombi at 25, 35, 75, or 100 s^{-1}. Rates of transiently interacting (recruitment, rolling, and release) and firmly adhered cells were quantified using fluorescent video capture. Solid lines indicate inhibitor-treated blood. Dashed lines are vehicle-treated blood. Data are represented as means ± SEM of 3 individual experiments.

Moreover, hirudin, rivaroxaban, or CTI reduced the total rate of interacting SW620 cells with thrombi to the levels observed on platelet aggregates in the absence of coagulation (Figure 6.6). Taken together, our data demonstrate a critical role for coagulation activation in potentiating tumor cell recruitment to thrombi under shear.

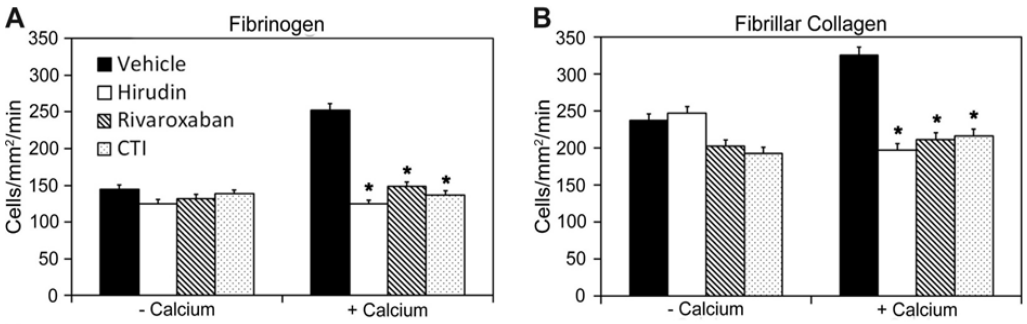

Figure 6.6 Role of coagulation factor X and thrombin in SW620 cell recruitment to thrombus under shear. Citrated anticoagulated blood was incubated with a thrombin inhibitor (hirudin; 20 μg/mL), a coagulation factor Xa inhibitor (rivaroxaban; 10 μM), or a coagulation factor XIIa inhibitor [corn trypsin inhibitor (CTI); 20 μg/mL]. Blood was perfused over a fibrinogen (A)- or fibrillar collagen (B)-coated surface (−Calcium). In selected experiments, whole blood was coperfused with calcium flow buffer (+Calcium). Fluorescent SW620 cells were then perfused and the total rates of interacting SW620 cells across all shear rates were calculated for each treatment. Data are represented as means ± SEM of 3 individual experiments. *$P < 0.05$ for coagulation inhibitor treatment compared with vehicle.

6.5.3 PMNs increase the rate of SW620 cell interactions to aggregates and thrombi under shear

Our next set of experiments was designed to determine whether thrombus-bound PMNs played a role in tumor cell recruitment and adhesion under shear. SW620 cells tethered to and adhered downstream of thrombus-bound PMNs (Figure 6.7A). The presence of thrombus-bound PMNs significantly increased the rate of SW620 transient interactions and firm adhesion (Figure 6.7B and C). The total interaction rates of SW620 cells with thrombi increased from 169 ± 16 cells/mm^2/min to 303 ± 31 cells/mm^2/min at 25 s^{-1} in the presence of thrombus-bound PMNs (Figure 6.7D).

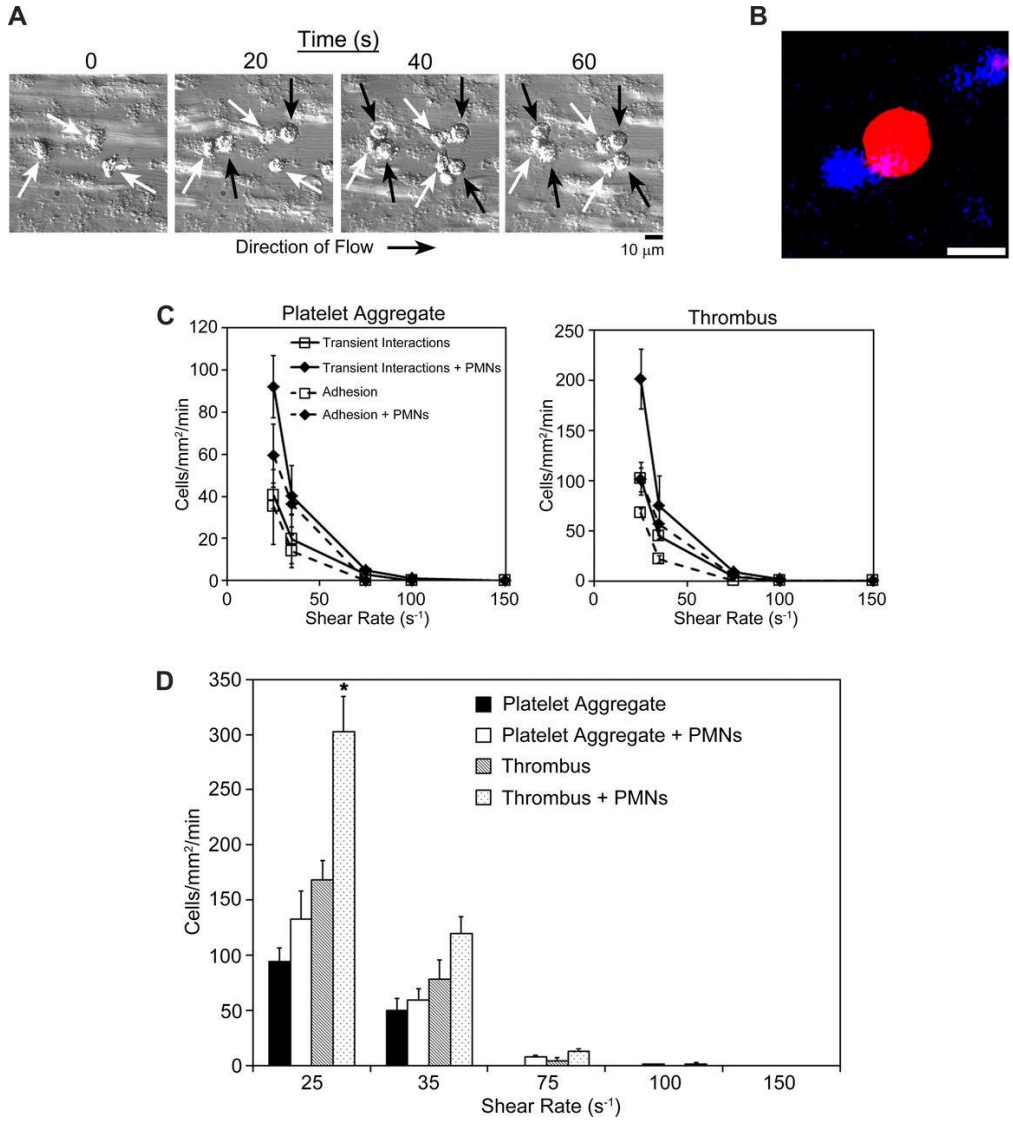

Figure 6.7 Polymorphonuclear leukocytes (PMNs) increase rate of SW620 adenocarcinoma cell recruitment to formed platelet aggregates or thrombi under shear. Platelet aggregates or thrombi were formed at 265 s^{-1} for 5 min over a fibrinogen-coated surface. Purified PMNs were fluorescently labeled with a dye (blue) that was spectrally distinct from the fluorescent dye used for SW620 cells (red). Fluorescently labeled PMNs were perfused over formed platelet aggregates or thrombi (1×10^6 PMNs/ml) at 265 s^{-1} for 1 min before perfusion of fluorescent SW620 cells at 25, 35, 75, 100, or 150 s^{-1}. The rates of transiently interacting (recruitment, rolling, and release) and firmly adhered SW620 cells were quantified using fluorescent video capture. A: representative ×40 DIC time-lapse images of PMNs recruiting SW620 cells to formed thrombi on a fibrinogen-coated surface. White arrows indicate adhered PMNs. Black arrows indicate SW620 cells. B: representative ×20 fluorescent image of a fluorescently labeled SW620 cell (red) adhering to a PMN (blue). Scale bar = 10 μm. C: rates of transiently interacting and firmly adhered SW620 cells to platelet aggregates (left) or thrombi (right) with or without PMNs (solid and dashed lines, respectively). D: total rate of interacting SW620 cells to platelet aggregates or thrombi in the absence or presence of PMNs for each shear rate. Data are represented as means ± SEM of 3 individual experiments. *$P < 0.05$ compared with the absence of PMNs.

6.6 Discussion

The main findings of this study are the following: 1) colon adenocarcinoma cells bind thrombi in a shear-dependent manner; 2) tumor cells interact with thrombi in a thrombin- and FXa-dependent manner; and 3) PMNs promote SW620 cell recruitment and adhesion to thrombi under shear.

6.6.1 SW620 cells interact with thrombi in a shear-dependent manner

Previous studies using purified systems have demonstrated the shear rate dependence of tumor cell-platelet interactions. In the present work, we found that tumor cell-thrombus interactions in the presence of coagulation decreased as shear rates increased from 25 to 75 s^{-1}. These shear rates coincide with the blood shear rates found in capillary beds (~32 to 43 s^{-1} reported for the human and mouse capillary bed, respectively) (Mayrovitz 1992; Cortinovis *et al.* 2006) and postcapillary venules (~35 to 560 s^{-1}) (Lawrence *et al.* 1990; Honn, Tang and Crissman 1992). Tumor cell arrest has been observed *in vivo* in both capillary beds (Chambers, Groom and MacDonald 2002; Mook *et al.* 2003; Enns *et al.* 2005) and postcapillary venules (Kong *et al.* 1996; Machan *et al.* 2012). Tumor cell arrest in capillaries has been hypothesized to be a passive process, wherein circulating tumor cells, which range in size from 9 to 12 μm in diameter in patient samples (Phillips and McCarty 2012; Phillips *et al.* 2012), are physically trapped in small capillaries, which range in size from 5 to 10 μm in diameter and number in the billions in the human body (Middelbeek *et al.* 2012). The SW620 cells used in this study ranged in size from 8 to 12 μm (Figures 6.1 and 6.2, A and B), which coincides with the sizes of circulating tumor cells trapped *in vivo*. For circulating tumor cells that make it through the metarterioles

and arteriovenous bypasses that regulate tissue perfusion, they next enter venules and veins. This vessel expansion through the postcapillary venules creates a reduction in blood velocity and an increase in pressure, which can result in small turbulent eddies at the edges of the expanding vessel (Pandhare and S.S.Jadhav 2009). Areas of turbulence or stagnant flow in the postcapillary venules may provide favorable conditions for tumor cell arrest in the vasculature during metastasis through both passive and active mechanisms (Thamilselvan *et al.* 2004).

We found that SW620 cell recruitment to thrombi formed on fibrillar collagen was significantly greater than the extent of recruitment to thrombi formed on fibrinogen. Fibrillar collagen is a potent platelet agonist and supports platelet recruitment, activation, and aggregate formation under high shear (Clemetson and Clemetson 2001). In parallel, collagen also activates FXII, initiating thrombin generation and fibrin formation (White-Adams *et al.* 2010). The discrete fibrillar nature of collagen results in three-dimensional thrombus formation being localized along the collagen fibers in the direction of shear flow (Baker, Phillips and McCarty 2012). In contrast, only a single layer of platelets forms on fibrinogen under shear, resulting in a "two-dimensional" platelet-rich thrombus forming in the presence of coagulation. The results indicate that thrombus formation on collagen creates a structure that is both physically and biochemically more active for tumor cell recruitment, *ex vivo*. Further, our results demonstrating that fibrin formed in plasma enhanced SW620 cells recruitment compared with fibrinogen support the notion that the conversion of fibrinogen to fibrin potentiates this receptor-ligand interaction (McCarty *et al.* 2002; Alves *et al.* 2008, 2009).

6.6.2 Role of thrombin and FXa in SW620 cell-thrombi interactions

Coagulation is triggered by the exposure of blood to ECM proteins and localized to the surface of activated platelets. The intrinsic and extrinsic pathways of coagulation converge to activate FX to FXa, which in turn activates prothrombin to generate thrombin, which in turn activates platelets and coagulation factors, cleaves fibrinogen to fibrin resulting in the formation of a thrombus or a hemostatic plug. Coagulation proteases, such as FXa and thrombin, have been shown to directly regulate cancer cell growth and motility (Huang, Li and Karpatkin 2000; Sampson and Kakkar 2002). Moreover, circumstantial evidence suggests that FXa and thrombin may support cancer metastasis via direct or indirect mechanisms (Tuszynski, Gasic and Gasic 1987; Donnelly *et al.* 1998; Nierodzik and Karpatkin 2006). For instance, studies have shown that targeting FXa with low-molecular weight heparin increases cancer survival (Altinbas *et al.* 2004; Klerk *et al.* 2005; Icli *et al.* 2007; Borensztajn, Peppelenbosch and Spek 2008). We show that inhibition of either FXa or thrombin significantly reduced the degree of SW620 cell recruitment to thrombi under shear, highlighting a role for these coagulation factors in promoting tumor cell-thrombus interactions. If thrombi that recruited tumor cells provide an environment that is favorable for survival and proliferation of circulating cancer cells, inhibition of thrombin generation could indeed provide anti-metastatic effects and survival benefit in patients.

6.6.3 PMNs promote SW620 cell adhesion and arrest to thrombi under shear

Numerous studies have reported a link between inflammation and cancer metastasis (Coussens and Werb 2002; Lin and Karin 2007; Mantovani *et al.* 2008; Grivennikov,

Greten and Karin 2010). It has been previously demonstrated that PMNs are capable of binding tumor cells in a shear-dependent manner in purified systems (Jadhav and Konstantopoulos 2002). It is also known that PMNs are often associated with and incorporated into developing thrombi (Gruber *et al.* 2007). Here we show that thrombus-bound PMNs promoted tumor cell recruitment and adhesion from blood under shear, *ex vivo*. In the vasculature, PMNs are recruited to the endothelium of inflamed postcapillary venules in a series of steps involving PMN capture, activation and rolling, firm adhesion, and migration. Studies also show that PMNs are recruited to experimental thrombi at sites of endothelial injury. Predominantly observed in the venous circulation, intravascular leukocyte migration within a thrombus has been shown to guide leukocytes toward a site of vascular injury (Ghasemzadeh *et al.* 2013). Our findings suggest that thrombus-bound PMNs may augment the recruitment of circulating tumor cells *in vivo*. This, in theory, could contribute to the seeding and proliferation of circulating cancer cells and accelerate the progression of metastatic cancer. Thrombus-associated leukocyte accumulation and tumor cell recruitment thus could provide a rationale for antithrombotic prophylaxis of cancer patients. However, it remains to be determined if the leukocyte-recruited cancer cell is in a microenvironment that favors proliferation.

Chapter 7: Conclusions and Future Directions

7.1 Summary

The techniques presented in Chapters 3-6 were developed to aid in characterizing primary and secondary hemostasis under static and fluid shear conditions, including assessing platelet function in the neonatal population and the role of coagulation in cancer metastasis. Use of the developed methodologies revealed the following main findings: activation of the coagulation cascade restricts thrombus growth formed under high physiologic arterial shear rates (Chapter 3); fibrin formation increases the density of thrombi while volume remains constant (Chapter 3); under static conditions, platelets form aggregates in a platelet concentration-dependent manner via GPIIb/IIIa (Chapter 4); in response to platelet GPCR and ITAM-signaling pathway agonists, neonate platelets have reduced activation compared with adult platelets (Chapter 5); under conditions of shear, neonatal platelets aggregate in a GPIIb/IIIa-dependent manner (Chapter 5); the presence of coagulation promotes metastatic colon adenocarcinoma cell adhesion to thrombi under shear (Chapter 6); and the addition of PMNs facilitates cancer cell recruitment to thrombi under venous shear rates (Chapter 6). The metrological techniques presented in this dissertation may be useful in future studies assessing platelet function and coagulation, evaluating efficacy of novel antithrombotic therapeutics, and investigating the biophysical properties of cellular specimens.

The following section discusses future methods that will be developed to extend the work presented in this dissertation.

7.2 Development of Microfluidic Device for Assessing Neonatal Platelet Function

The small volume assays presented in Chapter 5 of this dissertation utilize a total of 500 µL of anticoagulated whole blood to assess neonatal platelet adhesion and aggregation under static and fluid shear conditions. However, with recent advances in microfluidic technology, it is now possible to develop a "lab-on-a-chip" device that requires only microliter or nanoliter quantities of blood. We aim to develop a microfluidic device that would only require 1 µL or less of citrated whole blood to assess neonatal primary hemostasis. By reducing the sample volume to 1 µL, sample collection could be performed via finger prick without the need of a trained phlebotomist for routine use in clinics, emergency rooms, or homes. It has been reported that utilizing the electrical impedance of clotting blood or platelet aggregation is one of the best methods for assessing whole blood hemostasis (Blair *et al.* 1987). The proposed device will use electrical impedance monitoring for assessing neonatal platelet aggregation and will be rapid, easy to use, and amenable for use in a clinical setting.

Lei *et. al.* have recently developed an electrical impedance microfluidic device for monitoring whole blood coagulation (Lei *et al.* 2013). We aim to adapt their device for use in evaluating whole blood neonatal platelet aggregation. The microfluidic device will be made out of polydimethylsiloxane (PDMS; Sylgard® 184; Dow corning, Midland, MI) and have a pair of electrodes incorporated into the bottom of the PDMS wells on a glass substrate. A titanium/aluminum (Ti/Al) metal alloy will be added to a glass substrate via metal deposition and a photoresist (PR) mask will be added to the metal surface via spin-coating and photolithography. The metal will be etched around the PR

mask to form the electrodes. Polymethylmethacrylate (PMMA) will be micro-machined into a mold of the microfluidic wells. Liquid PDMS will be added to the mold and allowed to solidify, after which it will removed and bonded to the glass electrodes via oxygen plasma treatment. The proposed steps in fabricating the microfluidic device are shown in Figure 7.1.

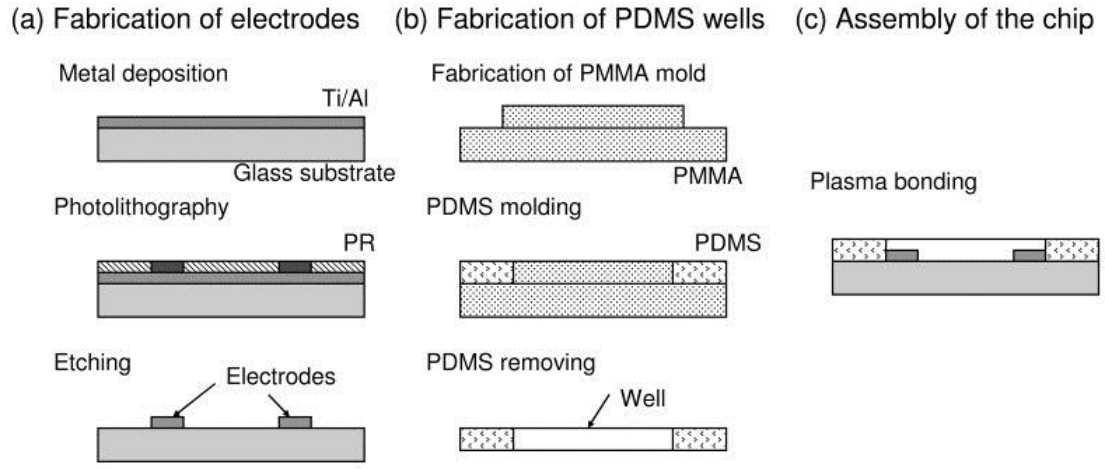

Figure 7.1 Example steps in fabrication of the electrode microfluidic device. (a) Electrode fabrication on a glass surface. Metal will be deposited onto a glass substrate. A photoresist (PR) mask will be added to the metal surface via spin-coating and photolithography. The metal will be etched to form the electrodes. (b) A PMMA mold will be made, PDMS will be poured around the mold and allowed to solidify, and the PDMS will then be removed. (c) The PDMS wells will be plasma bonded to the glass with electrodes to form the final electrode microfluidic device. Figure is adapted from ©Lei *et. al*., 2013, originally published in *PLoS One* (Lei *et al.* 2013).

The device will contain multiple wells to allow for testing of several blood samples with only one device. The device will be housed inside a temperature controller incubator set at 37^{o}C and the electrodes at the bottom of the wells will be attached to an impedance analyzer (VersaSTAT 4, Ametek, Beaverton, OR), as shown in Figure 7.2 (Lei *et al.* 2013). The wells will be pretreated with denatured BSA (5 mg/mL; Sigma-Aldrich) for 1 hr at 25^{o}C prior to use. Citrated whole blood will be pipetted into each well and the

impedance of the sample will be measured after the addition of the agonists TRAP-6 (10 µM; Tocris Bioscience), ADP (10 µM; Sigma-Aldrich), U46619 (10 µM; Tocris Bioscience), CRP (10 µg/mL; kind gift from Dr. Richard Farndale), epinephrine (10 µM; Chrono-Log), rhodocytin (300 nM; kindly provided by Dr. Johannes Eble), calcium ionophore A23187 (10 µM; Sigma-Aldrich), ristocetin (1 mg/mL; Chrono-Log), or vehicle to the blood to initiate platelet aggregation.

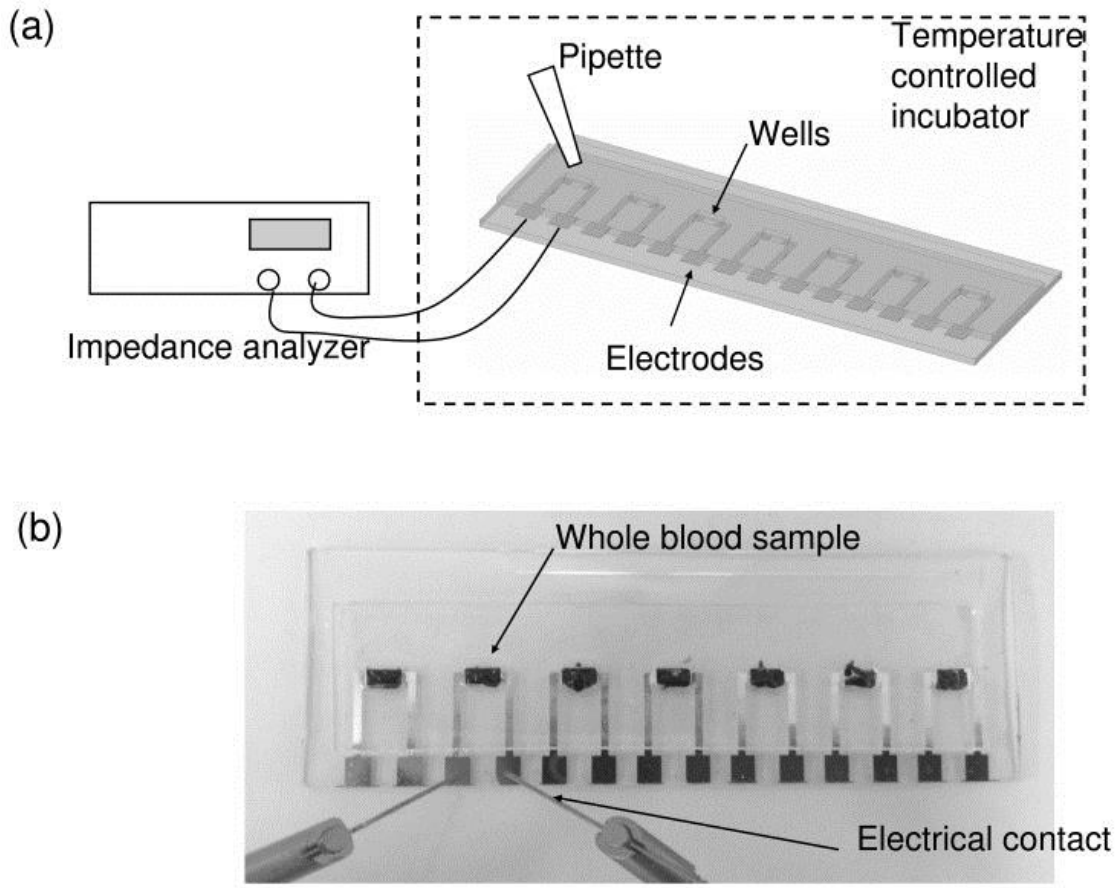

Figure 7.2 Assembled electrode microfluidic device. (a) The electrode microfluidic device will be housed in a temperature controlled incubator set at 37°C and will be connected to an electrical impedance analyzer. (b) Photo of the electrode microfluidic device loaded with a sample of whole blood. Figure is adapted from ©Lei *et. al*., 2013, originally published in *PLoS One* (Lei *et al.* 2013).

Previous studies have modeled the electrical impedance of whole blood clotting (Zhao, Jacobson and Ribbe 1993). We will adapt the model developed by Lei *et. al*. to measure the electrical impedance of whole blood platelet aggregation in the device well (Lei *et al.* 2013). An example electrical impedance model in the device and a representative trace of the impedance of whole blood clotting is shown in Figure 7.3.

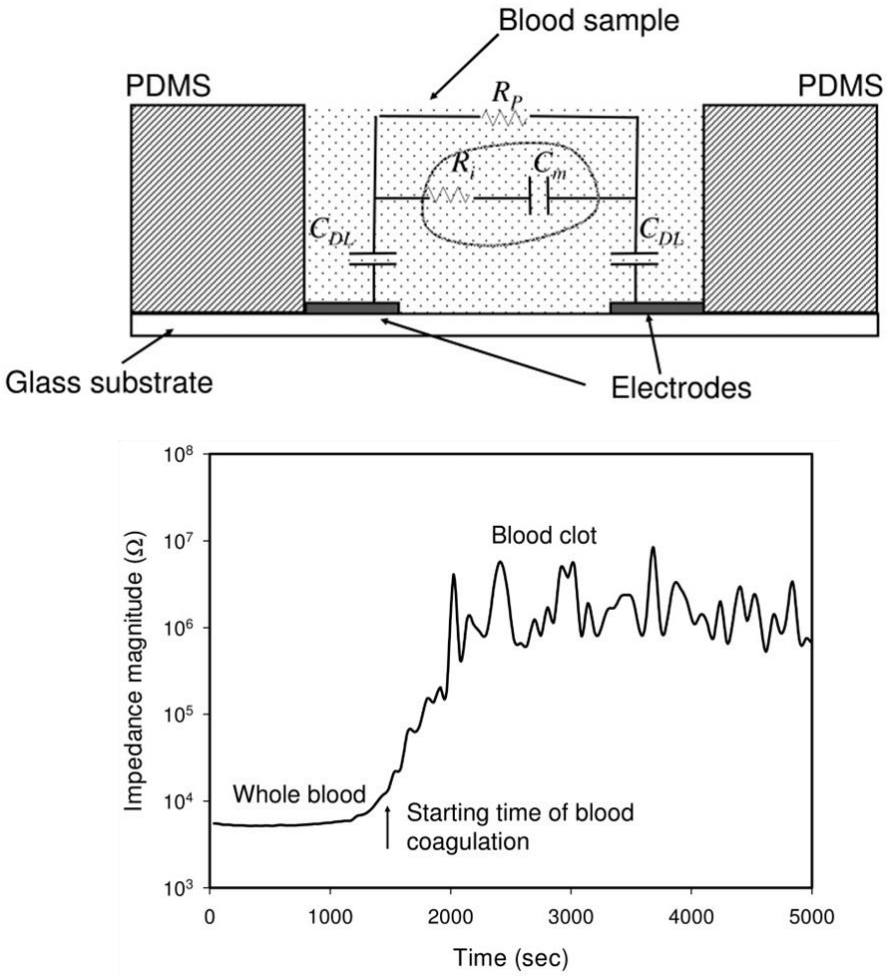

Figure 7.3 Impedance of whole blood coagulation. Whole blood is added to the PDMS wells and the addition of calcium initiates coagulation. The plasma resistance is R_P, the RBC resistance is R_i, the RBC capacitance is C_m, the double layer capacitance between the electrode and the electrolyte is C_{DL}. A representative impedance trace of whole blood clotting is shown. Figure is adapted from ©Lei *et. al*., 2013, originally published in *PLoS One* (Lei *et al.* 2013).

Initially we will use adult blood in the electrode microfluidic device to calibrate the impedance system. If adult platelet aggregation is not measurable for the device under resting (static) conditions, the device will be placed in a shaker plate (BioShake iQ, Quantifoil Instruments GmbH) and rotated at 1000 rpm to augment platelet-platelet interactions and aggregate formation. Once the impedance analyzer can correctly trace platelet aggregation of adult blood, we will test blood that has been incubated with inhibitors of GPIIb/IIIa (eptifibatide; 20 µg/mL; Millennium Pharmaceuticals) or GPIb (6D1; 20 µg/mL; kindly provided by Dr. Barry Coller) for 20 min at 25^{o}C prior to agonist treatment to determine whether the device is sensitive enough to measure platelet dysfunction. After the device is calibrated with adult blood, we will then test neonate whole blood collected via heel stick at 24 hrs of life into 3.8% sodium citrate. The developed electrode microfluidic device will be useful in studying neonatal primary hemostasis and could be adapted for use with portable electronic devices for point-of-care use in clinics, emergency rooms, or homes (Spence 2002).

7.3 Development of a Multi-Photon Microscopy System for Measuring the Physical Biology of Angiogenesis *In Vivo*

Angiogenesis, which is the process of new blood vessel growth, plays a key role in tissue development, wound repair, and various pathological states, such as inflammatory, malignant, and immune disorders. While the signaling pathways governing the process of angiogenesis in response to biochemical agents are well characterized, less is known about the role of mechanical cues in angiogenesis. *In vivo* assays are useful in angiogenesis research because they mimic angiogenesis in normal and pathological

states, which is extremely important for evaluating efficacy of agents during drug development. However, the inability to quantify mechanics of cells in *in vivo* angiogenesis systems has limited their use in cell mechanobiology research. This study aims to utilize the well characterized chicken chorioallantoic membrane (CAM) *in vivo* angiogenesis assay and fluorescent polylactic acid (PLA) scaffolds with known elastic properties in conjunction with multi-photon imaging to quantify the mechanics of migrating angiogenic endothelial cells.

The initial stages of this study will consist of designing and building a multi-photon microscopy system. Multi-photon fluorescence imaging utilizes pulsed long wavelength (near-infrared) light to excite fluorophores in a specimen. The fluorophore absorbs the combined energy from two or three low energy, long wavelength photons to emit a photon of shorter wavelength (Zipfel, Williams and Webb 2003). Long wavelength light penetrates deep into tissues (~1 mm) with minimal damage to cells due to its inherent low energy. Additionally, multi-photon imaging has no absorption (photobleaching) out of the focal plane to allow for 3D optical sectioning, making it ideal for long term *in vivo* imaging (Horton *et al.* 2013). Typically, multi-photon microscopy utilizes raster scanning with scanning mirrors (SMs) to move the focused laser beam across the specimen and the emitted fluorescence is collected with a photomultiplier tube (PMT) to generate images. The multi-photon microscopy setup for this study will include a pulsed near-infrared (IR) laser that will need to be properly aligned and routed to pass by a series of lens, SMs, a dichroic mirror, a microscope objective, and a PMT. A schematic of the proposed multi-photon microscopy system is shown in Figure 7.4.

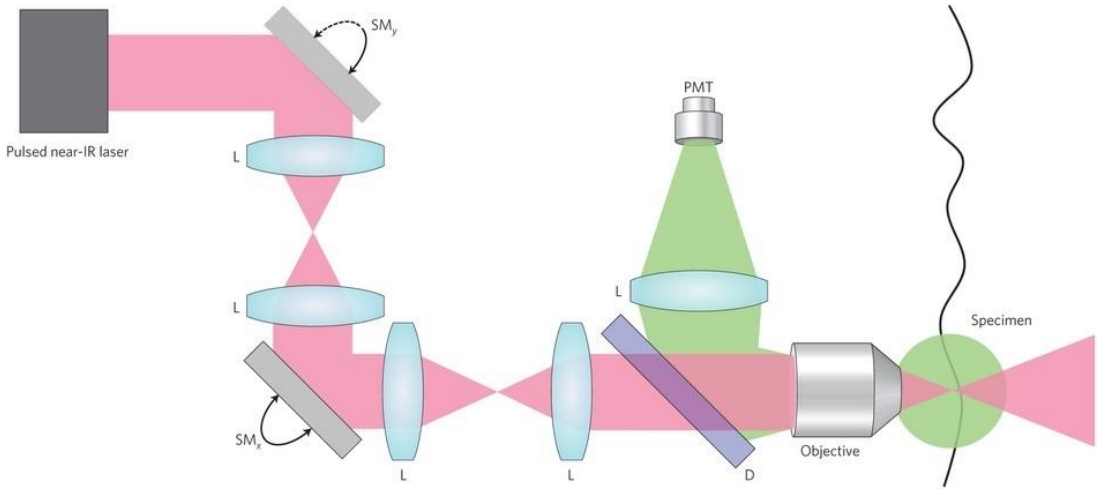

Figure 7.4 Schematic of a multi-photon microscopy system. Typically for multi-photon microscopy, a pulsed near-IR laser (700 – 1,300 nm) is used in conjunction with SMs, lens (L), and a dichroic mirror (D) to image a specimen and collect the emitted fluorescence with a PMT. Figure was reprinted with permission from ©Hoover *et. al*., 2013, originally published in *Nature Photonics* (Hoover and Squier 2013).

Once the multi-photon microscopy system is built, we will develop an *in vivo* angiogenesis assay that will utilize fluorescent PLA scaffolds with known elastic properties incorporated into the highly vascularized CAM of the developing chicken embryo. Fertilized *Gallus gallus* eggs (Granjas Gibert, Tarragona, Spain) will be washed and incubated at 37ºC and relative humidity of 90% for 3 days. On incubation day 3, the eggs will be broken and the embryos will be transferred to sterile petri dishes. On day 7, PLA scaffolds (a generous gift from Dr. Oscar Castaño at the Institute for Bioengineering of Catalonia, Barcelona, Spain) with known elastic properties containing 0.1% FITC or 0.1, 0.01, or 0.001% rhodamine will be cut into 2 × 2, 1 × 1, or 1 × 0.5 cm rectangles and added to the embryo CAM in a planar or rolled orientation.

To allow for visualization of blood vessels, on day 10 of incubation, embryos will be injected via a CAM vein with 100 µL of 10 kDa Cascade Blue-dextran (1 mg/mL; Life Technologies), 2 MDa FITC-dextran (1 mg/mL; Sigma-Aldrich), or FITC-lectin from *Lycopersican esculentum* (0.1 mg/mL; Sigma-Aldrich) using a micropipette made from G-1 borosilicate capillary tubes (Narishige, Tokyo, Japan) pulled with a P-97 Flaming/Brown micropipette puller (Sutter Instruments, Novato, CA). To secure the scaffold and minimize movement during imaging, embryos will be placed in a custom designed, 3D printed chamber (Figure 7.5).

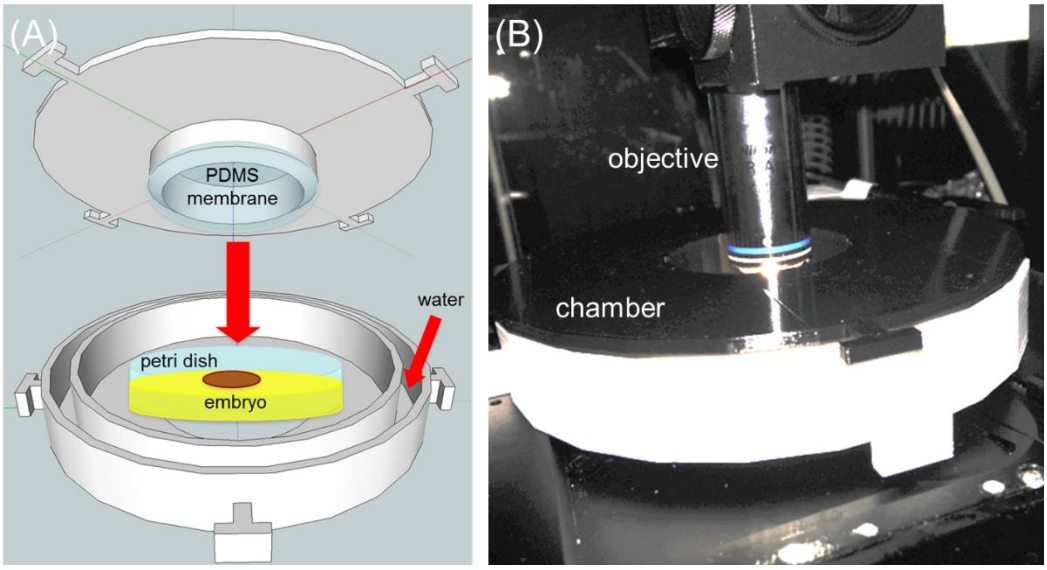

Figure 7.5 Schematic of chicken embryo chamber. (A) 3D drawing of designed chicken embryo chamber. A polydimethylsiloxane (PDMS) membrane is placed over the lid objective opening and is pressed down into the embryo in the petri dish. The outside well contains sterile water to maintain humidity during imaging. (B) Image of the 3D printed chamber assembled on the microscope stage with the objective aligned over the embryo.

Time-lapse, 3D images of scaffold deformation from new blood vessel growth will be acquired using the developed multi-photon microscopy system. Traction forces will then be calculated using a custom MATLAB program using finite element analysis. Embryos

will be sacrificed at day 13 with 10 mL of 10% PFA for 1 hr at 37^{o}C and scaffolds will be excised from the CAM for confocal imaging.

The excised scaffolds will be incubated overnight at -20^{o}C with an optimal cutting temperature (OCT) cryostat-embedding compound (Tissue-Tek, Torrance, CA), cryosectioned into 10 µm thick slices using a Leica Cryostat (Leica Biosystems, Germany), and slices will be placed onto StarFrost microscope slides (FisherScientific). Cryosectioned samples will be incubated with blocking buffer (1.5 mg/mL glycine in PBS; 6% BSA) for 1 hr at 37^{o}C, followed by staining with a primary rabbit anti-chicken CD144/VE-cadherin polyclonal antibody (1:100; ThermoFisher Scientific) in blocking buffer overnight at 4^{o}C. Samples will then be washed 3 times for 15 min in wash buffer (1.5 mg/mL glycine in PBS), incubated with a secondary goat anti-rabbit Alexa Fluor 350 antibody (1:300; Life Technologies) diluted in blocking buffer for 1 hr at 37^{o}C, and washed 3 times with wash buffer for 15 min each wash. The samples will then be stained with FITC-lectin (0.1 mg/mL) for 2 hr at 25^{o}C and washed with wash buffer. Stained samples will then be mounted with Mowiol 4-88 mounting medium (Sigma-Aldrich) and imaged with a confocal microscope.

To determine the PLA scaffold rhodamine concentration that produces a fluorescence signal in the dynamic range of the PMTs, scaffolds with 0.1, 0.01, or 0.001% rhodamine were added to embryos and imaged with the multi-photon microscopy system. We found that 0.001% rhodamine yielded the optimal scaffold fluorescence for resolving images with the developed system. To investigate the fluorescence intensity of different stains in

blood vessels, a 1 mg/mL 10 kDa Cascade Blue-dextran, 1 mg/mL 2 MDa FITC-dextran, or 0.1 mg/mL FITC-lectin were injected into a CAM vein and imaged over 2 hrs with the system. Our preliminary results found that the use of FITC-lectin or 2 MDa dextran resulted in the optimal vessel fluorescence for the duration of imaging (Figure 7.6).

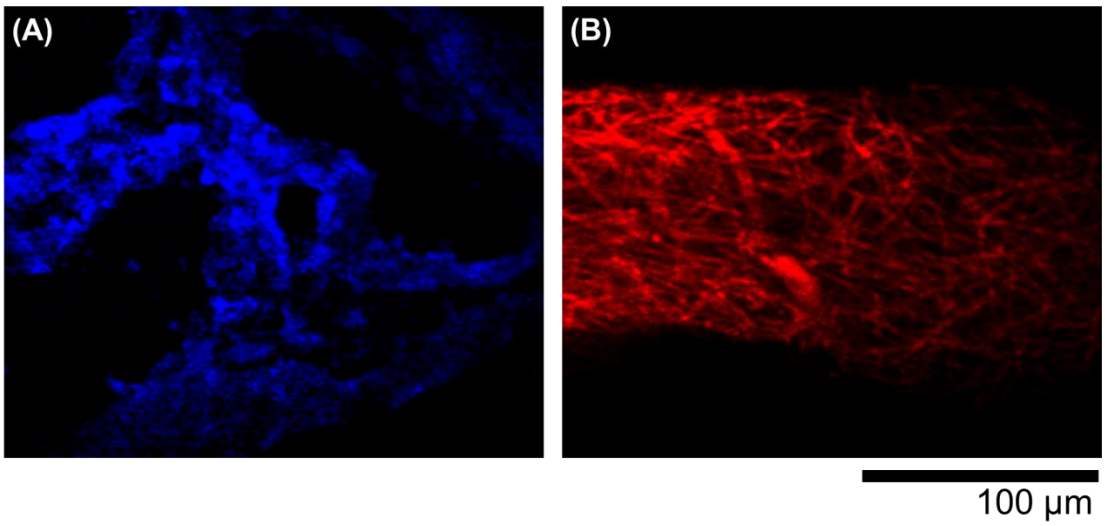

Figure 7.6 Multi-photon microscopy imaging. (A) Multi-photon microscopy image of a chicken embryo CAM blood vessel injected with fluorescent 2 MDa dextran. (B) Multi-photon image of PLA scaffold containing 0.001% rhodamine.

To determine embryo survival after injection with fluorescent stains, we compared the hours embryos were alive following injection with either 1 mg/mL dextran or 0.1 mg/mL lectin. We found that injection of dextran increased embryo survival by 83.3% compared with lectin injection (Figure 7.7). Although dextran is more biocompatible and less toxic than lectins, our results indicate that either stains can be used for 2 hrs of imaging. However, for longer imaging experiments that will be performed for 12 hrs, only dextran will be injected into embryos.

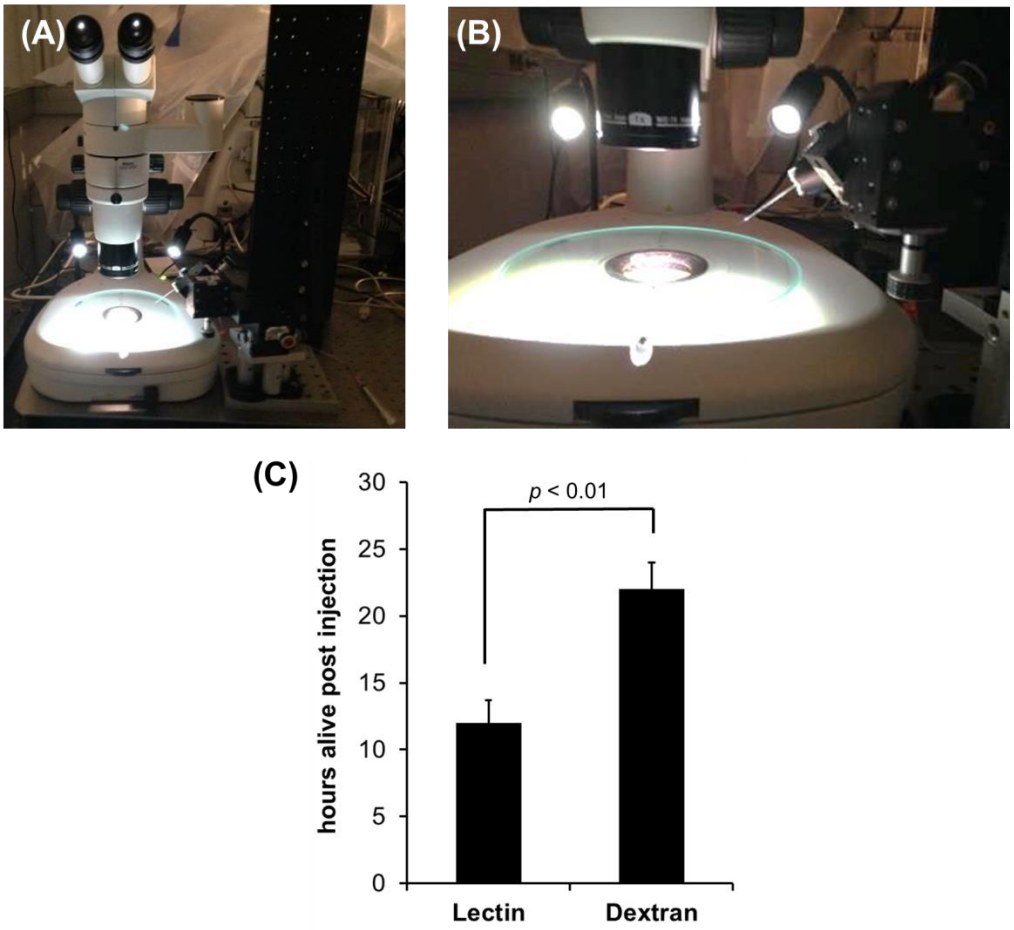

Figure 7.7 Injection setup and embryo survival rate. (A) Injection micromanipulator and light microscope setup for injecting dextran or lectin into chicken embryo CAM veins. (B) Detailed image of micromanipulator injection apparatus and light microscope. (C) Mean hours chicken embryos alive following lectin or dextran injection. Error bars are SEM.

In early experiments, it was noted that blood vessel growth varied depending on the orientation and size of the PLA scaffolds. To determine a scaffold orientation that results in the desired degree of vessel growth, we cut PLA scaffolds into 2 × 2, 1 × 1, or 1 × 0.5 cm rectangles and added them to the embryo CAM in a planar or rolled orientation. After 3 days of incubation with the scaffolds, the embryos were fixed, scaffolds were removed from the CAM, and scaffolds were cryosectioned and stained with Alexa Fluor 350-

CD144/VE-cadherin, and FITC-lectin, as previously described. Confocal imaging revealed maximal blood vessel interactions for 1 × 0.5 cm scaffolds in the rolled orientation (Figure 7.8).

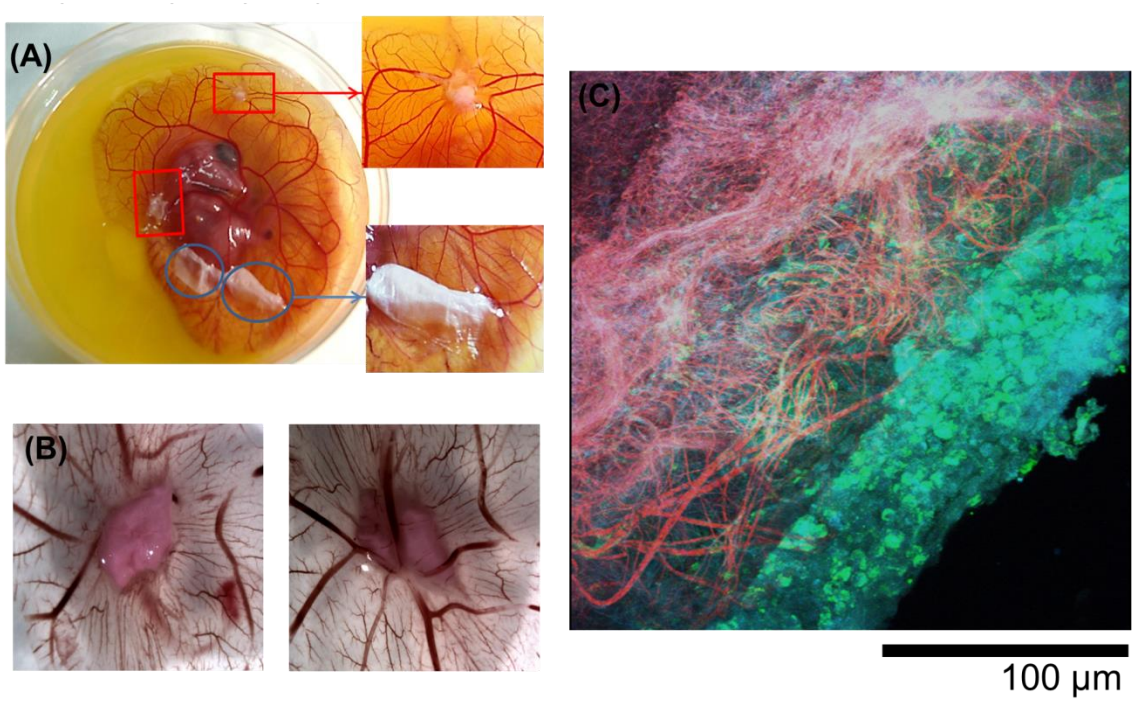

Figure 7.8 Chicken CAM blood vessel growth into scaffolds. (A) Left: Chicken embryo at developmental day 10 with rhodamine PLA scaffolds integrated into the CAM. Top right: 1 × 0.5 cm rhodamine PLA scaffold in rolled orientation. Bottom right: 1 × 1 cm rhodamine PLA scaffold in rolled orientation. (B) Representative images of a rhodamine scaffold in rolled orientation removed from the embryo CAM as viewed from above (left) and below (right). (C) Confocal fluorescent image of a cryosectioned rhodamine scaffold (red) in rolled orientation stained with FITC-lectin and a primary CD144/VE-cadherin antibody and an Alexa Fluor 350 secondary antibody.

This project will provide a novel setup for measuring the mechanical forces exerted by endothelial cells during angiogenesis *in vivo*. Use of this model will further our understanding of the fundamental biophysical mechanisms of *in vivo* angiogenesis, possibly providing a foundation for the development of new medical interventions for treating diseases associated with angiogenesis.

References

Aarts PA, Bolhuis PA, Sakariassen KS *et al.* Red blood cell size is important for adherence of blood platelets to artery subendothelium. *Blood* 1983;**62**:214–7.

Aeed PA, Nakajima M, Welch DR. The role of polymorphonuclear leukocytes (PMN) on the growth and metastatic potential of 13762nf mammary adenocarcinoma cells. *Int J Cancer* 1988;**42**:748–59.

Ahn KC, Jun AJ, Pawar P *et al.* Preferential binding of platelets to monocytes over neutrophils under flow. *Biochem Biophys Res Commun* 2005;**329**:345–55.

Altinbas M, Coskun HS, Er O *et al.* A randomized clinical trial of combination chemotherapy with and without low-molecular-weight heparin in small cell lung cancer. *J Thromb Haemost* 2004;**2**:1266–71.

Alves CS, Burdick MM, Thomas SN *et al.* The dual role of CD44 as a functional P-selectin ligand and fibrin receptor in colon carcinoma cell adhesion. *Am J Physiol - Cell Physiol* 2008;**294**:C907–16.

Alves CS, Yakovlev S, Medved L *et al.* Biomolecular characterization of CD44-fibrin(ogen) binding: distinct molecular requirements mediate binding of standard and variant isoforms of CD44 to immobilized fibrin(ogen). *J Biol Chem* 2009;**284**:1177–89.

Andrew M, Paes B, Johnston M. Development of the hemostatic system in the neonate and young infant. *Am J Pediatr Hematol Oncol* 1990;**12**:95–104.

Ariëns RAS, Lai T-S, Weisel JW *et al.* Role of factor XIII in fibrin clot formation and effects of genetic polymorphisms. *Blood* 2002;**100**:743–54.

Armand J. Q. A study of the coagulation defect in hemophilia and in jaundice. *Am J Med Sci* 1935;**190**:501–10.

Arnison MR, Cogswell CJ, Smith NI *et al.* Using the Hilbert transform for 3D visualization of differential interference contrast microscope images. *J Microsc* 2000;**199**:79–84.

Ascensao JL, Oken MM, Ewing SL *et al.* Leukocytosis and large cell lung cancer. A frequent association. *Cancer* 1987;**60**:903–5.

Aslan JE, Baker SM, Loren CP *et al.* The PAK system links Rho GTPase signaling to thrombin-mediated platelet activation. *Am J Physiol - Cell Physiol* 2013;**305**:C519–28.

Baker-Groberg SM, Bornstein S, Zilberman-Rudenko J *et al.* Effect of ionizing radiation on the physical biology of head and neck squamous cell carcinoma cells. *Cell Mol Bioeng* 2015:1–9.

Baker-Groberg SM, Phillips KG, McCarty OJT. Quantification of volume, mass, and density of thrombus formation using brightfield and differential interference contrast microscopy. *J Biomed Opt* 2013;**18**:016014–016014.

Baker SM, Phillips KG, McCarty OJT. Development of a label-free imaging technique for the quantification of thrombus formation. *Cell Mol Bioeng* 2012;**5**:488–92.

Bambace NM, Holmes CE. The platelet contribution to cancer progression. *J Thromb Haemost* 2011;**9**:237–49.

Barer R. Determination of dry mass, thickness, solid and water concentration in living cells. *Nature* 1953;**172**:1097–8.

Bergmeier W, Stefanini L. Platelet ITAM signaling. *Curr Opin Hematol* 2013;**20**:445–50.

Berny-Lang MA. Thrombin, thrombus, thrombi mechanisms of thrombus formation under flow. *Sch Arch* 2010.

Berny MA, Munnix ICA, Auger JM *et al.* Spatial distribution of factor Xa, thrombin, and fibrin(ogen) on thrombi at venous shear. *PLoS ONE* 2010;**5**:e10415.

Blair P, Flaumenhaft R. Platelet alpha-granules: basic biology and clinical correlates. *Blood Rev* 2009;**23**:177–89.

Blair SD, Menashi S, Samson D *et al.* Whole blood clotting tests: an evaluation of five methods. *Clin Lab Haematol* 1987;**9**:91–4.

Boccardo P, Remuzzi G, Galbusera M. Platelet dysfunction in renal failure. *Semin Thromb Hemost* 2004;**30**:579–89.

Bockhorn M, Jain RK, Munn LL. Active versus passive mechanisms in metastasis: do cancer cells crawl into vessels, or are they pushed? *Lancet Oncol* 2007;**8**:444–8.

Bolton-Maggs PHB, Perry DJ, Chalmers EA *et al.* The rare coagulation disorders--review with guidelines for management from the United Kingdom Haemophilia Centre Doctors' Organisation. *Haemoph Off J World Fed Hemoph* 2004;**10**:593–628.

Borensztajn K, Peppelenbosch MP, Spek CA. Factor Xa: at the crossroads between coagulation and signaling in physiology and disease. *Trends Mol Med* 2008;**14**:429–40.

Borsig L, Wong R, Feramisco J *et al.* Heparin and cancer revisited: mechanistic connections involving platelets, P-selectin, carcinoma mucins, and tumor metastasis. *Proc Natl Acad Sci U S A* 2001;**98**:3352–7.

Boulaftali Y, Hess PR, Kahn ML *et al.* Platelet immunoreceptor tyrosine-based activation motif (ITAM) signaling and vascular integrity. *Circ Res* 2014;**114**:1174–84.

Bowman M, Hopman WM, Rapson D *et al.* A prospective evaluation of the prevalence of symptomatic von Willebrand disease (VWD) in a pediatric primary care population. *Pediatr Blood Cancer* 2010;**55**:171–3.

Bromberg ME, Konigsberg WH, Madison JF *et al.* Tissue factor promotes melanoma metastasis by a pathway independent of blood coagulation. *Proc Natl Acad Sci U S A* 1995;**92**:8205–9.

Broze GJ, Girard TJ. Tissue factor pathway inhibitor: structure-function. *Front Biosci Landmark Ed* 2012;**17**:262–80.

von Brühl M-L, Stark K, Steinhart A *et al.* Monocytes, neutrophils, and platelets cooperate to initiate and propagate venous thrombosis in mice in vivo. *J Exp Med* 2012;**209**:819–35.

Camerer E, Kolstø AB, Prydz H. Cell biology of tissue factor, the principal initiator of blood coagulation. *Thromb Res* 1996;**81**:1–41.

Camerer E, Qazi AA, Duong DN *et al.* Platelets, protease-activated receptors, and fibrinogen in hematogenous metastasis. *Blood* 2004;**104**:397–401.

Campbell RA, Overmyer KA, Selzman CH *et al.* Contributions of extravascular and intravascular cells to fibrin network formation, structure, and stability. *Blood* 2009;**114**:4886–96.

Cardinal DC, Flower RJ. The electronic aggregometer: a novel device for assessing platelet behavior in blood. *J Pharmacol Methods* 1980;**3**:135–58.

Cattaneo M. Molecular defects of the platelet P2 receptors. *Purinergic Signal* 2011;**7**:333–9.

Chambers AF, Groom AC, MacDonald IC. Metastasis: dissemination and growth of cancer cells in metastatic sites. *Nat Rev Cancer* 2002;**2**:563–72.

Choi SH, Smith SA, Morrissey JH. Polyphosphate is a cofactor for the activation of factor XI by thrombin. *Blood* 2011;**118**:6963–70.

Cho Y-I, Cho DJ. Hemorheology and microvascular disorders. *Korean Circ J* 2011;**41**:287–95.

Cines DB, Pollak ES, Buck CA *et al.* Endothelial cells in physiology and in the pathophysiology of vascular disorders. *Blood* 1998;**91**:3527–61.

Clemetson KJ, Clemetson JM. Platelet collagen receptors. *Thromb Haemost* 2001;**86**:189–97.

Corby DG, O'Barr TP. Decreased alpha-adrenergic receptors in newborn platelets: cause of abnormal response to epinephrine. *Dev Pharmacol Ther* 1981;**2**:215–25.

Cortinovis A, Crippa A, Cavalli R *et al.* Capillary blood viscosity in microcirculation. *Clin Hemorheol Microcirc* 2006;**35**:183–92.

Coussens LM, Werb Z. Inflammation and cancer. *Nature* 2002;**420**:860–7.

Crawley JTB, Zanardelli S, Chion CKNK *et al.* The central role of thrombin in hemostasis. *J Thromb Haemost* 2007;**5**:95–101.

Dahlbäck B. Blood coagulation. *The Lancet* 2000;**355**:1627–32.

Dahlback B, Villoutreix BO. The anticoagulant protein C pathway. *Febs Lett* 2005;**579**:3310–6.

Daly ME. Determinants of platelet count in humans. *Haematologica* 2011;**96**:10–3.

Dardik R, Kaufmann Y, Savion N *et al.* Platelets mediate tumor cell adhesion to the subendothelium under flow conditions: involvement of platelet GPIIb-IIIa and tumor cell alpha(v) integrins. *Int J Cancer J Int Cancer* 1997;**70**:201–7.

De Clerck LS, Bridts CH, Mertens AM *et al.* Use of fluorescent dyes in the determination of adherence of human leucocytes to endothelial cells and the effect of fluorochromes on cellular function. *J Immunol Methods* 1994;**172**:115–24.

De Cuyper IM, Meinders M, van de Vijver E *et al.* A novel flow cytometry-based platelet aggregation assay. *Blood* 2013;**121**:e70–80.

Del Vecchio A, Motta M, Romagnoli C. Neonatal platelet function. *Clin Perinatol*, DOI: 10.1016/j.clp.2015.04.015.

Di Carlo E, Forni G, Lollini P *et al.* The intriguing role of polymorphonuclear neutrophils in antitumor reactions. *Blood* 2001;**97**:339–45.

Donnelly KM, Bromberg ME, Milstone A *et al.* Ancylostoma caninum anticoagulant peptide blocks metastasis in vivo and inhibits factor Xa binding to melanoma cells in vitro. *Thromb Haemost* 1998;**79**:1041–7.

Duke WW. The relation of blood platelets to hemorrhagic disease. By W.W. Duke. *JAMA J Am Med Assoc* 1983;**250**:1201–9.

Du X. Signaling and regulation of the platelet glycoprotein Ib-IX-V complex. *Curr Opin Hematol* 2007;**14**:262–9.

Dvorak HF, Van DeWater L, Bitzer AM *et al.* Procoagulant activity associated with plasma membrane vesicles shed by cultured tumor cells. *Cancer Res* 1983;**43**:4434–42.

Dzierzak E, Philipsen S. Erythropoiesis: development and differentiation. *Cold Spring Harb Perspect Med* 2013;**3**:a011601.

Enns A, Korb T, Schlüter K *et al.* αvβ5-Integrins mediate early steps of metastasis formation. *Eur J Cancer* 2005;**41**:1065–72.

Falati S, Gross P, Merrill-Skoloff G *et al.* Real-time in vivo imaging of platelets, tissue factor and fibrin during arterial thrombus formation in the mouse. *Nat Med* 2002;**8**:1175–81.

Favaloro EJ, Funk DM, Lippi G. Preanalytical and postanalytical variables: the leading causes of diagnostic error in hemostasis? *Lab Med* 2012;**43**:1–10.

Felding-Habermann B, Habermann R, Saldívar E *et al.* Role of beta3 integrins in melanoma cell adhesion to activated platelets under flow. *J Biol Chem* 1996;**271**:5892–900.

Ferrer-Marin F, Chavda C, Lampa M *et al.* Effects of in vitro adult platelet transfusions on neonatal hemostasis. *J Thromb Haemost JTH* 2011;**9**:1020–8.

Ferrer-Marin F, Stanworth S, Josephson C *et al.* Distinct differences in platelet production and function between neonates and adults: implications for platelet transfusion practice. *Transfusion (Paris)* 2013;**53**:2814–21.

Frank J, Altmeyer S, Wernicke G. Non-interferometric, non-iterative phase retrieval by Green's functions. *J Opt Soc Am A Opt Image Sci Vis* 2010;**27**:2244–51.

Friedl P, Alexander S. Cancer invasion and the microenvironment: plasticity and reciprocity. *Cell* 2011;**147**:992–1009.

Fulkerson PC, Rothenberg ME. Targeting eosinophils in allergy, inflammation and beyond. *Nat Rev Drug Discov* 2013;**12**:117–29.

Furie B, Furie BC. Molecular and cellular biology of blood coagulation. *N Engl J Med* 1992;**326**:800–6.

Furie B, Furie BC, Flaumenhaft R. A journey with platelet P-selectin: the molecular basis of granule secretion, signalling and cell adhesion. *Thromb Haemost* 2001;**86**:214–21.

Garcia D, Libby E, Crowther MA. The new oral anticoagulants. *Blood* 2010;**115**:15–20.

Gasic GJ, Gasic TB, Stewart CC. Antimetastatic effects associated with platelet reduction. *Proc Natl Acad Sci U S A* 1968;**61**:46–52.

Gay LJ, Felding-Habermann B. Platelets alter tumor cell attributes to propel metastasis: programming in transit. *Cancer Cell* 2011;**20**:553–4.

Gelman B, Setty BN, Chen D *et al.* Impaired mobilization of intracellular calcium in neonatal platelets. *Pediatr Res* 1996;**39**:692–6.

Ghasemzadeh M, Kaplan ZS, Alwis I *et al.* The CXCR1/2 ligand NAP-2 promotes directed intravascular leukocyte migration through platelet thrombi. *Blood* 2013;**121**:4555–66.

Ghoshal K, Bhattacharyya M, Ghoshal K *et al.* Overview of platelet physiology: its hemostatic and nonhemostatic role in disease pathogenesis. *Sci World J* 2014;**2014**:e781857.

Gramatikov B. *Handbook of Biomedical Optics*. Boas D, Pitris C, Ramanujam N (eds.). New York, NY: CRC Press, 2012.

Granger DN, Rodrigues SF, Yildirim A *et al.* Microvascular responses to cardiovascular risk factors. *Microcirculation* 2010;**17**:192–205.

Gresele P, Born GVR, Patrono C *et al.* eds. *Antiplatelet Agents*. Berlin, Heidelberg: Springer Berlin Heidelberg, 2012.

Grivennikov SI, Greten FR, Karin M. Immunity, inflammation, and cancer. *Cell* 2010;**140**:883–99.

Gruber A, Marzec UM, Bush L *et al.* Relative antithrombotic and antihemostatic effects of protein C activator versus low-molecular-weight heparin in primates. *Blood* 2007;**109**:3733–40.

Haier J, Nicolson GL. Tumor cell adhesion under hydrodynamic conditions of fluid flow. *APMIS* 2001;**109**:241–62.

Haley KM, Recht M, McCarty OJT. Neonatal platelets: mediators of primary hemostasis in the developing hemostatic system. *Pediatr Res* 2014;**76**:230–7.

Hanke AA, Roberg K, Monaca E *et al.* Impact of platelet count on results obtained from multiple electrode platelet aggregometry (Multiplate^{TM}). *Eur J Med Res* 2010;**15**:214.

Hanley W, McCarty O, Jadhav S *et al.* Single-molecule binding of CD44 to fibrin versus P-selectin predicts their distinct shear-dependent interactions in cancer. *J Biol Chem* 2003;**278**:10556–61.

Harrison P, Mackie I, Mumford A *et al.* Guidelines for the laboratory investigation of heritable disorders of platelet function. *Br J Haematol* 2011;**155**:30–44.

Heisig N. *Functional Analysis of the Microcirculation in the Exocrine Pancreas*. 1st ed. Harders (ed.). Basel, NY: S. Karger, 1967.

van Herrewegen F, Meijers JCM, Peters M *et al.* Clinical practice. *Eur J Pediatr* 2012;**171**:207–14.

Hiramoto R, Bernecky J, Jurandowski J *et al.* Fibrin in human tumors. *Cancer Res* 1960;**20**:592–3.

Hiramoto R, Yagi Y, Pressman D. Immunohistochemical studies of antibodies in anti-murphy lymphosarcoma sera. *Cancer Res* 1959;**19**:874.

Honn KV, Tang DG, Crissman JD. Platelets and cancer metastasis: A causal relationship? *Cancer Metastasis Rev* 1992;**11**:325–51.

Hoover EE, Squier JA. Advances in multiphoton microscopy technology. *Nat Photonics* 2013;**7**:93–101.

Horton NG, Wang K, Kobat D *et al.* In vivo three-photon microscopy of subcortical structures within an intact mouse brain. *Nat Photonics* 2013;**7**:205–9.

Horton S, Augustin S. Activated clotting time (ACT). *Methods Mol Biol Clifton NJ* 2013;**992**:155–67.

Huang Y-Q, Li J-J, Karpatkin S. Thrombin inhibits tumor cell growth in association with up-regulation of p21(waf/cip1) and caspases via a p53-independent, STAT-1-dependent pathway. *J Biol Chem* 2000;**275**:6462–8.

Icli F, Akbulut H, Utkan G *et al.* Low molecular weight heparin (LMWH) increases the efficacy of cisplatinum plus gemcitabine combination in advanced pancreatic cancer. *J Surg Oncol* 2007;**95**:507–12.

Ishikawa M, Koga Y, Hosokawa M *et al.* Augmentation of B16 melanoma lung colony formation in C57BL/6 mice having marked granulocytosis. *Int J Cancer J Int Cancer* 1986;**37**:919–24.

Israels SJ. Diagnostic evaluation of platelet function disorders in neonates and children: an update. *Semin Thromb Hemost* 2009;**35**:181–8.

Israels SJ, Cheang T, McMillan-Ward EM *et al.* Evaluation of primary hemostasis in neonates with a new in vitro platelet function analyzer. *J Pediatr* 2001;**138**:116–9.

Israels SJ, Cheang T, Roberston C *et al.* Impaired signal transduction in neonatal platelets. *Pediatr Res* 1999;**45**:687–91.

Israels SJ, Rand ML, Michelson AD. Neonatal platelet function. *Semin Thromb Hemost* 2003;**29**:363–72.

Itakura A, McCarty OJT. Pivotal role for the mTOR pathway in the formation of neutrophil extracellular traps (NETs) via regulation of autophagy. *Am J Physiol Cell Physiol* 2013, DOI: 10.1152/ajpcell.00108.2013.

Iversen LH, Thorlacius-Ussing O. Systemic coagulation reactivation in recurrence of colorectal cancer. *Thromb Haemost* 2003;**89**:726–34.

Ivy AC, Nelson D, Bucher G. The standardization of certain factors in the cutaneous "venostasis" bleeding time technique. *J Lab Clin Med* 1941;**26**:1812–22.

Jadhav S, Bochner BS, Konstantopoulos K. Hydrodynamic shear regulates the kinetics and receptor specificity of polymorphonuclear leukocyte-colon carcinoma cell adhesive interactions. *J Immunol* 2001;**167**:5986–93.

Jadhav S, Konstantopoulos K. Fluid shear- and time-dependent modulation of molecular interactions between PMNs and colon carcinomas. *Am J Physiol - Cell Physiol* 2002;**283**:C1133–43.

Jung SM, Takemura Y, Imamura Y *et al.* Collagen-type specificity of glycoprotein VI as a determinant of platelet adhesion. *Platelets* 2008;**19**:32–42.

Keuren JFW, Wielders SJH, Ulrichts H *et al.* Synergistic effect of thrombin on collagen-induced platelet procoagulant activity is mediated through protease-activated receptor-1. *Arterioscler Thromb Vasc Biol* 2005;**25**:1499–505.

Kitayama J, Tsuno N, Sunami E *et al.* E-selectin can mediate the arrest type of adhesion of colon cancer cells under physiological shear flow. *Eur J Cancer Oxf Engl 1990* 2000;**36**:121–7.

Kitchen S, Makris M. Laboratory tests of hemostasis. In: Key N, Kris M, O'Shaughnessy D, et al. (eds.). *Practical Hemostasis and Thrombosis*. Wiley-Blackwell, 2009, 7–16.

Klerk CPW, Smorenburg SM, Otten H-M *et al.* The effect of low molecular weight heparin on survival in patients with advanced malignancy. *J Clin Oncol* 2005;**23**:2130–5.

Kong L, Dunn GD, Keefert LK *et al.* Nitric oxide reduces tumor cell adhesion to isolated rat postcapillary venules. *Clin Exp Metastasis* 1996;**14**:335–43.

Konstantopoulos K, Thomas SN. Cancer cells in transit: the vascular interactions of tumor cells. *Annu Rev Biomed Eng* 2009;**11**:177–202.

Koutsi A, Papapanagiotou A, Papavassiliou AG. Thrombomodulin: from haemostasis to inflammation and tumourigenesis. *Int J Biochem Cell Biol* 2008;**40**:1669–73.

Kroll MH, Hellums JD, McIntire LV *et al.* Platelets and shear stress. *Blood* 1996;**88**:1525–41.

Kühne T, Imbach P. Neonatal platelet physiology and pathophysiology. *Eur J Pediatr* 1998;**157**:87–94.

Kundu SK, Heilmann EJ, Sio R *et al.* Description of an in vitro platelet function analyzer--PFA-100. *Semin Thromb Hemost* 1995;**21**:106–12.

Labelle M, Begum S, Hynes RO. Direct signaling between platelets and cancer cells induces an epithelial-mesenchymal-like transition and promotes metastasis. *Cancer Cell* 2011;**20**:576–90.

Lammle B, Wuillemin W, Huber I *et al.* Thromboembolism and bleeding tendency in congenital factor XII deficiency-a study on 74 subjects from 14 Swiss families. *Thromb Haemost* 1991;**65**:117–21.

Langdell RD, Wagner RH, Brinkhous KM. Effect of antihemophilic factor on one-stage clotting tests; a presumptive test for hemophilia and a simple one-stage antihemophilic factor assay procedure. *J Lab Clin Med* 1953;**41**:637–47.

de Lange F de, Cambi A, Huijbens R *et al.* Cell biology beyond the diffraction limit: near-field scanning optical microscopy. *J Cell Sci* 2001;**114**:4153–60.

Läubli H, Stevenson JL, Varki A *et al.* L-selectin facilitation of metastasis involves temporal induction of Fut7-dependent ligands at sites of tumor cell arrest. *Cancer Res* 2006;**66**:1536–42.

Lawrence MB, Smith CW, Eskin SG *et al.* Effect of venous shear stress on CD18-mediated neutrophil adhesion to cultured endothelium. *Blood* 1990;**75**:227–37.

Lee CA, Berntorp EE, Hoots WK. *Textbook of Hemophilia*. John Wiley & Sons, 2008.

Lee S-H, Roichman Y, Yi G-R *et al.* Characterizing and tracking single colloidal particles with video holographic microscopy. *Opt Express* 2007;**15**:18275–82.

Leger AJ, Jacques SL, Badar J *et al.* Blocking the protease-activated receptor 1-4 heterodimer in platelet-mediated thrombosis. *Circulation* 2006;**113**:1244–54.

Lei KF, Chen K-H, Tsui P-H *et al.* Real-time electrical impedimetric monitoring of blood coagulation process under temperature and hematocrit variations conducted in a microfluidic chip. *PLoS ONE* 2013;**8**, DOI: 10.1371/journal.pone.0076243.

Lin W-W, Karin M. A cytokine-mediated link between innate immunity, inflammation, and cancer. *J Clin Invest* 2007;**117**:1175–83.

Lipowsky HH. Microvascular rheology and hemodynamics. *Microcirc N Y N 1994* 2005;**12**:5–15.

Litalien C, Jacqz-Aigrain E. Risks and benefits of nonsteroidal anti-inflammatory drugs in children: a comparison with paracetamol. *Paediatr Drugs* 2001;**3**:817–58.

Li Y-SJ, Haga JH, Chien S. Molecular basis of the effects of shear stress on vascular endothelial cells. *J Biomech* 2005;**38**:1949–71.

Luz LT da, Nascimento B, Rizoli S. Thrombelastography (TEG®): practical considerations on its clinical use in trauma resuscitation. *Scand J Trauma Resusc Emerg Med* 2013;**21**:29.

Luzzatto G, Schafer AI. The prethrombotic state in cancer. *Semin Oncol* 1990;**17**:147–59.

Machan M, Kroh J-M, Hunt E *et al.* Letter: Basal cell carcinoma with vascular invasion. *Dermatol Online J* 2012;**18**:13.

Mackman N. New insights into the mechanisms of venous thrombosis. *J Clin Invest* 2012;**122**:2331–6.

Maloney SF, Brass LF, Diamond SL. P2Y12 or P2Y1 inhibitors reduce platelet deposition in a microfluidic model of thrombosis while apyrase lacks efficacy under flow conditions. *Integr Biol Quant Biosci Nano Macro* 2010;**2**:183–92.

Mammen EF. Coagulation abnormalities in liver disease. *Hematol Oncol Clin North Am* 1992;**6**:1247–57.

Mannucci PM, Cattaneo M, Teresa Canciani M *et al.* Early presence of activated ("exhausted") platelets in malignant tumors (breast adenocarcinoma and malignant melanoma). *Eur J Cancer Clin Oncol* 1989;**25**:1413–7.

Mantovani A, Allavena P, Sica A *et al.* Cancer-related inflammation. *Nature* 2008;**454**:436–44.

Marossy A, Svorc P, Kron I *et al.* Hemorheology and circulation. *Clin Hemorheol Microcirc* 2009;**42**:239–58.

Mayrovitz HN. Skin capillary metrics and hemodynamics in the hairless mouse. *Microvasc Res* 1992;**43**:46–59.

McCarty OJT, Abulencia JP, Mousa SA *et al.* Evaluation of platelet antagonists in in vitro flow models of thrombosis. *Methods Mol Med* 2004;**93**:21–34.

McCarty OJT, Calaminus SDJ, Berndt MC *et al.* von Willebrand factor mediates platelet spreading through glycoprotein Ib and αIIbβ3 in the presence of botrocetin and ristocetin, respectively. *J Thromb Haemost* 2006;**4**:1367–78.

McCarty OJT, Jadhav S, Burdick MM *et al.* Fluid shear regulates the kinetics and molecular mechanisms of activation-dependent platelet binding to colon carcinoma cells. *Biophys J* 2002;**83**:836–48.

McCarty OJT, Larson MK, Auger JM *et al.* Rac1 is essential for platelet lamellipodia formation and aggregate stability under flow. *J Biol Chem* 2005;**280**:39474–84.

McCarty OJT, Mousa SA, Bray PF *et al.* Immobilized platelets support human colon carcinoma cell tethering, rolling, and firm adhesion under dynamic flow conditions. *Blood* 2000;**96**:1789–97.

McKee C. Excess leukocytosis (leukemoid reactions) associated with malignant diseases. *South Med J* 1985;**78**:1475–82.

McNicol A, Israels SJ. Platelet dense granules: structure, function and implications for haemostasis. *Thromb Res* 1999;**95**:1–18.

van der Meijden PEJ, Munnix ICA, Auger JM *et al.* Dual role of collagen in factor XII–dependent thrombus formation. *Blood* 2009;**114**:881–90.

Michelson AD. Flow cytometry: a clinical test of platelet function. *Blood* 1996;**87**:4925–36.

Michelson AD. Platelet function testing in cardiovascular diseases. *Circulation* 2004;**110**:e489–93.

Middelbeek J, Kuipers AJ, Henneman L *et al.* TRPM7 is required for breast tumor cell metastasis. *Cancer Res* 2012;**72**:4250–61.

Mócsai A. Diverse novel functions of neutrophils in immunity, inflammation, and beyond. *J Exp Med* 2013;**210**:1283–99.

Monroe DM, Hoffman M. What does it take to make the perfect clot? *Arterioscler Thromb Vasc Biol* 2006;**26**:41–8.

Mook ORF, Van Marle J, Vreeling-Sindelárová H *et al.* Visualization of early events in tumor formation of eGFP-transfected rat colon cancer cells in liver. *Hepatology* 2003;**38**:295–304.

Moroi M, Jung SM, Okuma M *et al.* A patient with platelets deficient in glycoprotein VI that lack both collagen-induced aggregation and adhesion. *J Clin Invest* 1989;**84**:1440–5.

Mozaffarian D, Benjamin EJ, Go AS *et al.* Heart disease and stroke statistics--2015 update: a report from the American Heart Association. *Circulation* 2015;**131**:e29–322.

Müller F, Mutch NJ, Schenk WA *et al.* Platelet polyphosphates are proinflammatory and procoagulant mediators in vivo. *Cell* 2009;**139**:1143–56.

van Munster EB, van Vliet LJ, Aten JA. Reconstruction of optical pathlength distributions from images obtained by a wide-field differential interference contrast microscope. *J Microsc* 1997;**188**:149–57.

Naess IA, Christiansen SC, Romundstad P *et al.* Incidence and mortality of venous thrombosis: a population-based study. *J Thromb Haemost* 2007;**5**:692–9.

Neuenschwander PF, Fiore MM, Morrissey JH. Factor VII autoactivation proceeds via interaction of distinct protease-cofactor and zymogen-cofactor complexes. Implications of a two-dimensional enzyme kinetic mechanism. *J Biol Chem* 1993;**268**:21489–92.

Nierodzik ML, Karpatkin S. Thrombin induces tumor growth, metastasis, and angiogenesis: Evidence for a thrombin-regulated dormant tumor phenotype. *Cancer Cell* 2006;**10**:355–62.

Nieswandt B, Hafner M, Echtenacher B *et al.* Lysis of tumor cells by natural killer cells in mice is impeded by platelets. *Cancer Res* 1999;**59**:1295–300.

Offermanns S. Activation of platelet function through G protein-coupled receptors. *Circ Res* 2006;**99**:1293–304.

O'Meara R a. Q. Coagulative properties of cancers. *Ir J Med Sci* 1958;**33**:474–9.

O'Meara R a. Q, Jackson RD. Cytological observations on carcinoma. *Ir J Med Sci* 1958;**33**:327–8.

van Ommen CH, Peters M. The bleeding child. Part I: primary hemostatic disorders. *Eur J Pediatr* 2012;**171**:1–10.

Orr FW, Mokashi S. Effect of leukocyte activation on the formation of heterotypic tumor-cell aggregates in vitro. *Int J Cancer* 1985;**35**:101–6.

Paganin D, Nugent KA. Noninterferometric phase imaging with partially coherent light. *Phys Rev Lett* 1998;**80**:2586–9.

Palumbo JS, Kombrinck KW, Drew AF *et al.* Fibrinogen is an important determinant of the metastatic potential of circulating tumor cells. *Blood* 2000;**96**:3302–9.

Palumbo JS, Potter JM, Kaplan LS *et al.* Spontaneous hematogenous and lymphatic metastasis, but not primary tumor growth or angiogenesis, is diminished in fibrinogen-deficient mice. *Cancer Res* 2002;**62**:6966–72.

Palumbo JS, Talmage KE, Massari JV *et al.* Platelets and fibrin(ogen) increase metastatic potential by impeding natural killer cell-mediated elimination of tumor cells. *Blood* 2005;**105**:178–85.

Pandhare AP, S.S.Jadhav. *Fluid Mechanics*. Technical Publications, 2009.

Papaioannou TG, Stefanadis C. Vascular wall shear stress: basic principles and methods. *Hell J Cardiol HJC Hellēnikē Kardiologikē Epitheōrēsē* 2005;**46**:9–15.

Pauer H-U, Renné T, Hemmerlein B *et al.* Targeted deletion of murine coagulation factor XII gene-a model for contact phase activation in vivo. *Thromb Haemost* 2004;**92**:503–8.

Perry DJ, Fitzmaurice DA, Kitchen S *et al.* Point-of-care testing in haemostasis. *Br J Haematol* 2010;**150**:501–14.

Phillips KG, Baker-Groberg SM, McCarty OJT. Quantitative optical microscopy: measurement of cellular biophysical features with a standard optical microscope. *J Vis Exp JoVE* 2014.

Phillips KG, Jacques SL, McCarty OJT. Measurement of single cell refractive index, dry mass, volume, and density using a transillumination microscope. *Phys Rev Lett* 2012;**109**:118105.

Phillips KG, Kolatkar A, Rees KJ *et al.* Quantification of cellular volume and sub-cellular density fluctuations: comparison of normal peripheral blood cells and circulating tumor cells identified in a breast cancer patient. *Front Oncol* 2012;**2**:96.

Phillips KG, McCarty OJT. Optical quantification of cellular mass, volume, and density of circulating tumor cells identified in an ovarian cancer patient. *Front Cancer Mol Targets Ther* 2012;**2**:72.

Polanowska-Grabowska R, Raha S, Gear AR. Adhesion efficiency, platelet density and size. *Br J Haematol* 1992;**82**:715–20.

Popel AS, Johnson PC. Microcirculation and hemorheology. *Annu Rev Fluid Mech* 2005;**37**:43–69.

Popescu G. Quantitative phase imaging of nanoscale cell structure and dynamics. *Methods Cell Biol* 2008;**90**:87–115.

Popescu G, Park Y, Choi W *et al.* Imaging red blood cell dynamics by quantitative phase microscopy. *Blood Cells Mol Dis* 2008;**41**:10–6.

Preza C, van Munster EB, Aten JA *et al.* Determination of direction-independent optical path length distribution of cells using rotational-diversity transmitted-light differential-interference-contrast (DIC). In: Cogswell CJ, Conchello J-A, Lerner JM, et al. (eds.). 1998, 60–70.

Puy C, Tucker EI, Wong ZC *et al.* Factor XII promotes blood coagulation independent of factor XI in the presence of long-chain polyphosphates. *J Thromb Haemost* 2013;**11**:1341–52.

Rajasekhar D, Kestin AS, Bednarek FJ *et al.* Neonatal platelets are less reactive than adult platelets to physiological agonists in whole blood. *Thromb Haemost* 1994;**72**:957–63.

Ratnoff OD, Colopy JE. A familial hemorrhagic trait associated with a deficiency of a clot-promoting fraction of plasma. *J Clin Invest* 1955;**34**:602–13.

Reitsma PH, Versteeg HH, Middeldorp S. Mechanistic view of risk factors for venous thromboembolism. *Arterioscler Thromb Vasc Biol* 2012;**32**:563–8.

Renné T, Gailani D. Role of Factor XII in hemostasis and thrombosis: clinical implications. *Expert Rev Cardiovasc Ther* 2007;**5**:733–41.

Riewald M, Ruf W. Mechanistic coupling of protease signaling and initiation of coagulation by tissue factor. *Proc Natl Acad Sci U S A* 2001;**98**:7742–7.

Roberts DE, McNicol A, Bose R. Mechanism of collagen activation in human platelets. *J Biol Chem* 2004;**279**:19421–30.

Roschitz B, Sudi K, Köstenberger M *et al.* Shorter PFA-100 closure times in neonates than in adults: role of red cells, white cells, platelets and von Willebrand factor. *Acta Paediatr Oslo Nor 1992* 2001;**90**:664–70.

Rosenthal RL, Dreskin OH, Rosenthal N. New hemophilia-like disease caused by deficiency of a third plasma thromboplastin factor. *Proc Soc Exp Biol Med Soc Exp Biol Med N Y N* 1953;**82**:171–4.

Ruggeri ZM. Platelets in atherothrombosis. *Nat Med* 2002;**8**:1227–34.

Sadler JE. Redeeming ristocetin. *Blood* 2010;**116**:155–6.

Sakariassen KS, Nievelstein PF, Coller BS *et al.* The role of platelet membrane glycoproteins Ib and IIb-IIIa in platelet adherence to human artery subendothelium. *Br J Haematol* 1986;**63**:681–91.

Salles I, Broos K, Fontayne A *et al.* Development of a high-throughput ELISA assay for platelet function testing using platelet-rich plasma or whole blood. *Thromb Haemost* 2010;**104**:392–401.

Salooja N, Perry DJ. Thrombelastography. *Blood Coagul Fibrinolysis Int J Haemost Thromb* 2001;**12**:327–37.

Sampson MT, Kakkar AK. Coagulation proteases and human cancer. *Biochem Soc Trans* 2002;**30**:201–7.

Santoro SA. Identification of a 160,000 dalton platelet membrane protein that mediates the initial divalent cation-dependent adhesion of platelets to collagen. *Cell* 1986;**46**:913–20.

Saving KL, Mankin PE, Gorman MJ. Differences in adhesion receptor expression between immature and older platelets and red blood cells of neonates and adults. *J Pediatr Hematol Oncol* 2002;**24**:120–4.

Saxonhouse MA, Garner R, Mammel L *et al.* Closure times measured by the platelet function analyzer PFA-100 are longer in neonatal blood compared to cord blood samples. *Neonatology* 2010;**97**:242–9.

Schlegel N, Bardet V, Kenet G *et al.* Diagnostic and therapeutic considerations on inherited platelet disorders in neonates and children. *Klin Pädiatr* 2010;**222**:209–14.

Schmugge M, Rand ML, Bang KWA *et al.* The relationship of von Willebrand factor binding to activated platelets from healthy neonates and adults. *Pediatr Res* 2003;**54**:474–9.

Sharma G, Berger JS. Platelet activity and cardiovascular risk in apparently healthy individuals: a review of the data. *J Thromb Thrombolysis* 2011;**32**:201–8.

Shattil SJ, Kashiwagi H, Pampori N. Integrin signaling: the platelet paradigm. *Blood* 1998;**91**:2645–57.

Shoenfeld Y, Tal A, Berliner S *et al.* Leukocytosis in non hematological malignancies—A possible tumor-associated marker. *J Cancer Res Clin Oncol* 1986;**111**:54–8.

Sitaru AG, Holzhauer S, Speer CP *et al.* Neonatal platelets from cord blood and peripheral blood. *Platelets* 2005;**16**:203–10.

Smith SA, Choi SH, Davis-Harrison R *et al.* Polyphosphate exerts differential effects on blood clotting, depending on polymer size. *Blood* 2010;**116**:4353–9.

Smyth SS, Woulfe DS, Weitz JI *et al.* G-protein-coupled receptors as signaling targets for antiplatelet therapy. *Arterioscler Thromb Vasc Biol* 2009;**29**:449–57.

Sola-Visner M. Platelets in the neonatal period: developmental differences in platelet production, function, and hemostasis and the potential impact of therapies. *ASH Educ Program Book* 2012;**2012**:506–11.

Spence N. Electrical impedance measurement as an endpoint detection method for routine coagulation tests. *Br J Biomed Sci* 2002;**59**:223–7.

Starkey JR, Liggitt HD, Jones W *et al.* Influence of migratory blood cells on the attachment of tumor cells to vascular endothelium. *Int J Cancer* 1984;**34**:535–43.

Stegner D, Nieswandt B. Platelet receptor signaling in thrombus formation. *J Mol Med Berl Ger* 2011;**89**:109–21.

Strauss T, Sidlik-Muskatel R, Kenet G. Developmental hemostasis: primary hemostasis and evaluation of platelet function in neonates. *Semin Fetal Neonatal Med* 2011;**16**:301–4.

Sutor AH. Vitamin K deficiency bleeding in infants and children. *Semin Thromb Hemost* 1995;**21**:317–29.

Tesselaar MET, Romijn FPHTM, Van Der Linden IK *et al.* Microparticle-associated tissue factor activity: a link between cancer and thrombosis? *J Thromb Haemost JTH* 2007;**5**:520–7.

Thamilselvan V, Patel A, Voort van Zyp J van der *et al.* Colon cancer cell adhesion in response to Src kinase activation and actin-cytoskeleton by non-laminar shear stress. *J Cell Biochem* 2004;**92**:361–71.

Trousseau A. *Clinique médicale de l'Hôtel-Dieu de Paris*. 5th ed. J.-B. Baillière, 1865.

Tuszynski GP, Gasic TB, Gasic GJ. Isolation and characterization of antistasin. An inhibitor of metastasis and coagulation. *J Biol Chem* 1987;**262**:9718–23.

Uçar T, Gurman C, Arsan S *et al.* Platelet aggregation in term and preterm newborns. *Pediatr Hematol Oncol* 2005;**22**:139–45.

Valastyan S, Weinberg RA. Tumor metastasis: molecular insights and evolving paradigms. *Cell* 2011;**147**:275–92.

Versteeg HH, Heemskerk JWM, Levi M *et al.* New fundamentals in hemostasis. *Physiol Rev* 2013;**93**:327–58.

Wada H, Matsumoto T, Yamashita Y. Diagnosis and treatment of disseminated intravascular coagulation (DIC) according to four DIC guidelines. *J Intensive Care* 2014;**2**:15.

Wasiluk A, Mantur M, Szczepański M *et al.* The effect of gestational age on platelet surface expression of CD62P in preterm newborns. *Platelets* 2008;**19**:236–8.

Watson SP, Auger JM, McCARTY OJT *et al.* GPVI and integrin αIIbβ3 signaling in platelets. *J Thromb Haemost* 2005;**3**:1752–62.

Wei AH, Schoenwaelder SM, Andrews RK *et al.* New insights into the haemostatic function of platelets. *Br J Haematol* 2009;**147**:415–30.

Weiss HJ. von Willebrand factor and platelet function. *Ann N Y Acad Sci* 1991;**614**:125–37.

Welch DR, Schissel DJ, Howrey RP *et al.* Tumor-elicited polymorphonuclear cells, in contrast to "normal" circulating polymorphonuclear cells, stimulate invasive and

metastatic potentials of rat mammary adenocarcinoma cells. *Proc Natl Acad Sci* 1989;**86**:5859–63.

White-Adams TC, Berny MA, Patel IA *et al.* Laminin promotes coagulation and thrombus formation in a factor XII-dependent manner. *J Thromb Haemost JTH* 2010;**8**:1295–301.

White CR, Frangos JA. The shear stress of it all: the cell membrane and mechanochemical transduction. *Philos Trans R Soc Lond B Biol Sci* 2007;**362**:1459–67.

White TC, Berny MA, Robinson DK *et al.* The leech product saratin is a potent inhibitor of platelet integrin α2β1 and von Willebrand factor binding to collagen. *FEBS J* 2007;**274**:1481–91.

Wirtz D, Konstantopoulos K, Searson PC. The physics of cancer: the role of physical interactions and mechanical forces in metastasis. *Nat Rev Cancer* 2011;**11**:512–22.

Woldhuis B, Tangelder GJ, Slaaf DW *et al.* Concentration profile of blood platelets differs in arterioles and venules. *Am J Physiol* 1992;**262**:H1217–23.

Wu QD, Wang JH, Condron C *et al.* Human neutrophils facilitate tumor cell transendothelial migration. *Am J Physiol Cell Physiol* 2001;**280**:C814–22.

Xiao T, Takagi J, Coller BS *et al.* Structural basis for allostery in integrins and binding to fibrinogen-mimetic therapeutics. *Nature* 2004;**432**:59–67.

Yang W-J. *Biothermal-Fluid Sciences: Principles and Applications*. Garland Science, 1989.

Zhang Y, Zhao Y, Lu S *et al.* A high-throughput biotin-avidin-ELISA for studying expression of platelet membrane glycoproteins and its clinical application. *Tohoku J Exp Med* 2010;**222**:83–8.

Zhao TX, Jacobson B, Ribbe T. Triple-frequency method for measuring blood impedance. *Physiol Meas* 1993;**14**:145–56.

Zipfel WR, Williams RM, Webb WW. Nonlinear magic: multiphoton microscopy in the biosciences. *Nat Biotechnol* 2003;**21**:1369–77.

Biographical Sketch

Sandra Michelle Baker was born on April 25, 1988 in Portland, Oregon to Julie and Daniel Baker. On October 6, 2012, she was married to Thiago Groberg.

Sandra attended Aloha High School and, upon graduation, enrolled at Oregon State University (OSU). During her undergraduate studies, she became involved in a variety of research areas through internships at Oregon Freeze Dry, SolarWorld Industries of America, the laboratory of Dr. Janine Trempy at OSU, and the laboratory of Dr. Willie "Skip" Rochefort at OSU. In June of 2011, she earned her Bachelor of Science degree in Bioengineering.

Sandra continued her education at Oregon Health & Science University (OHSU), joining the laboratory of Dr. Owen McCarty in the Department of Biomedical Engineering in July 2011. She received a Whitaker fellowship to conduct her third year of graduate school in the laboratory of Dr. Xavier Trepat at the Institute for Bioengineering of Catalonia in Barcelona, Spain. Sandra returned from Europe to finish her graduate research centered on the development of small volume platelet function assays to evaluate neonatal platelet adhesion, activation, and aggregation.

During her graduate studies at OHSU, Sandra was awarded an International Society on Thrombosis and Haemostasis Young Investigator Award and received research funding through a N.L. Tartar Research scholarship. She has presented her research in peer-reviewed journals and at international conferences throughout North America and Europe. Current publications and presentations are listed below:

Publications

1. **Baker SM**, Phillips KG, McCarty OJT. "Development of a label-free imaging technique for the quantification of thrombus formation." *Cellular and Molecular Bioengineering.* 2012 Sep; 5(4):488-492.

2. Aslan JE, Itakura A, Haley KM, Tormoen GW, Loren CP, **Baker SM**, Pang J, Chernoff J, McCarty OJT. "p21 activated kinase signaling coordinates glycoprotein receptor VI-mediated platelet aggregation, lamellipodia formation and aggregate stability under shear." *Arteriosclerosis, Thrombosis, and Vascular Biology.* 2013 Jul; 33(7):1544-51.

3. Aslan JE, **Baker SM**, Haley KM, Loren CP, Itakura A, Pang J, Greenberg DL, David LL, Chernoff J, Manser E, McCarty OJT. "The PAK system links Rho GTPase signaling to thrombin-mediated platelet activation." *American Journal of Physiology: Cell Physiology.* 2013 Sep; 305(5):C519-28.

4. **Baker-Groberg SM**, Phillips KG, McCarty OJT. "Quantification of volume, mass, and density of thrombus formation using bright field and differential interference contrast microscopy." *Journal of Biomedical Optics.* 2013 Jan; 18(1):0160141-0160144.

5. Jones CM, **Baker-Groberg SM**, Cianchetti FA, Glynn JJ, Healy LD, Lam WY, Nelson JW, Parrish DC, Phillips KG, Scott-Drechsel DE, Tagge IJ, Zelaya JE, Hinds MT, McCarty OJT. "Measurement science in the circulatory system." *Cellular and Molecular Bioengineering.* 2013 Dec; 7(1):1-14.

6. **Baker-Groberg SM**, Itakura A, Gruber A, McCarty OJT. "Recruitment of colon adenocarcinoma cells to thrombus under shear." *American Journal of Physiology: Cell Physiology.* 2013 Nov; 305(9):C951-C959.

7. Phillips KG, **Baker-Groberg SM**, McCarty OJT. "Quantitative optical microscopy: Measurement of cellular biophysical features with a standard optical microscope." *Journal of Visualized Experiments.* 2014 Apr; (86), e50988.

8. **Baker-Groberg SM**, Cianchetti FA, Phillips KG, McCarty OJT. "Development of a method to quantify platelet adhesion and aggregation under static conditions." *Cellular and Molecular Bioengineering.* 2014 Apr; 7(2):285-290.

9. King MR, Phillips KG, Mitrugno A, Lee TR, de Guillebon AME, Chandrasekaran S, McGuire MJ, Carr RT, **Baker-Groberg SM**, Rigg RA, Kolatkar A, Luttgen M, Bethel K, Kuhn P, Decuzzi P, McCarty OJT. "A physical sciences network characterization of circulating tumor cell aggregate transport." *American Journal of Physiology: Cell Physiology*. 2015 May; 308(10):C792-802.

10. **Baker-Groberg SM**, Bornstein S, Zilberman-Rudenko J, Schmidt M, Tormoen GW, Kernan C, Thomas CR, Wong MH, Phillips KG, McCarty OJT. "Effect of ionizing radiation on the physical biology of head and neck squamous cell carcinoma cells." *Cellular and Molecular Bioengineering.* 2015 May; doi:10.1007/s12195-015-0393-8.

11. **Baker-Groberg SM**, Phillips KG, Healy LD, Itakura A, Porter JE, Newton PK, Nan X, McCarty OJT. "Critical behavior of subcellular density organization during neutrophil

activation and migration." *Cellular and Molecular Bioengineering.* 2015 Jun; doi: 10.1007/s12195-015-0400-0.

12. Aslan JE, Rigg RA, Nowak MS, Loren CP, **Baker-Groberg SM**, Pang J, David LL, McCarty OJT. (in press). "Lysine acetyltransfer supports platelet function." *Journal of Thrombosis and Haemostasis*. 2015 Aug; doi: 10.1111/jth.13070.

Presentations

1. **Baker SM**, McCarty OJT, Berny-Lang MA, Tormoen GW. "Characterization of the role of cancer cells in the promotion of thrombus formation under shear." *Scientific & Standardization Committee of the ISTH*, Liverpool, United Kingdom (June, 2012).

2. **Baker SM**, McCarty OJT, Phillips KG, Rees KJ. "Development of a novel imaging technique for the quantification of mass, volume, and density of thrombus formation", *Scientific & Standardization Committee of the ISTH*, Liverpool, United Kingdom (June, 2012).

3. **Baker SM**, King MR, Decuzzi P, Phillips KG, Kolatkar A, Luttgen M, Bethel K, Kuhn P, McCarty OJT. "Circulating tumor microemboli interactions with blood cells and plasma in the vascular microenvironment", *NCI Scripps Physics Oncology*, San Diego, CA (October, 2012).

4. Haley KM, Aslan JE, Tormoen GT, **Baker SM**, Loren CP, Chernoff J, McCarty OJT. "The PAK signaling system links Rho GTPase activation to platelet lamellipodia formation, aggregation and aggregate stability under shear." *Annual Meeting of the American Society of Hematology*, Atlanta, GA (December, 2012).

5. **Baker SM**, Phillips KG, McCarty OJT. "Label-free volume determination using differential interference contrast microscopy: quantification of *in vitro* platelet aggregate and thrombus volumes under physiological shear rates." *BiOS SPIE Photonics West - Biomedical Spectroscopy, Microscopy, and Imaging; Imaging, Manipulation, and Analysis of Biomolecules, Cells, and Tissues XI Section*, San Francisco, CA (February, 2013).

6. **Baker-Groberg SM**, Itakura A, Gruber A, McCarty OJT. "Colon adenocarcinoma cell recruitment to platelets and thrombi under shear." *Third Annual Physical Sciences – Oncology Centers (PS-OCs) Network Investigators' Meeting*, Scottsdale, AZ (April, 2013).

7. **Baker-Groberg SM**, Phillips KG, Leung PY, Tucker EI, Gruber A, McCarty OJT. "Quantitative imaging of thrombus formation under shear." *XXIV Congress of the International Society on Thrombosis and Haemostasis*, Amsterdam, The Netherlands (June, 2013).

8. **Baker-Groberg SM**, Itakura A, Gruber A, McCarty OJT. "Colon adenocarcinoma cell recruitment to platelets and thrombi under shear." *XXIV Congress of the International Society on Thrombosis and Haemostasis,* Amsterdam, The Netherlands (June, 2013).

9. **Baker-Groberg SM**, Zalvidea D. "Development of a multi-photon microscopy setup for measuring 3D traction forces during *in vivo* angiogenesis." *Whitaker International Program Enrichment Seminar*. Rome, Italy (March, 2014).

10. **Baker-Groberg SM**, Zalvidea D. "Development of a multi-photon microscopy setup for measuring traction forces during *in vivo* angiogenesis." *2014 Biomedical Engineering Society Annual Meeting*, San Antonio, TX (October, 2014).

11. **Baker-Groberg SM**, Haley K, Dovlatova N, Recht M, McCarty OJT. "Development of a small volume, whole blood, platelet function assay to assess neonatal platelet adhesion, activation, and aggregation." *XXV Congress of the International Society on Thrombosis and Haemostasis*, Toronto, Canada (June, 2015).